STUDY OF WING-BODY INTERFERENCE AND DESIGN OF AN AERODYNAMICALLY COMPENSATED PITOT-STATIC TUBE

BY

SATISH CHANDER GUPTA

DEPARTMENT OF AERONAUTICAL ENGINEERING

INDIAN INSTITUTE OF TECHNOLOGY KANPUR

JUNE 1971

STUDY OF WING-BODY INTERFERENCE AND DESIGN OF AN AERODYNAMICALLY COMPENSATED PITOT-STATIC TUBE

A Thesis submitted

In Partial Fulfilment of the requirements

for the degree of

MASTER OF TECHNOLOGY

by

SATISH CHANDER GUPTA

to the

DEPARTMENT OF AERONAUTICAL ENGINEERING
INDIAN INSTITUTE OF TECHNOLOGY/ KANPUR

June 1971

CERTIFICATE

Certified that this work 'Study of Wing-Body Interference and Design of an Aerodynamically Compensated Pitot-Static Tube' has been carried out under my supervision and that this has not been submitted elsewhere for a degree.

S.M. Ramachandra

S.M. RAMACHANDRA
Professor, Department of
Aeronautical Engineering
Indian Institute of Technology
Kanpur

ACKNOWLEDGEMENT

This investigation was done under a grants-in-aid project entitled Wing-Body Interference sponsored by the Ministry of Defence, Government of India. I feel highly obliged to take the opportunity to pay my indomitable thanks to Professor S.M. Ramachandra for his versatile guidance throughout the period of this work.

ABSTRACT

Theory is presented on the lift and pressure distribution of bodies, wings and wing-body combinations at subsonic speeds. It is found that varying source ring distribution over body helps to simulate the wing-body interference effects. To study the phenomenon of wing-body interference, various mathematical models representing the given configurations are studied.

The design of an aerodynamically compensated pitot-static tube is made to nullify the position error. Aerodynamic compensation and insensitivity to angle of attack are the important features of designed pitot-static tubes.

CONTENTS

LIST OF FIGURES

LIST OF FIGURES.....

NOMENCLATURE

A	Aspect ratio
b	Span
c	Chord
d	Distance (fig.1-h)
2D	Fuselage diameter
D(k), E(k), K(k)	Elliptic integrals
K	Mach factor
l	Length over which each singularity is distributed
L	Panel sweep
M	Mach number
m	Line source strength per unit length
p_o	Free stream static pressure
ρ_o	Free stream density
p	local static pressure
q	Source-sink strength per unit length
q_{mB}	Source-sink strength per unit length required to satisfy tangential flow boundary condition in the presence of wing
Re	Real part
S(x)	Cross section area
u,v,w	Perturbation velocities in x,y,z directions
Δu	Pressure discontinuty across wing panel
Δu_{mW}	Pressure discontinuty required to satisfy tangential flow boundary condition in the presence of the body

Nomenclature (Continued)

v_{qx}	Horizontal component of perturbed velocity due due to source ring.
v_{qr}	Radial component of perturbed velocity due source ring
u_x	Horizontal component of perturbed velocity due to source ring
v_y	Lateral component of perturbed velocity due to source ring
w_z	Vertical component of perturbed velocity due to source ring
U	Free stream velocity
x,y,z	Cartesian coordinates
r'	Source ring radius
r,θ	Angular coordinates
x,r ϕ	Cylindrical coordinate system
Λ	Leading edge sweep
ξ,η	Integration variables
ϕ	Velocity potential function
ϕ^W	Velocity potential for wing
ϕ^B	Velocity potential for body
ϕ^P	Velocity potential for pitot-static tube
ϕ_M	Velocity potential for a given wing-body configuration
ϕ^i	Interference velocity potential due to wing-body combination
ϕ^{Wi}	Interference potential due to the presence of wing in the vicinity of body
ϕ^{Bi}	Interference potential function due to the presence of body in the vicinity of wing

Nomenclature (Continued)

ϕ^{MW}	Total potential for wing in the presence of body
ϕ^{MB}	Total potential for body in the presence of wing
C_{p_c}	Compensating pressure coefficient

Subscripts:

k	Corner point
n	Number
r	Radial
θ	Tangential
o	Free stream condition
W	Wing
B	Body
M,m	Model (Wing-body combination)
i	Interference

PART - A

STUDY OF WING BODY INTERFERENCE

CHAPTER - 1

INTRODUCTION

1.1 The presence of wing around body, puts the body at an angle of attack to an otherwise undisturbed stream of fluid parallel to the body axis. This change of direction of fluid around body results in the wing interference. To simulate this effect the body can be represented by a varying source ring distribution. The wing-body interference effects become more and more predominent with increasing yawing and pitching moments and angle of attack. The flow around a wing-body combination is studied for zero angle of attack. For other angles of attack the body starts shedding vortices of comparable strength over the wing vortices. The modified wing vortex distribution changes entirely when the presence of body vortices are considered. The flow being at a zero angle of attack, the effect of vortex distribution on body is considered negligible (Nielsen[1]). This assumption is not valid for high angles of attack. The effect of body vortices must be taken into account for $\alpha > 10^{\circ}$. The effect of body shedding vortices has been compared with the low angle theory and the verification has been made by the experimental work carried out by H.Schlichting[2]. To simulate the effect of wing interference, we rely upon varying source distribution since the angle of attack is taken to be zero.

A study of wing-body interference has been made for several wing-body configurations.

CHAPTER - 2

MATHEMATICAL FORMULATION

2.1 In order to study the flow field of wing-body combination, the wing, body and wing-body combination is represented by a set of singularities. The strengths of which are found by satisfying the tangential flow boundary conditions at the selected control points to get the given configuration. The shrouded part of the wing is considered to be of zero camber and zero thickness. The theory applies to both subsonic and supersonic flows, since the linearised potential function and Prandtl-Glauert equation hold for these flows. The similarity solution of Von Karman[3] may be used to extend this theory for transonic flow.

2.2 Wing alone:

The potential function for the wing satisfies the linearised Prandtl-Glauert equation[4].

$$(1-M^2)\,\phi^{W}_{xx} + \phi^{W}_{yy} + \phi^{W}_{zz} = 0 \qquad \ldots\ldots\ldots 2.1$$

The failure of lifting line theory for swept back wings lights up the idea of surface discontinuties. The wing plane is assumed to be a horizontal plane. This plane is divided into a large number of panels. Over each panel a singularity of constant strength is distributed. The downwash at each control point is determined. The strength of

each panel pressure discontinuity is determined to satisfy the flow tangency boundary condition required to obtain the given camber line.

The expression for potential function for constant pressure singularities is given by[4]

$$\phi^W = \frac{K}{\pi} \iint \left(\frac{z(x-\xi)}{(y-\eta)^2 + z^2} \right) \frac{d\xi \, . d\eta}{\sqrt{(x-\xi)^2 + (1-M^2)\left[(y-\eta)^2 + z^2\right]}}$$

$$+ \frac{(1-K)}{\pi} \iint \frac{z \, d\xi \, d\eta}{(y-\eta)^2 + z^2} \qquad \ldots\ldots 2.2$$

where $K = 0.5$ for $M < 1$

and $K = 1.0$ for $M > 1$

$$x = x_p - x_k$$

$$y = y_p - y_k$$

$$z = z_p$$

The limits of integration are defined by the panel boundaries. For one corner element the potential function is given by

$$\phi_k^W = \frac{K \Delta u}{2\pi} \left[(x - ly).(F3+F4) + z\{(L^2+1-M^2).F2 - L(F1-F5) - yF6\} \right] \qquad \ldots\ldots\ldots 2.3$$

where 2. Δu = pressure discontinuity across panel

$$F1 = \mathrm{Re}\left[\log \frac{x+d}{\sqrt{|1-M^2|}} - r\right]$$

$$F2 = \frac{1}{\sqrt{L^2+1-M^2}} \mathrm{Re}\left(\log \frac{x' + d'}{r'\sqrt{|1-M^2|}}\right)$$

$$F3 = \mathrm{Re}\left[\tan^{-1}\left(\frac{zd}{Lr - xy}\right)\right]$$

$$F4 = \tan^{-1}\frac{y}{z} \quad \text{for } M < 1$$

$$= 0 \qquad \text{for } M > 1$$

$$F5 = \log \frac{L\sqrt{y^2+z^2}}{\sqrt{(x-Ly)^2+(L^2+1-M^2)z^2}}$$

$$= \log \frac{Lr}{r'} \quad \text{for } M < 1$$

$$= 0 \qquad \text{for } M > 1$$

$$F6 = \frac{x+d}{r^2} \quad \text{for } M < 1$$

$$= \frac{d}{r^2} \quad \text{for } M > 1$$

$$r = \sqrt{y^2 + z^2}$$

$$d = \sqrt{x^2+(1-M^2)\,r^2}$$

$$x' = Lx + (1-M^2)y$$

$$y' = x - Ly$$

$$r' = \sqrt{(x - Ly)^2 + (L^2 + 1 - M^2)\, z^2}$$

$$d' = \sqrt{x'^2 + (1-M^2)\, r'^2}$$

The potential at a point P (x_p, y_p, z_p) is given by

$$\phi^W(P) = \phi^W_1 - \phi^W_2 - \phi^W_3 + \phi^W_4 \qquad \text{.....2.4}$$

where $\phi^W_{K'}$ $K = 1.....4$

is the potential due to one corner element of constant pressure discontinuity:

The perturbation velocity components are given by

$$u = \frac{\partial \phi}{\partial x} \qquad v = \frac{\partial \phi}{\partial y} \qquad w = \frac{\partial \phi}{\partial z} \qquad \text{.....2.5}$$

The partial derivative of eqn.(2.3) gives the perturbation velocity component due to each corner element of constant pressure panel.

$$\left.\begin{aligned} u_k &= \frac{K\,\Delta u}{2\pi}\,(F3 + F4) \\ v_k &= \frac{K\,\Delta u}{2\pi}\,\left[L(F3+F4) - z.F6\right] \\ w_k &= \frac{K\,\Delta u}{2\pi}\,\left[(L^2 + 1 - M^2)\,F2 - L\,(F1-F5) - y.F6\right] \end{aligned}\right\} \ldots 2.6$$

The perturbation velocity components due to vortex panel at any point $p(x_p, y_p, z_p)$ are given by

$$u(p) = u_1 - u_2 - u_3 + u_4$$

$$v(p) = v_1 - v_2 - v_3 + v_4 \qquad \text{.....2.7}$$

$$w(p) = w_1 - w_2 - w_3 + w_4$$

$w(p)$ = slope at the control points (p) x free stream velocity. This gives a set of n simultaneous linear equations for n control points. The solution of these equations gives the value of pressure discontinuities across the panels.

Using the linearised form of Bernoulli's equation for study, compressible flow, the pressure coefficient becomes

$$C_p = \frac{p - p_\infty}{\frac{1}{2} \rho U^2} = \frac{-2u}{U} \qquad \text{.....2.8}$$

The pressure discontinuity across the panel is given by the linearised Bernoulli's equation.

$$C_p = C_{p_{lower}} - C_{p_{upper}}$$

$$\text{or} \quad C_p = 2.\left(\frac{\Delta u}{U}\right) \qquad \text{.....2.9}$$

To study the pressure distribution and lift distribution of the wing, three configurations are chosen. A tapered wing, delta wing and constant chord wing have been treated with the described mathematical formulation.

The lift and pressure distributions are plotted and compared in figs.(1-15). The details of the wings dimentions are given below:

WING	A	s	C_r	C_t	T.R.	Λ
Tapered wing	2.9	10	5	2	2.5	45°
Delta wing	2.9	10	5	0	∞	-do-
Constant chord wing	4	10	3.2	3.2	1	-do-

The pressure distribution increases toward the tip of the constant chord wing. This is because of the leading edge sweep. The center of pressure, therefore, moves away from the root section. The delta wing has the nearest center of pressure to the wing root, as compared to other wings.

2.3 Body alone:

The potential function for body satisfies the linearised Prandtl-Glauert equation[4]

$$(1-M^2)\ \phi^B_{xx} + \phi^B_{yy} + \phi^B_{zz} = 0 \qquad \ldots 2.10$$

The body is represented by a constant source sink distribution. A source ring is a distribution of sources of constant strength along a circle.[5]

The velocity induced by element of strength q.ds of a source ring of radius r' at a point (x,r,ϕ) is given by fig.(1-f)

$$\overrightarrow{dv} = \frac{q.\ ds\ \overrightarrow{R}}{4\pi\ R^2\ R}$$

Taking the integration around the circumference of the ring we obtain for the velocity components in cylindrical coordinates.

$$v_{qx}(x,r) = \frac{q}{4\pi r'} \int_0^{2\pi} \frac{x}{\sqrt{x^2+r^2+1-2r\,\mathrm{Cos}(\phi-\phi')}^3} d\phi'$$

$$\text{and } v_{qr}(x,r) = \frac{q}{4\pi r'} \int_0^{2\pi} \frac{r-\mathrm{Sin}\,\phi'}{\sqrt{x^2+r^2+1-2r\,\mathrm{Cos}(\phi-\phi')}^3} d\phi' \qquad \ldots 2.11$$

where $x = x/r'$

$r = r/r'$

For simplicity only the x and r are replaced by non-dimensionalized values of x and r

r' = source - ring radius

x = distance of control point from source ring

r = distance of control point from x axis.

These integrals are reduced to complete elliptic integrals. The expression for velocity components are given by the followings:

$$v_{qx}(x,r) = \frac{q}{2\pi r'} \frac{2x}{\left[\sqrt{x^2+(r+1)^2}\right]\left[x^2+(r-1)^2\right]} E(k)$$

$$v_{qr}(x,r) = \frac{q}{2\pi r' r \sqrt{x^2+(r+1)^2}} \left[K(k) - \left(1 - \frac{2r(r-1)}{x^2+(r-1)^2}\right) E(k) \right] \qquad \ldots\ldots.2.12$$

where $K(k) = \int_0^{\pi/2} \frac{1}{\sqrt{1-k^2 \sin^2\alpha}}\, d\alpha$

$$E(k) = \int_0^{\pi/2} \sqrt{1-k^2 \sin^2 \alpha}\, d\alpha$$

$$D(k) = \int_0^{\pi/2} \frac{\sin^2 \alpha}{\sqrt{1-k^2 \sin^2 \alpha}}\, d\alpha \qquad \ldots\ldots.2.13$$

$$= \frac{K-E}{k^2}$$

and $k^2 = \frac{4r}{x^2 + (r+1)^2}$

To simulate the effect of body volume, eighteen source rings are chosen with the control points placed between successive sources. The boundary conditions are satisfied to obtain tangential flow over the control points. Thus

$$\frac{v_{qr}(x,r)}{U} = \text{slope at any point } p\ (x,r)$$

Three bodies, an elipsoid of revolution, a Sears-Haack body and a Karman Ogive of the same length and volume are represented by this type of mathematical model. Their pressure distribution and the strength of equivalent

source-sink distribution is compared in figs.(33). .

The contours of the three types of bodies are expressed by the following equations.

1. Ellipsoid of revolution

$$\frac{x^2}{a^2} + \frac{y^2}{b^2} = 1.0 \text{ with } a/b = 10/1 \qquad \ldots.2.14$$

2. Sears-Haack body

$$S(x) = \frac{16.\ \text{Volume}}{3\pi l}\left[1-(1-\frac{2x}{l})^2\right]^{3/2} \qquad \ldots.2.15$$

where $S(x)$ = X-sectional area of the body at any distance x from the origin

l = length of it's axis

volume $= \frac{4}{3}\ a\ \pi\ b^2$ (volume of ellipsoid of revolution)

3. Karman Ogive

$$S(\theta) = \frac{S(l)}{\pi}\ (\pi-\theta+\frac{1}{2}\ \text{Sin}2\theta) \qquad \ldots.2.16$$

where $\theta = \text{Cos}^{-1}(1-\frac{2x}{l})$

$S(l)$ = maximum X-sectional area

2.4 Wing-Body Combination:

For the combined flow field of a wing body combination, the total velocity potential is not a simple sum of the potentials of the body ϕ^B and the wing ϕ^W alone. The resultant flow should satisfy the boundary conditions on both wing and body together. For a wing body combination, the resultant potential function may be written as

$$\phi_M = \phi^B + \phi^W + \phi^i \qquad \text{.....2.17}$$

Many approximate mathematical theories have been put forward for the explicit expression of the interference velocity potential function.[7,8,9,10] Interference potential can be expressed as algebric sum of interference potential due to wing on body and due to body on wing[12]. So the expression for ϕ^i can be written as

$$\phi^i = \phi^{Wi} + \phi^{Bi}$$

The expression for ϕ_M through this equation is written as

$$\phi_M = \phi^B + \phi^W + \phi^{Wi} + \phi^{Bi}$$

$$= (\phi^W + \phi^{Bi}) + (\phi^B + \phi^{Wi})$$

$$= \phi^{MW} + \phi^{MB}$$

where $\phi^{MW} - = \phi^{W} + \phi^{Bi}$

and $\phi^{MB} = \phi^{B} + \phi^{Wi}$ 2.18

ϕ^{MW} is the potential function of wing in the presence of body and ϕ^{MB} is the potential function of body in the presence of wing. These potential functions satisfy the linearised Prandtl-Glauert equation for all Mach numbers except $M = 1$

$$(1-M^2)\,\phi^{MW}_{xx} + \phi^{MW}_{yy} + \phi^{MW}_{zz} = 0 \qquad .....2.19$$

$$(1-M^2)\,\phi^{MB}_{xx} + \phi^{MB}_{yy} + \phi^{MB}_{zz} = 0 \qquad .....2.20$$

To determine the expression for velocity potential function, the wing is replaced by the pressure discontinuities across the horizontal panel and the body is replaced by a distribution of source ring singularities.

The potential function for constant pressure singularities is given by eqn.(2.2) and the vertical component of perturbed velocity by eqn.(2.6). The potential for the wing and the induced velocity may be written in the form $\phi^{MW}(p) = \phi^{MW}_{1} - \phi^{MW}_{2} - \phi^{MW}_{3} + \phi^{MW}_{4}$

and $$W_k = \frac{K \Delta u_{mW}}{2\pi} \left[(L^2 + 1-M^2).F2-L(F1-F5)-YF6 \right] \quad \ldots 2.21$$

The downwash at any point $P(x_p, y_p, z_p)$ is given by

$$w(p) = w_1 - w_2 - w_3 + w_4$$

$$= C_W \cdot u_{mW} \quad \ldots\ldots 2.22$$

where $$C_W = \frac{K}{2\pi} \left[\left\{ (L^2 + 1-M^2) \cdot F2 - L(F1-F5) - YF6 \right\}_{k=1} - \left\{ (L^2 + 1-M^2).F2-L(F1-F5)-YF6 \right\}_{k=2} - \left\{ L^2 + 1-M^2). F2-L(F1-F5)-YF6 \right\}_{k=3} + \left\{ L^2 +1-M^2). F2-L(F1-F5) -YF6 \right\}_{k=4} \right] \quad \ldots 2.23$$

No explicit analytical expression can be given for the velocity potential function of a varying source ring distribution, however, numerical values can be obtained by graphical integration of velocity field.

When the axis of body of revolution is inclined to free stream the varying source - ring distribution is taken as singularity. This simulates the effect of wing interference on body. The use of additional vortex distribution on body is not required, since the problem is studied for zero angle of attack. Only at high angles of attack, the body starts shedding vortices of strengths

comparable to the wing vortices. This modified theory for high angle of attack is discussed by Nelson[1]. The potential theory with vortex distribution on body is in good agreement with low angle of attack theory. The departure of the two curves for normal load distribution starts at an angle of attack of about 10°. Ref.[1].

The expression for velocity components of a source distribution of varying strength on a circle[5] are given below:

$$u_x(x,r,\phi) = \frac{q_{MB}}{2\pi r'} \frac{2x(2K(k)-2D(k)-E(k))}{(x^2+(r-1)^2)\sqrt{x^2+(r+1)^2}} \sin\phi$$

$$v_y(x,r,\phi) = \frac{q_{MB}}{2\pi r'} \frac{\sin 2\phi}{(x^2+(r-1)^2)\sqrt{x^2+(r+1)^2}}$$

$$\left[\left(r - \frac{8}{k^2}\right)(2K(k)-2D(k)-E(k)) + 8(K(k)-D(k))-E(k) \right]$$

$$w_z(x,r,\phi) = \frac{q_{MB}}{2\pi r'} \frac{1}{(x^2+(r-1)^2)\sqrt{x^2+(r+1)^2}}$$

$$\left[2r \sin^2\phi + \frac{8}{k^2}(1-2\sin^2\phi)(2K(k)-2D(k)-E(k)) \right.$$

$$\left. -8(1-2\sin^2\phi)(K(k)-D(k))-2\sin^2\phi\, E(k) \right]$$

.....2.24

and

$$w_z(x,r,\phi) = D_B\, q_{mB} \qquad \text{.....2.25}$$

where $D_B = \dfrac{\sin 2\phi}{2\pi r'} \dfrac{1}{(x^2+(r-1)^2)\sqrt{x^2+(r+1)^2}}$

$$\left[\left(r - \frac{8}{k^2}\right)\left((2K(k)-2D(k)-E(k))+8(E(k)-D(k))-E(k)\right]\right.$$

The resultant vertical component of velocity due source-sink ring and vortex distribution is given by algebric sum of the two velocity components.

For n pressure panel singularities and m source ring singularities, there are n control points on the wing and n control points on the body. The total downwash at any control point of the wing is given by algebraic sum of the velocity due to wing pressure singularities eqn.(2.23) and those due to source ring singularities (eqn.2.25)

$$w_W = \sum_{i=1}^{n} C_{WW,i}\, \Delta u_{mW,i} + \sum_{j=1}^{m} D_{BW,j}\, q_{mB,j} \qquad \text{.....2.26}$$

The downwash at any of the body control points is given by

$$w_B = \sum_{i=1}^{n} C_{WB,i}\, \Delta u_{mW,i} + \sum_{j=1}^{m} D_{BB,j}\, q_{mB,j} \qquad \text{.....2.27}$$

The downwash on (m+n) control points is given by

$$w_{mn} = \sum_{i=1}^{n} C_{W,i} \Delta u_{mW,i} + \sum_{j=1}^{n} D_{B,j} \quad q_{mB,j} \qquad \text{.....2.28}$$

$\frac{w_{mn}}{U}$ = surface slope at the (m+n) control point.

The system of simultaneous linear equations is solved by Gauss-Jordon method to satisfy the tangential flow conditions. The final values of constant pressure discontinuties and varying source ring distribution are obtained. The new potential function for the wing in the presence of the body is given by

$$\phi_k^{mW} = \frac{K \Delta u_{mW}}{2\pi} \left[(x-Ly).(F3+F4) + z \left\{ (L^2+1-M^2)\, F2 - L(F1-F5) - yF6 \right\} \right] \qquad \text{.....2.29}$$

where $2\Delta u_{mW}$ is the pressure discontinuity across the panel. The value of new potential function at any point $P(x_p, y_p, z_p)$ is given by

$$\phi^{mW}(p) = \phi_1^{mW} - \phi_2^{mW} - \phi_3^{mW} + \phi_4^{mW} \qquad \text{.....2.30}$$

The value of the interference potential due to body on wing is given by eqn.(2.18) thus at any point P

$$\phi^{Bi}(p) = \phi^{MW}(p) - \phi^{W}(p) \qquad \ldots\ldots 2.31$$

The expression for the body potential due to the source ring distribution is given by

$$\phi^{B} = \int_{o}^{r} v_{qx}\,dr + \int_{o}^{x} v_{qr}\,r\,dx \qquad \ldots\ldots 2.32$$

The expression for potential function for varying source ring distribution is given by

$$\phi^{MB} = \int_{o}^{x} u\,dx + \int_{o}^{y} v\,dy + \int_{o}^{z} w\,dz \qquad \ldots\ldots 2.33$$

The expressions for v_{qx}, v_{qr}, u, v, w, are given by eqns.(2.12 and 2.24) so the expressions for ϕ^{B} and ϕ^{MB} are known. The interference potential due to a wing on a body is defined by eqn.(2.18.)

$$\begin{aligned}\phi^{Wi} &= \phi^{MB} - \phi^{B} \\ &= \int_{o}^{x} u\,dx + \int_{o}^{y} v\,dy + \int_{o}^{z} w\,dz - \int_{o}^{r} v_{qx}\,dr \\ &\quad - \int_{o}^{x} v_{qr}\,r\,dx \end{aligned} \qquad \ldots\ldots 2.34$$

The mathematical model described to simulate the given configurations can work upto $\pm 10^{o}$ of angle of attack. Beyond this range of angle of attack the shed vortices of body are to be taken into account. To take care of body vortices, the body in the interference region is divided into a large number of panels. Each panel represents a constant pressure singularity. The tangential flow boundary conditions are applied to determine the strength of these singularities.

CHAPTER - 3

RESULTS AND DISCUSSION

The study of wind-body interference involves the importance of satisfying the tangential flow boundary conditions both on wing and body. The effect of interference due to body on wing is high in the vicinity of body only. The wing interference is found to be predominent over a long distance on the body. As the length of the nose of the wing-body configuration increases, the center of pressure moves outward on the wing, therefore, a short nose-body should be preferred for high manoeuverability. The combination of elliptic body, Sears-Haack body and Karman Ogive body with tapered wing, delta wing and constant chord wing has been studied for three locations of wing on the major axis of body.

For a long nose shaped constant chord wing-body combination, the center of pressure lies outward to the point of center of pressure for a delta wing-body combination. The change in lift distribution of the constant chord wing due to the presence of body is not effected much as compared to the change in lift distribution of tapered and delta wings. The change in source sink singularities and wing pressure distribution is found maximum for a delta wing and Sears Haack body combination. The change in lift distribution of wing due the presence of Karman-Ogive body is least as compared to the

presence of elliptic or Sears-Haack body. The magnitude of interference pressure coefficient due to a delta wing and Sears-Haack body combination is maximum than the value of interference pressure coefficient due to any other combination.

Short nose elliptic body and tapered wing combination is found to be the best case for least interference. The center of pressure of the wing, therefore, does not shift much due to the presence of the body.

The wing-body interference phenomenon can be studied and the values of the interference pressure coefficients and lift distributions can be found through the computer programming given in appendix A. The values of pressure coefficient of a wing-body flow field may be found at any location. The value of pressure coefficient may be used for the design of an aerodynamically compensated pitot-static tube described in Part B.

PART - B

DESIGN OF AN AERODYNAMICALLY COMPENSATED PITOT-STATIC TUBE

CHAPTER - 4
INTRODUCTION

4.1 Pitot pressure and free stream static pressure are required to determine the altitude, rate of climb and air speed of the airplane. The presence of a static port in the disturbed flow field created by the airplane causes it's port to sense inaccurate static pressure. To meet the need of the present day busy airports and high performance airplanes it is very important to know the accurate speed and altitude. The error in static pressure sensing is a function of Mach number, angle of attack and change of configuration of the airplane. The change in configuration of the airplane means the operation of flaps, elevators or ailerons. The operation of flaps can cause a non-negligible change of static pressure at the static port location. The error in static pressure sensing port due to the perturbed field of the airplane is known as the position error. The design of the pitot-static tube is so made as to provide a negative compensation to the flow field perturbation created by the airplane. This is known as aerodynamic compensation for the static pressure sensing port. The data for the design of the aerodynamic compensator is obtained from Part A. The aerodynamic compensator is designed to sense the accurate static pressure over a large range of Mach number.

The design of a pitot static tube for sensing accurate static pressure must take into account the static pressure variation with Mach number and angle of attack. These static pressure variations can be minimised by a suitable location of the static

pressure sensing port in the vicinity of the airplane. The best location for the pitot-static tube mounting is found to be the nose boom, ahead of the body of the airplane, since the variations of the static pressure perturbations with Mach number and angle of attack is a minimum at this location. The nose boom location for the pitot static tube has disadvantages of maintenance and storage and the increased length of the aircraft complicates the ground movement problems.

Since the effect of the upwash field of the wing is predominent in the vicinity of the wing, therefore, the second preferred location of the static port is found to be the fuselage dorsal mounting. The third preferred location on high performance airplanes for static pressure sensing port is the wing tip.

A pitot-static tube design has been tailor made to sense almost the exact free stream static pressure over a large range of Mach number and angle of attack. The designed contours of the pitot static tubes, shown in figs.(55,57, 59) are aerodynamically compensated for the Mach numbers ranging between (0.3 to 0.85). The linearised theory used here can not be applied for $M<0.3$ due to the high angle of attack involved. For $0.3<M<0.9$, the error ΔC_{p_c} in the cancellation of the static pressure perturbation is less than 0.075 of C_{p_c}, the compensating static pressure. In the following Chapters of Part B the procedure for the design of aerodynamically compensated pitot-static head is discussed for the three pitot

head locations. For this purpose an elliptic fuselage with a 45° swept wing centerly mounted on it is assumed. Other wings and fuselage shapes and positions may be considered on a same procedure to design the pitot-static tube.

CHAPTER - 5

DESIGN FOR AERODYNAMIC COMPENSATION

5.1 Description of the aerodynamic compensator:

In Part A the static pressure perturbations, were calculated for several combinations of wing-body shapes and locations. The perturbation field created by the fuselage and the wing, is plotted against Mach number for the three positions of the pitot-static tube viz.(i) ahead of body (ii) dorsal side of the fuselage (iii) ahead of the wing tip. The contour of the pitot-static tube is now sought to develope a negative static pressure perturbation at the location of the static pressure sensing port to canel the static pressure perturbation due to the wing-fuselage combination. The static pressure sensing port is made insensitive to angle of attack. For this purpose the static pressure sensing ports are located diagonaly opposite in the lateral direction. The shape of the aerodynamic compensator is made smooth to avoid abrupt compression and expansion of flow. We can also determine the perturbation field created by the airplane at any location using numerically the computer programme given in appendix A. Appendix B gives the computer programme for obtaining the nose contour of an aerodynamically compensated pitot-static tube. Giving the length of the pitot-static nose contour and pressure coefficient required for negative compensation as the input data, the desired compensating shape of the nose contour can be obtained.

We have the Bernoulli's equation for compressible steady flow between the free stream and the point of location of static pressure sensing port.

$$\frac{1}{2}U^2 + \frac{\gamma}{\gamma-1}\frac{p_o}{\rho_o} = \frac{1}{2}V^2 + \frac{\gamma}{\gamma-1}\frac{p}{\rho} \qquad \ldots\ldots 5.1$$

The local static pressure is expressed as a function of the free stream static pressure by

$$p = p_o(1+\epsilon) \qquad \ldots\ldots\ldots 5.2$$

For an undisturbed flow the perturbation velocities u, v, w are zero and hence ϵ is zero. Thus in the undisturbed flow we can sense the correct static pressure.

Combining eqns. (5.1) and (5.2) we have

$$\frac{1}{2}U^2 + \frac{\gamma}{\gamma-1}\frac{p_o}{\rho_o} = \frac{1}{2}V^2 + \frac{\gamma}{\gamma-1}\frac{p_o(1+\epsilon)}{\rho} \qquad \ldots\ldots 5.3$$

where $V = \sqrt{(U+u)^2 + v^2 + w^2}$

from which ϵ can be written as

$$\epsilon = -\frac{\rho}{p_o}\left[Uu + \frac{1}{2}\left((1-M^2)u^2 + v^2 + w^2\right)\right] \qquad \ldots\ldots 5.4$$

Another expression for ϵ fallows from eqn. (5.2) as

$$\epsilon = \frac{p - p_o}{p_o}$$

Defining the pressure coefficient as

$$C_p = \frac{p - p_o}{\frac{1}{2}\rho U^2} \qquad \ldots\ldots 5.5$$

The expression for pressure coefficient can be written as

$$C_p = \frac{-\left[Uu + \frac{1}{2}\left((1-M^2)\,u^2+v^2+w^2\right)\right]}{\frac{1}{2}U^2} \qquad \ldots\ldots 5.6$$

Combining eqns. (5.2) and (5.5)

$$C_p = \frac{p_o\,(1+\epsilon) - p_o}{\frac{1}{2}\,\rho\,U^2}$$

so that

$$\epsilon = \frac{C_p\ \frac{1}{2}\ \rho\ a_o^2\ M_o^2}{p_o} = \frac{\gamma\ M_o^2\ C_p}{2} \qquad \ldots\ldots 5.7$$

For a given airplane geometry, ϵ is a function of Mach number and angle of attack. The perturbation ϵ as a function of M and α, should vary least for the best location of the static pressure sensing port. This variation is found suitable for the nose boom location of the pitot-static tube fig. (55-A). The shape of the pitot port is so designed that it ca n sense the pitot-pressure accurately upto $\pm$ 15° of angle of attack.

5.2 Pitot-head design for nose boom location:

For subsonic flow, the fuselage causes significant compression of air ahead of it. This results in a static pressure error. The static pressure field ahead of the fuselage axis is plotted in fig.(55-B). The pressure coefficient falls in a non-linear manner ahead of the body

In the plane of the symmetry of the aircraft, the lateral perturbation velocity is zero. The vertical perturbation velocity is created by the flow field on the wing. The

expression for C_p in the plane of symmetry is given by

$$C_p = \frac{-\left[Uu + \frac{1}{2}\left((1-M^2)\,u^2 + w^2\right)\right]}{\frac{1}{2}U^2} \qquad \ldots\ldots 5.8$$

Now we go for the design of the contour of the pitot-static head to comtensate for the positive static pressure perturbation at the static pressure sensing port. To avoid abrupt compression, a sufficient length of pitot head is provided. Smooth curvature ahead of the static port is given to avoid flow seperation. The static port location is taken at 0.55D ahead of the body where the static pressure coefficient is found to be 0.1217 for a 45° swept tapered wing-elliptic body combination. The body is assumed to be of fineness ratio 1:10. At a distance of 0.55 D forward of the body, the value of the wing-body perturbation static pressure coefficient is neutralised by the expansion of the subsonic flow over the pitot head at the static port. To make the static pressure sensing port insensitive to the angle of attack, we choose two static port locations, which are diagonally opposite to each other and lie in the lateral direction. fig. (55-B). These static ports are not sensitive to the flow direction since they lie parallel to the flow direction created by the wing. The use of a single set of static ports in Rosemount tube[22] is a contradicting statement to the use of four static ports placed diagionally opposite.[21] The advantage of a single set of ports for both subsonic and supersonic flows is stated to obviate the need for computation of correction

within the central air data computer.[22] The single set of ports chosen for the Rosemount tube[22] are very sensitive to angle of attack. The two sets of ports used in the Rosemount tube[21] are placed diagonally opposite to compensate for pitching, yawing or rolling motions. In our present pitot-static head design the use of a single set of diagonally opposite static ports is considered to nullify the effects of pitching, yawing or rolling motions. The position of the static ports is set diagonally opposite in the lateral direction to avoid the necessity of using computed corrections within the central air data computer. To make the static pressure sensing port insensitive to the vertical perturbation velocity and angle of attack, we set the value of the vertical perturbation velocity created by the pitot-static tube at the static port location equal to zero. The mathematical formulation for the design of the aerodynamic compensator is described below.

5.3 Mathematical formulation:

The effect of pitot - static tube shape is simulated by a linearly varying line source singularity. The strength of this singularity is determined to get the required shape of the pitot-static tube. The potential function due to a line source of constant strength located along the x-axis between x = o and x = 1 is given by the following expression:

$$\phi^P = m \int_0^1 \frac{-\xi \, d\xi}{\sqrt{(x-\xi)^2 + (1-M^2)r^2}} \qquad \ldots\ldots.5.9$$

m = strength of source per unit length. The integration is carried out between the limits $\xi = 0$ and $\xi = 1$ and resulting potential may be written as

$$\phi^P = \mathrm{Re}\ \left(d_1 - d_2 - x_1 \log \frac{x_1 + d_1}{x_2 + d_2}\right) \qquad \ldots\ldots\ldots 5.10$$

where $d_1 = \sqrt{x_1^2 + (1-M^2)\, r^2}$ $\quad x_1 = x - x_k$

$d_2 = \sqrt{x_2^2 + (1-M^2)\, r^2}$ $\quad x_2 = x - 1$

In subsonic flow the distances d_1 and d_2 may be taken from the origin and tail of the line source to the point P^* $(x, r\sqrt{1-M^2}\ )$ in the Prandtl-Glauert coordinate system, fig. (1-d). In supersonic flow d_1 and d_2 are both imaginary ahead of Mach cone from origin; d_1 is real and d_2 is imaginary between the Mach cone ahead of the body and the Mach cone aft of body. Behind the Mach cone both d_1 and d_2 and are real, the variation of d_1 and d_2 is shown in fig. (1-d). In supersonic flow the distance d_1 between the Mach cone ahead and aft of body is interpreted as the distance from the origin to the point P on the circle of diameter X, fig. (1-d).

The logarithmic term in eqn.(5.10) can be expressed as a function of hyperbolic sine and hyperbolic cosine for subsonic and supersonic domains respectively. The velocity components are given by the partial derivatives of potential

function , as follows:

$$u = \frac{\partial \phi}{\partial x} \qquad v = \frac{\partial \phi}{\partial y} \qquad w = \frac{\partial \phi}{\partial z}$$

After carrying out the partial differentiation the perturbation velocity components can be expressed as

$$u = m \ \mathrm{Re}\left[\log\left(\frac{x_2 + d_2}{x_1 + d_1}\right) + \frac{l}{d_2}\right] = m.c$$

$$v_r = \frac{m}{r} \ \mathrm{Re}\left(d_1 - \frac{d_1^2 - x_1 l}{d_2}\right) = m.d. \qquad \text{.....5.11}$$

The pressure coefficient through the Bernoulli's equation for compressible steady flow is given by

$$C_{p_c} = \frac{-\left[Uu + \frac{1}{2}\left((1-M^2)\,u^2 + v_r^2\right)\right]}{\frac{1}{2}U^2} \qquad \text{.....5.12}$$

The desired shape of the nose contour is simulated by a pair of line source and line sink singularities distributed over lengths l_1 and l_2 respectively as shown in fig. (5B).For a known length $l = l_1 + l_2$, of the nose contour, l_1 and l_2 are assumed equal for the sake of simplicity and the strengths m_1 and m_2 of the source-sink singularities is determined by eqns. (5.11) and (5.12).

The shape of the compensating nose contour which provides a negative pressure coefficient equal in magnitude

to the positive pressure coefficient due to the assumed wing body combination have been calculated and plotted in fig. (55-B).

5.4 Pitot head design for fuselage dorsal mounting:

The total perturbation pressure coefficient due to the wing-body combination is plotted on the fuselage dorsal side in fig.(56-B). The pitot static tube is assumed to be located at a distance of 0.5D above the top surface of the fuselage at the center. The variation of pressure coefficient at the static port location is plotted as a function of Mach number fig. (56-A). The pressure coefficient on the fuselage dorsal side has a negative value. The shape of the nose contour of the pitot-static tube is simulated by a combination of two line sources of strengths m_1 and m_3 and a line sink of strength m_2 as shown in fig. (57) The line source singularities are distributed over lengths l_1 and l_3, and the line sink singularity is distributed over length l_2. The lengths l_2 and l_3 are expressed as

$$l_1 = 2\, l_1 = 2l_3$$

The sink strength m_2 is chosen as half of the source strength m_1. The strengths m_1 and m_3 are determined through eqns. (5.11) and (5.12). The equations can be expressed as

$$u = m_1 c_1 + m_2 c_2 + m_3 c_3$$

$$v = m_1 d_1 + m_2 d_2 + m_3 d_3$$

where C_n and d_n, (n=1, 2, 3) are defined through eqns.(5.11) and (5.12) fig.(1-d). The third singularity m_3 is a line source singularity. This developes a curved surface aft of the static port. This causes a significant compression of air on the static port and develops a positive pressure coefficient. To get a smooth shape of the nose contour a proper choice of the length over which each singularity is distributed, has to be made. Care has been taken to keep the contour curvatures as smooth as possible to avoid abrupt compression and expansion of flow past it. The design of the pitot-static tube for fuselage dorsal side is complicated. The value of the pressure coefficient required to be neutralised on the fuselage dorsal side is high and negative (-0.1819) as compared to the value of pressure coefficient at the nose boom location (+0.1217). This is because the pitot-static tube and the wing are centerly mounted on the fuselage. The relative location of the pitot-static tube and the wing, on fuselage shall be decided to avoid the complicated design of the pitot head. The design of the nose contour follows a simple and smooth curvature for nose boom location. As in the case of the nose boom, the static pressure sensing port is made diagnally opposite in the lateral direction for the dorsally mounted pitot-static tube. This makes the static port insensitive to angle of attack. The nose contour of the dorsally mounted pitot-static tube can be computed for a given pressure coefficient due to wing-body combination by using the programme given in appendix B.

Though simple in design, the lengthy pitot-static tube is not preferable. The design of a medium size pitot-static tube is made to provide the negative pressure coefficient to neutralise the pressure coefficient existing due to the wing-body combination. One disadvantage of this location is apparent that the nearer we approach the wing tip, the greater is the variation of pressure coefficient with Mach number and angle of attack. The effect of angle of attack can be readly eliminated by the proper location of the static port on the nose contour fig.(59-B). The variation of pressure coefficient with Mach number for this location can be neglected over the increased length of pitot tube for any other better location ahead of the wing tip. The pitot tube designed for wing tip location is free from position error for the Mach number ranging between (0.3→0.8). Giving the input data, that is the distance of the static port location from the wing tip and the value of the perturbed pressure coefficient at this location, the design of the tube can be computed by using the programme given in appendix B.

CHAPTER - 6

6.1 Results and Discussion:

The application of the above method of analysis has been done for the steady subsonic flow. The aerodynamic compensation extends over a large range of Mach number. Static pressure sensing ports are made insensitive to angle of attack. The error in static pressure sensing due to a change in angle of attack is least at the nose boom location.[21] The static pressure sensing port lies parallel to the plane of symmetry and is independent of the flow direction at any angle of attack. At very high angles of attack the flow seperates on the bottom and the topside of pitot-static tube. The location of the static port is thus free from seperation of flow at any angle of attack. The best location for an aerodynamically compensated pitot-static tube is the nose boom since the pressure distribution ahead of the nose boom does not vary much with Mach number and angle of attack. For short nosed airplanes to minimise the effect of angle of attack, the length of the pitot-static tube should be increased since as we go forward of the body the variation in pressure coefficient with Mach number and angle of attack decreases.

The variation of pressure coefficient with Mach number is more at the fuselage dorsal side as compared to it's variation at the nose boom location. Where the pressure

coefficient has a high negative value, a large compression of air is required to provide the positive pressure coefficient at the static port location. For this reason the shape of the nose contour consists of double curvature. To avoid abrupt compression and expansion the nose contour is made smooth. The increased length of the nose contour does not effect the overall length of the pitot-static tube. The effect of angle of attack is minimised by lateral location of static ports.

In the wing tip location of pitot-static tube the pressure coefficient varies significantly with Mach number and angle of attack. The pressure coefficient ahead of the wing changes steeply with distance. At one location pressure coefficient becomes zero. The design of the pitot-static tube involves no aerodynamic compensation for this location. The point of zero pressure coefficient lies at a sufficiently great distance from the wing tip. For this reason the length of pitot-tube has to be large. This has disadvantages from standpoint of maintenance and service, increased weight and cost. In addition to a long pitot-static tube an aerodynamically compensated pitot static tube is designed for a moderate length. In the vicinity of the wing tip, the pressure coefficient varies significantly with Mach number and angle of attack. This variation decreases with increasing distance from the wing tip. The pitot tube for the wing-tip location is, therefore, longer than the pitot-static tubes used at the nose boom or fuselage dorsal location.

Aerodynamic compensation and insensitivity to angle of attack are the important features of designed pitot-static tubes. The mathematical method can be applied to any airplane wing-body configuration. Using the computer programming for wing-body combination, the value of the pressure coefficient can be predicted at any point. With the pressure coefficient and the desired length of the nose contour of the pitot-static tube as the input data, the computer programme made for Part B gives the shapt of the aerodynamic compensator.

*****

REFERENCES

1. Jack N.Nelsen; J.Richard; and Frank Centolanzi., Aerodynamics of bodies, wings and wing-body combinations at high angle of attack and supersonic speed.' 'NACA-RM A55L13C, 1953.

2. H. Schlichting.,'Report on the special field 'Interference' to the Wind Tunnel Committee in Feb.,1965'. NACA T:M. 1347, Feb.,1965.

3. Von Karman.,'The similarity theory of transonic flow', J.Math.Phys.26,pp 182-190,1947

4. F.A. Woodward.,'A unified approach to the analysis and design of wing-body combinations at subsonic and supersonic speed', The Boeing Company, Renton, Washington, AIAA Paper No.68-55, Jan.,1968

5. Dietrich Kuchemann and Johanna Weber.,''Aerodynamics of Propulsion', McGraw-Hill Publishing Company Ltd.,New York, London, 1953.

6. Spreiter, John. R., 'Aerodynamic properties of slender wing-body combinations at subsonic, transonic and supersonic speeds.,NACA TN 1662, July 1948

7. H.R. Lawrence and A.H. Flax., 'Wing-body interference at subsonic and supersonic speeds ,Survey and new developments., J.Aero.Sci.,Vol.21,No.5,May 1954

8. Moskowitz,B.,'Approximate theory for calculation of lift of bodies,afterbodies and combination of bodies., NACA TN 2669, April 1952

9. Nielsen, J:N: and Pitts W.C., 'Wing-body interference at supersonic speeds with an application to combinations with rectangular wings'., NACA TN 2677, April 1952.

10. Laitone, E.V., '1st order wing-body interference effects'., J.Aero. Sci. Reader's Forum, Vol.16, No.8, pp-510, Aug.,1949

11. Woodward, F.A., Tinoco, E.N: Larsen, J.W., 'Analysis and design of supersonic wing-body combinations, including flow properties in the near field - Part 1 theory and applications'., NASA CR 73106, Aug 1967

References.....

12. Donovan, A.F. and Lawerence, H.R., 'Aerodynamic components of aircraft at high speeds'., Princeton Univ. Press, 1957

13. Jorgensen and Perkinsen., 'Wing-body interference'., NACA RM A55E31, 1953

14. Krenkel, A.R., 'Wing-body interference phenomenon'., Rep.No.3524, Mc.Donnell Aircraft Corp.March,1954

15. Nielsen, Jack N, Kaattari; George; and Anastasic, Robert. F., 'A method for calculating the lift and center of pressure of wing-body tail combination at subsonic,transonic and supersonic speeds'., NACA RM A53508, 1953

16. Moskowitz, B.,'Approximate theory for calculation of lift of bodies, afterbodies and combinations of bodies'., NACA TN 2669, 1952

17. Ferrari, C., 'Interference between wing and body at supersonic speeds - theory and numerical application., pp 317-336, June 1948

18. Ritchie, Virgils., 'Several methods for aerodynamic reduction of static pressure errors for aircraft at subsonic, near sonic and low supersonic speeds'., NASA TR 18, June 1958

19. Townsend, J.E.G., 'The development of a static tube which is insensitive to incidence at supersonic speeds'., Aeronautical Research Council (Great Britain) ARC 21, 644 FM 2908

20. Rosemount Engineering Company, Minnesota., 'Pitot and pitot-static tubes'., Bulletin 2661, Rosemount Engg. Company, October 1966

21. Rosemount Engineering Company, Minnesota., Model 655, Aerodynamically compensated pitot static tube, Models 850 and 852, Conventional pitot static tube, Bulletin 116010 Rosemount Engg. Co.,

22. Gracey, Wm., Coletti, D.E. and Russel, W.R., 'Wind tunnel investigation of a number of total pressure tubes at high angles of attack, supersonic speeds'., NACA TR 2661, January 1951

***

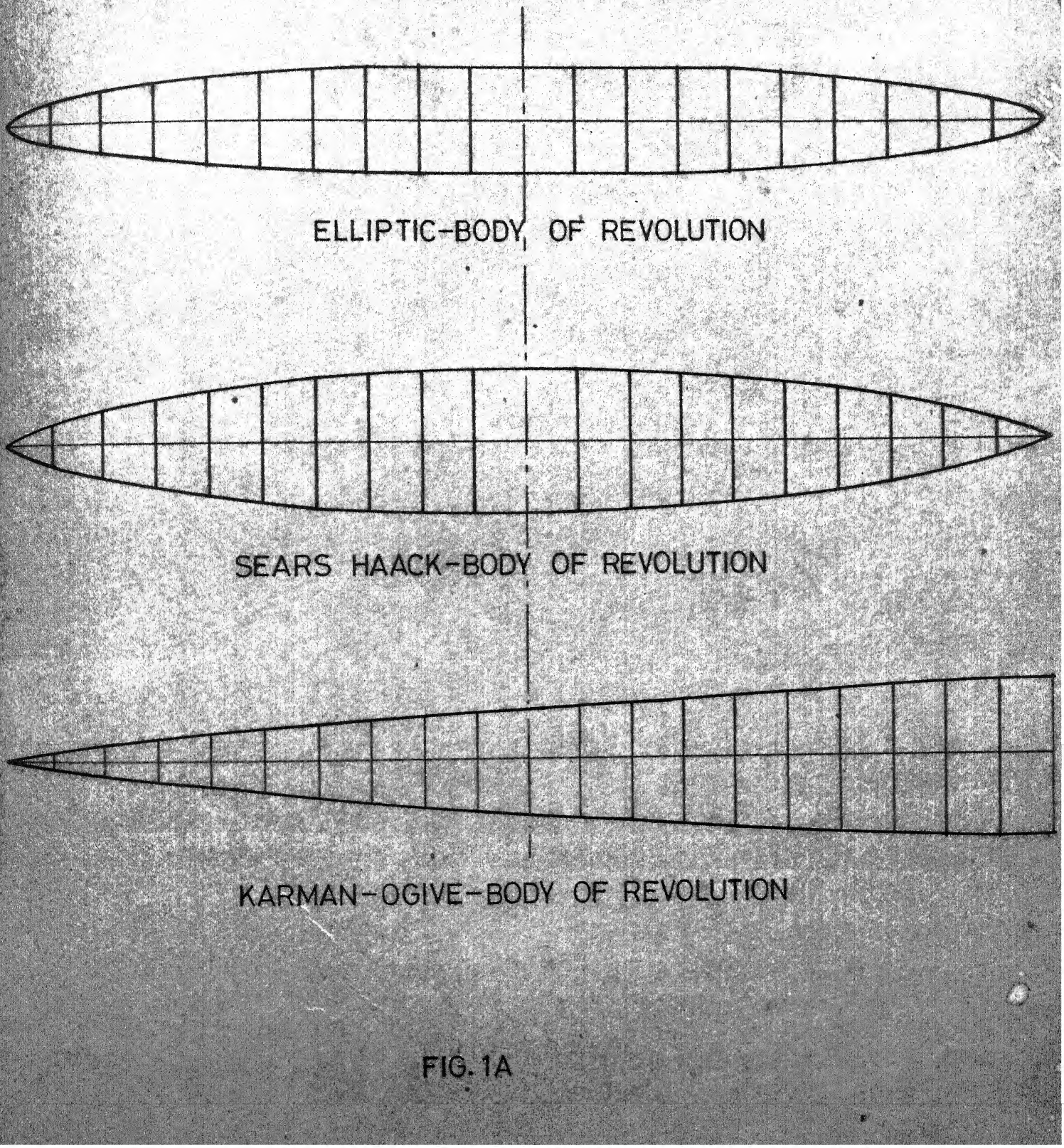
ELLIPTIC-BODY OF REVOLUTION
SEARS HAACK-BODY OF REVOLUTION
KARMAN-OGIVE-BODY OF REVOLUTION

FIG. 1A

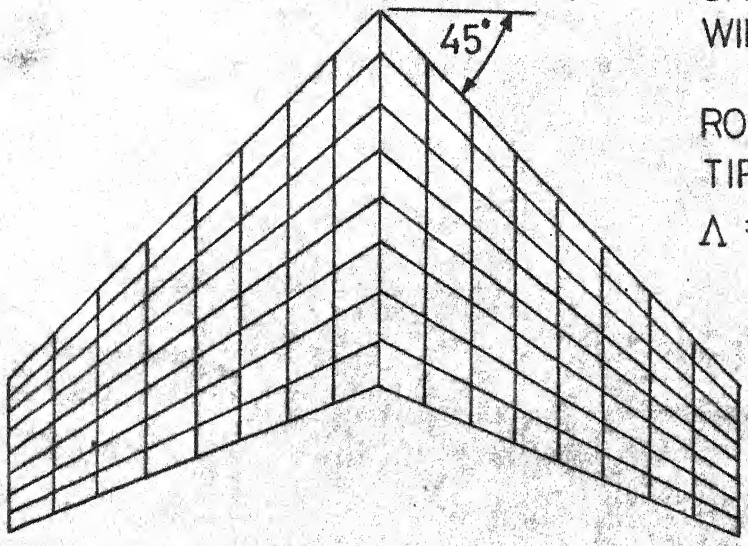

A = 2.87
SPAN = 10 UNITS
WING AREA = 34.9 UNITS SQ.
ROOT CHORD = 5 UNITS
TIP CHORD = 2 UNITS
$\Lambda = \pi/4$

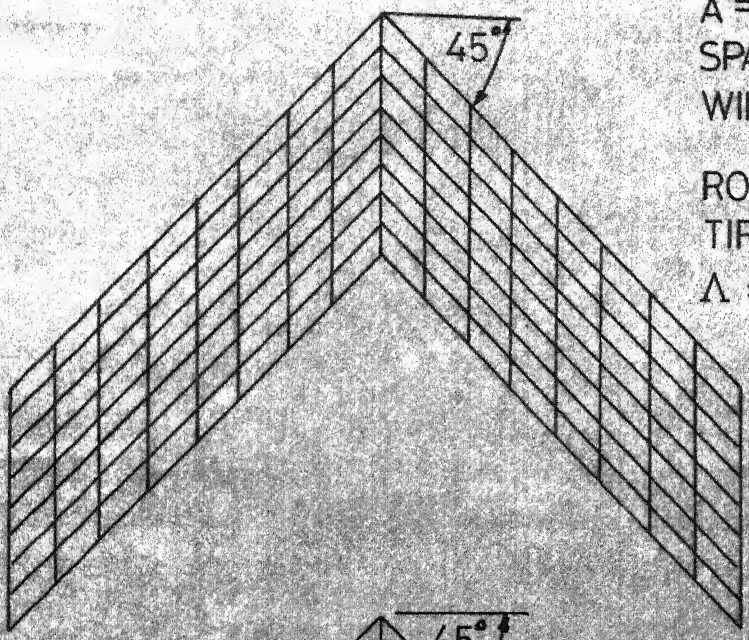

A = 2.87
SPAN = 10 UNITS
WING AREA = 34.9 UNITS SQ.
ROOT CHORD = 3.2 UNITS
TIP CHORD = 3.2 UNITS
$\Lambda = \pi/4$

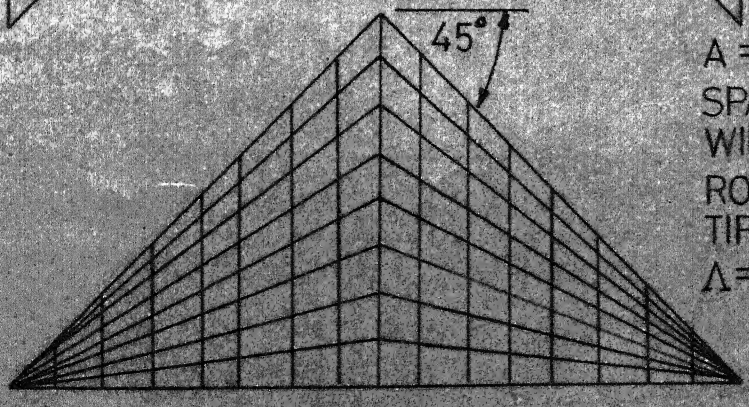

A = 4.00
SPAN = 10 UNITS
WING AREA = 25 UNITS SQ.
ROOT CHORD = 5 UNITS
TIP CHORD = 0
$\Lambda = \pi/4$

FIG._1b

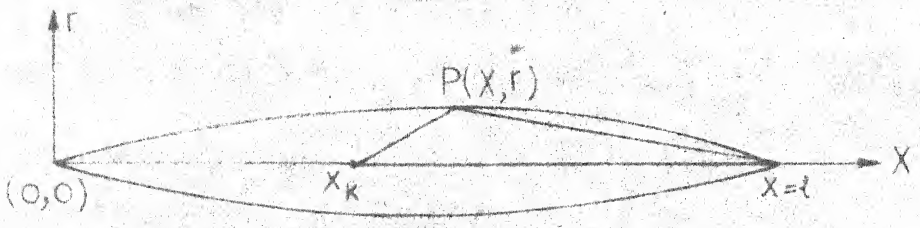

FIG. 1C

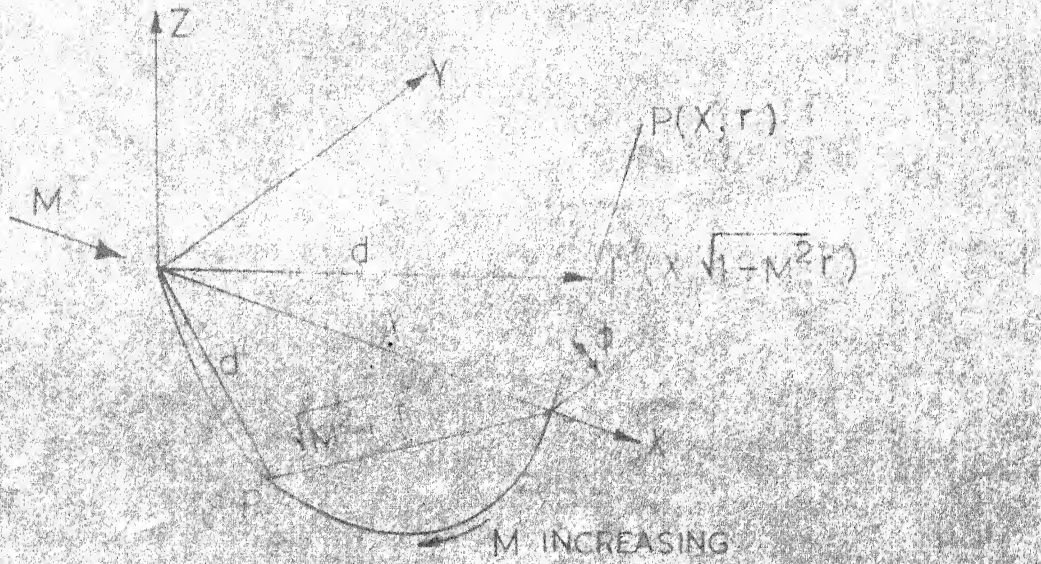

PRANDTL-GLAUERT COORDINATE SYSTEM

FIG. 1d

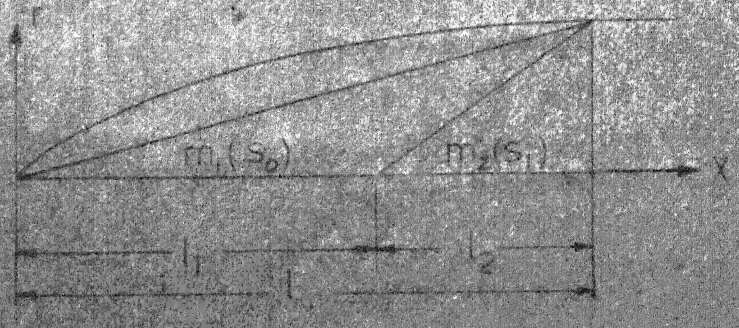

FIG. 1e

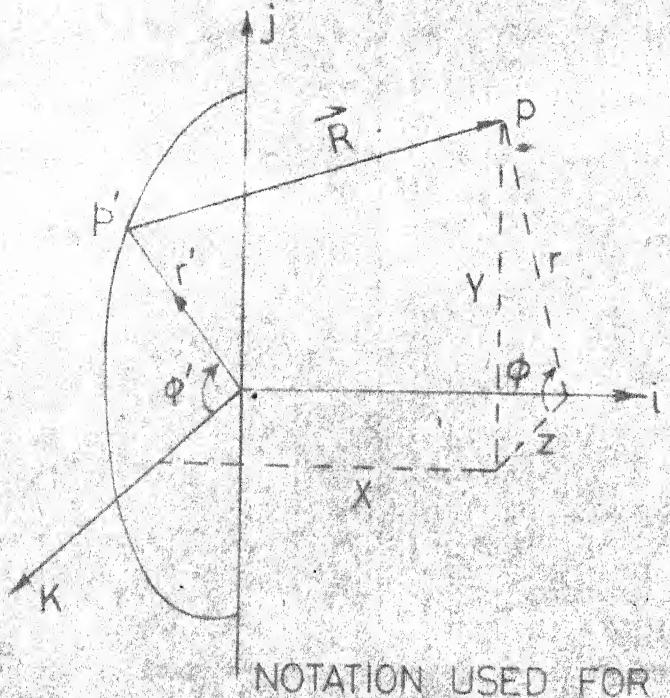

NOTATION USED FOR SOURCE - SINK DISTRIBUTION

FIG. 1.f

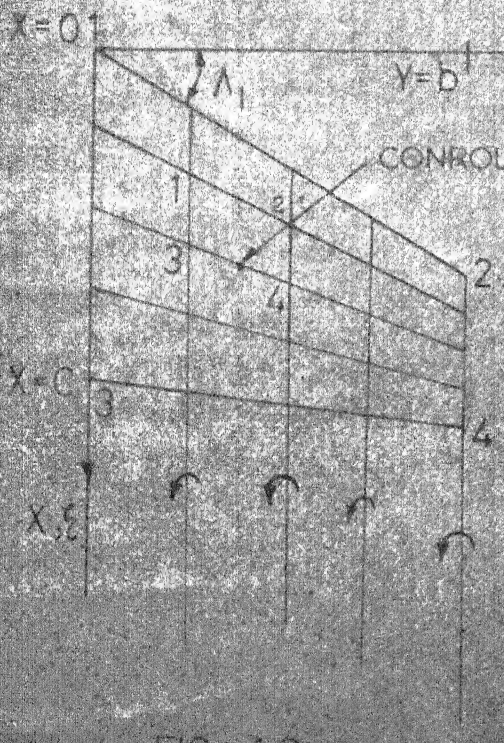

FIG. 1.G

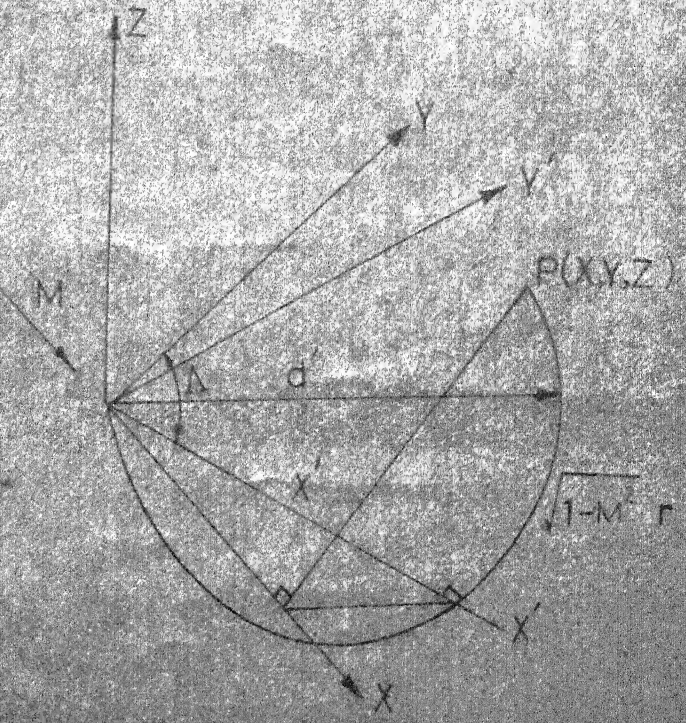

LORENTZ TRANSFORMATION OF LINE SOURCE

FIG. 1.H

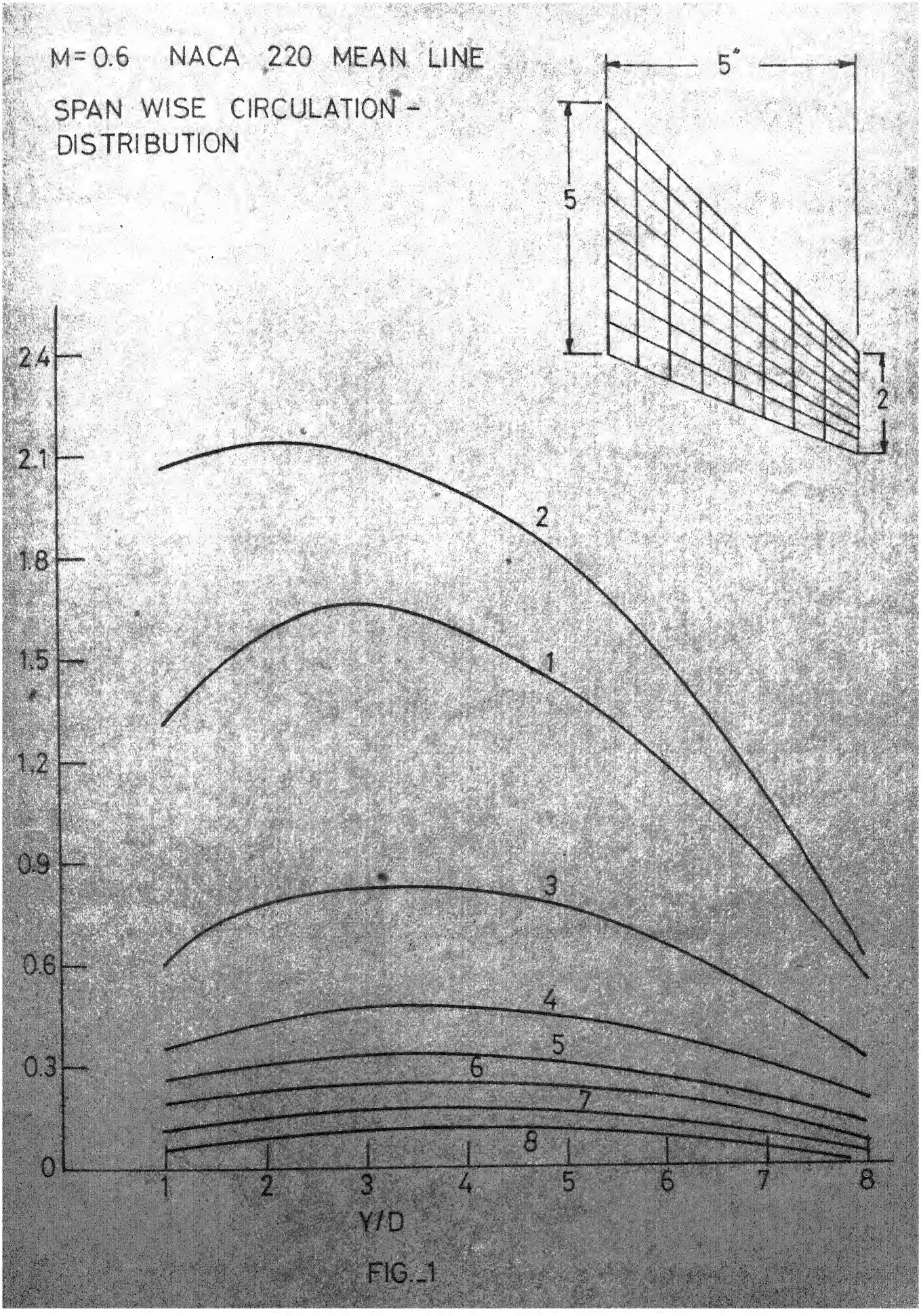
M= 0.6 NACA 220 MEAN LINE
SPAN WISE CIRCULATION -
DISTRIBUTION
5"
5
2
2.4
2.1
1.8
1.5
1.2
0.9
0.6
0.3
0
1
2
3
4
5
6
7
8
Y/D

FIG._1

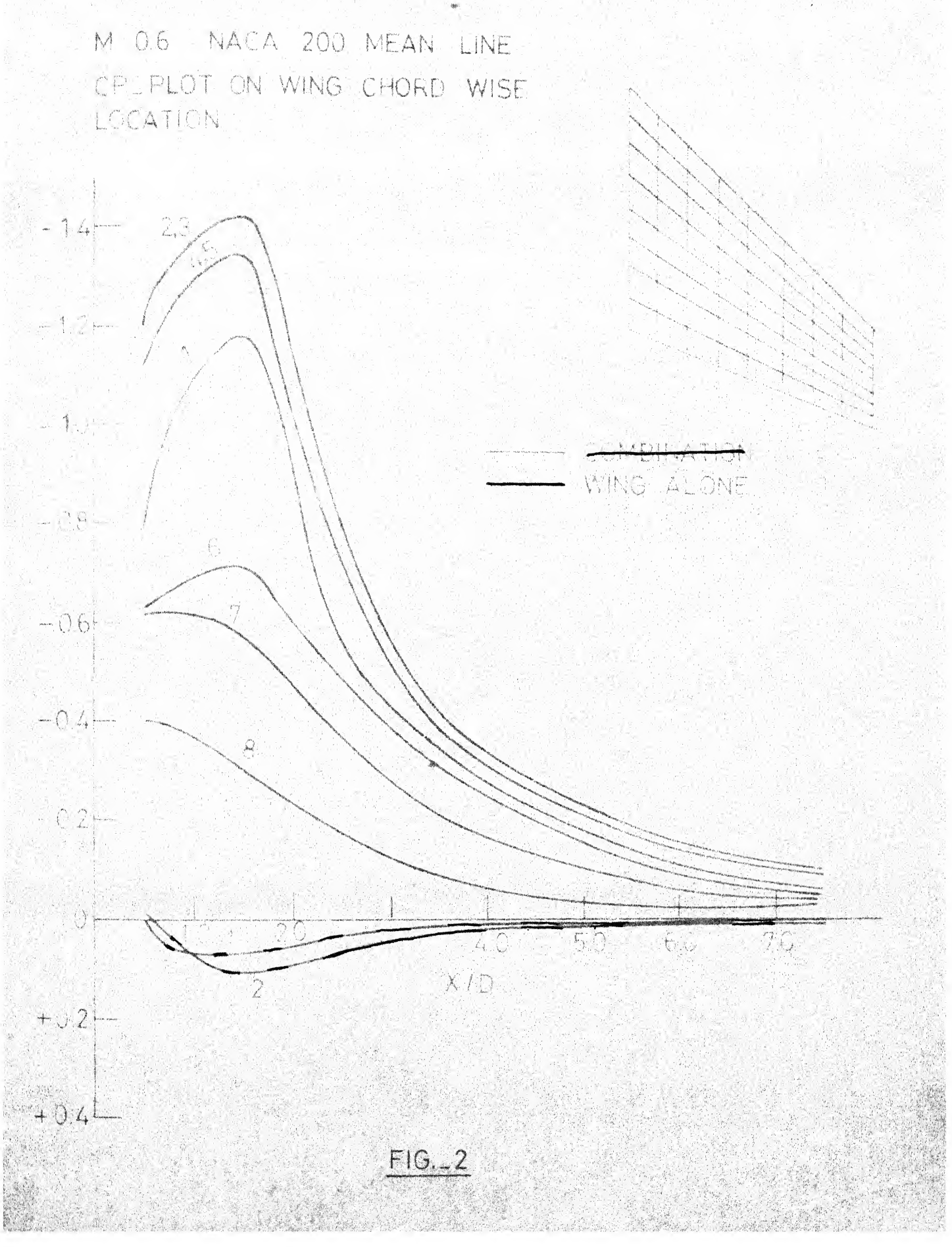
M 0.6 NACA 200 MEAN LINE
CP PLOT ON WING CHORD WISE LOCATION
WING ALONE
-1.4
-1.2
-1.0
-0.8
-0.6
-0.4
-0.2
0
+0.2
+0.4
2,3
6
7
8
1
2
1.0
2.0
4.0
5.0
6.0
7.0
X/D

FIG.-2

M= 0.6 NACA 220 MEAN LINE

SPAN WISE CIRCULATION DISTRIBUTION

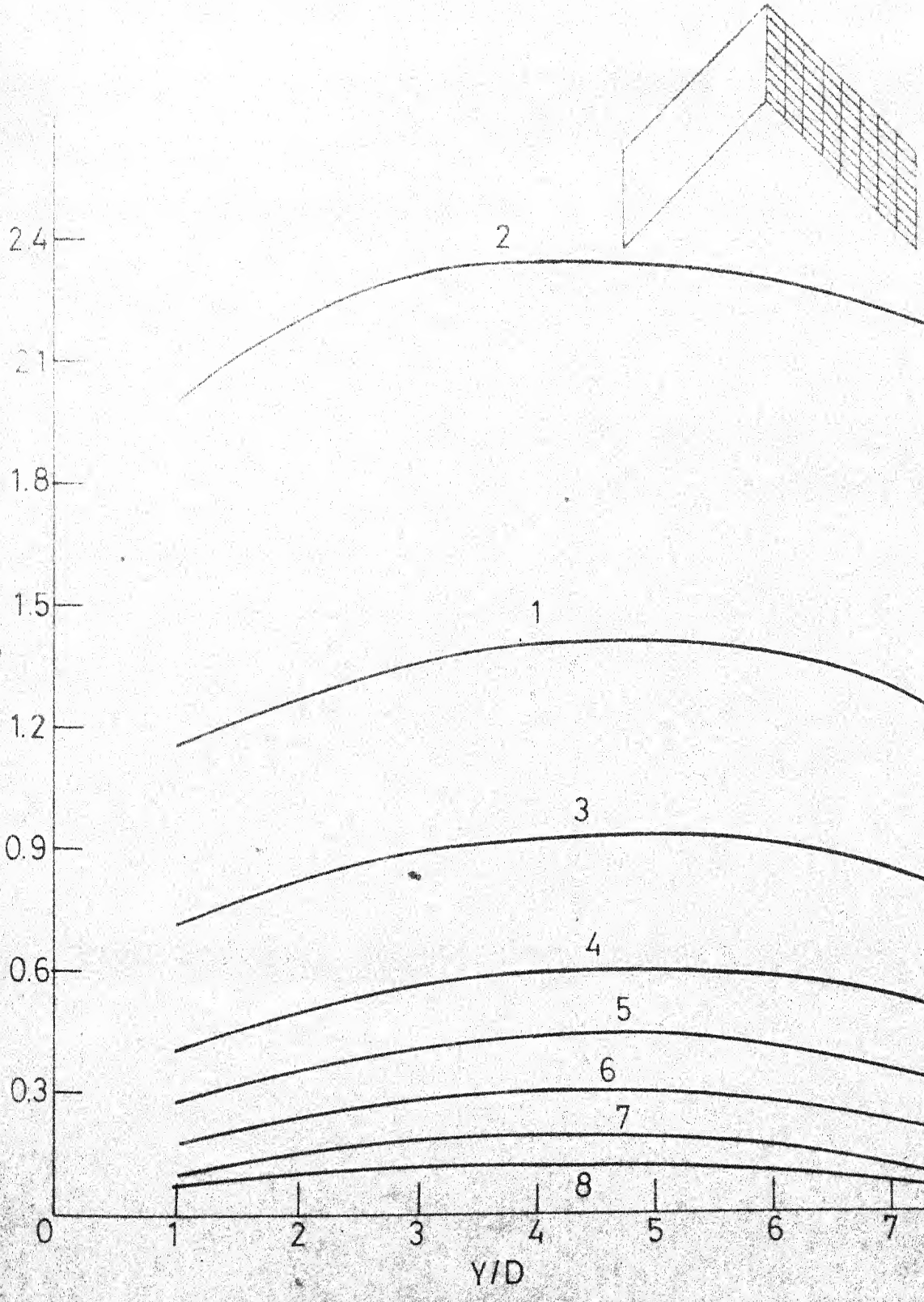

FIG._3

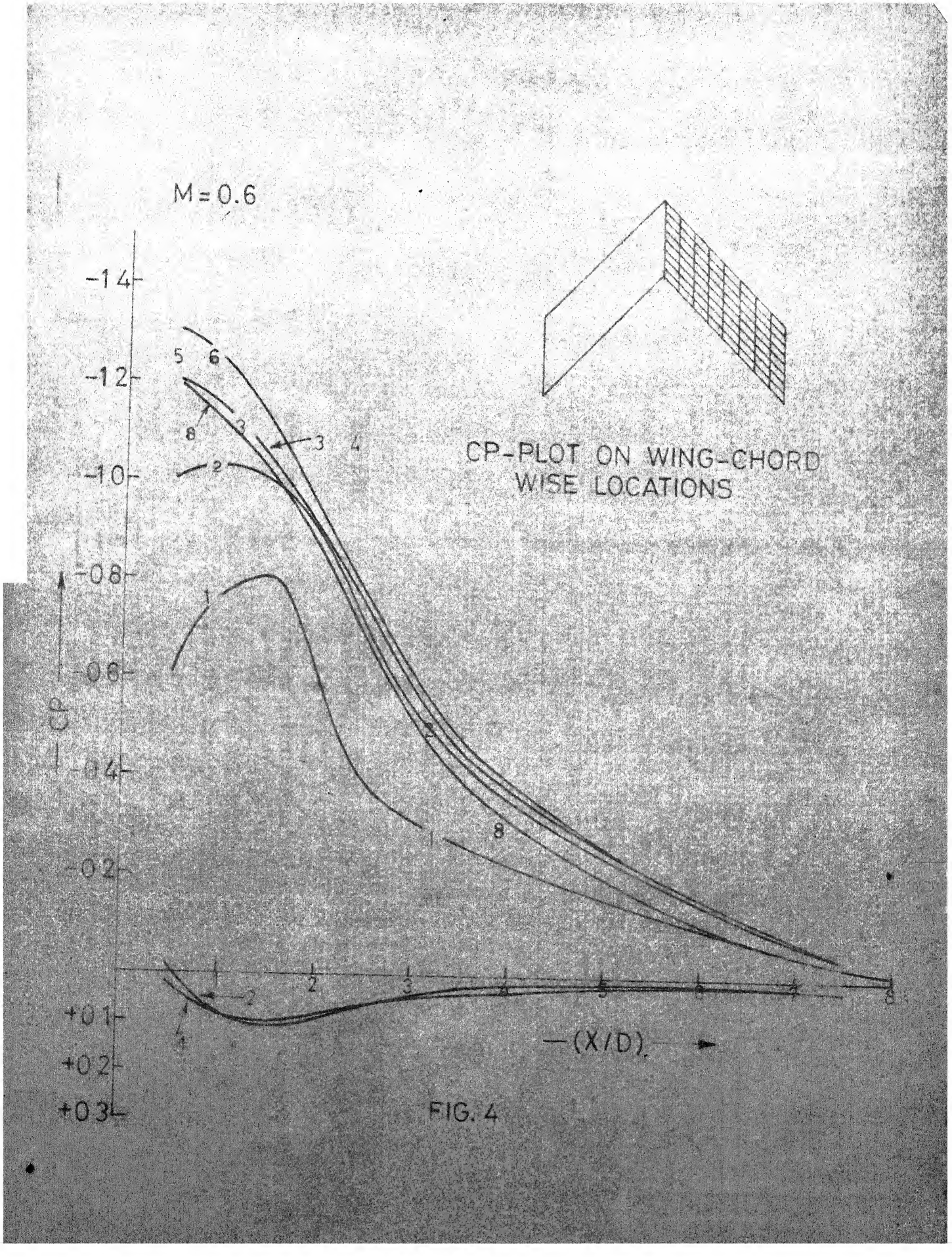
M = 0.6
-14
-12
-10
-08
-06
-04
-02
+01
+02
+03
Cp
—(X/D)
CP-PLOT ON WING-CHORD WISE LOCATIONS

FIG. 4

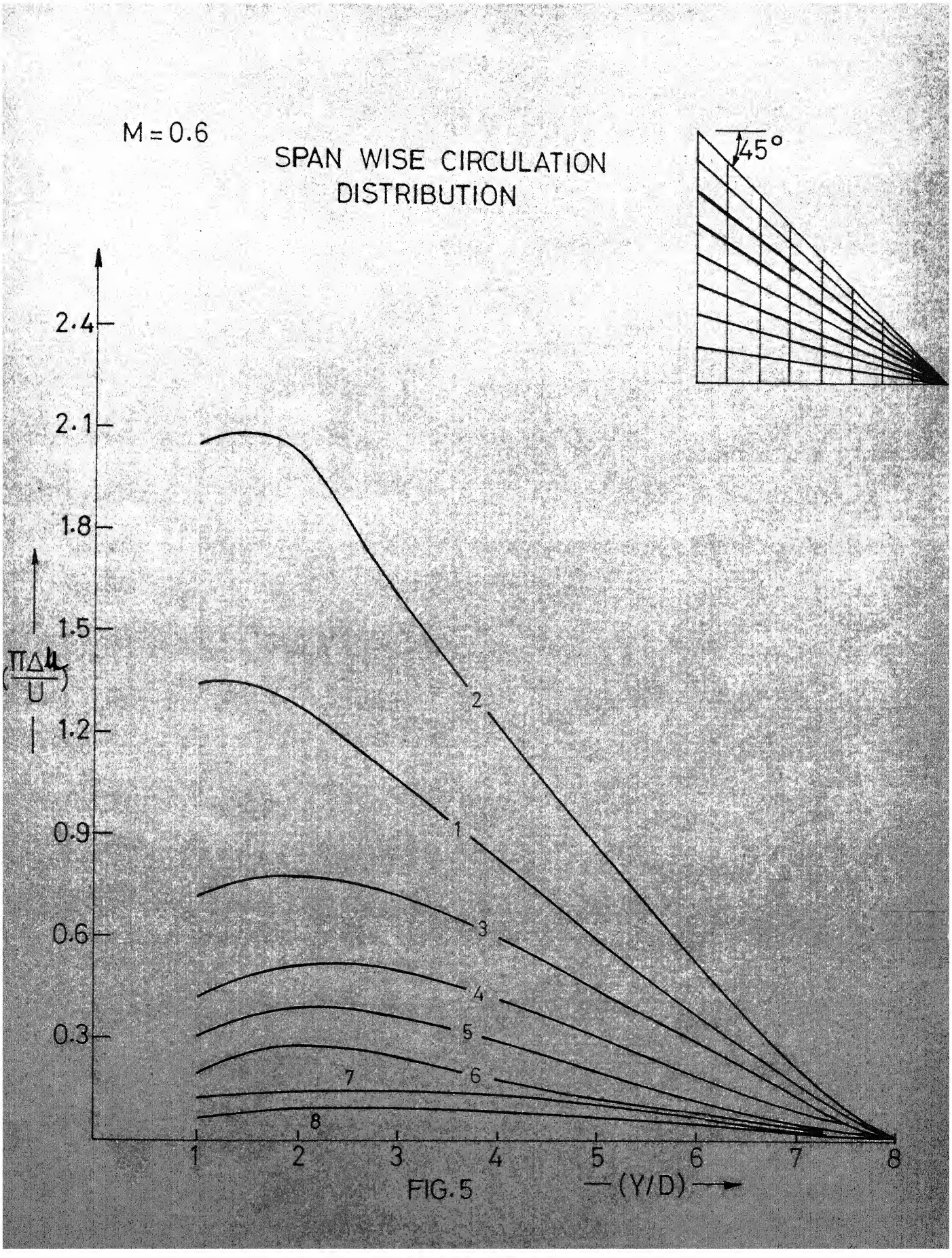
M = 0.6
SPAN WISE CIRCULATION
DISTRIBUTION
45°
2.4
2.1
1.8
1.5
1.2
0.9
0.6
0.3
(πΔ4/U)
1
2
3
4
5
6
7
8
— (Y/D) →

FIG. 5

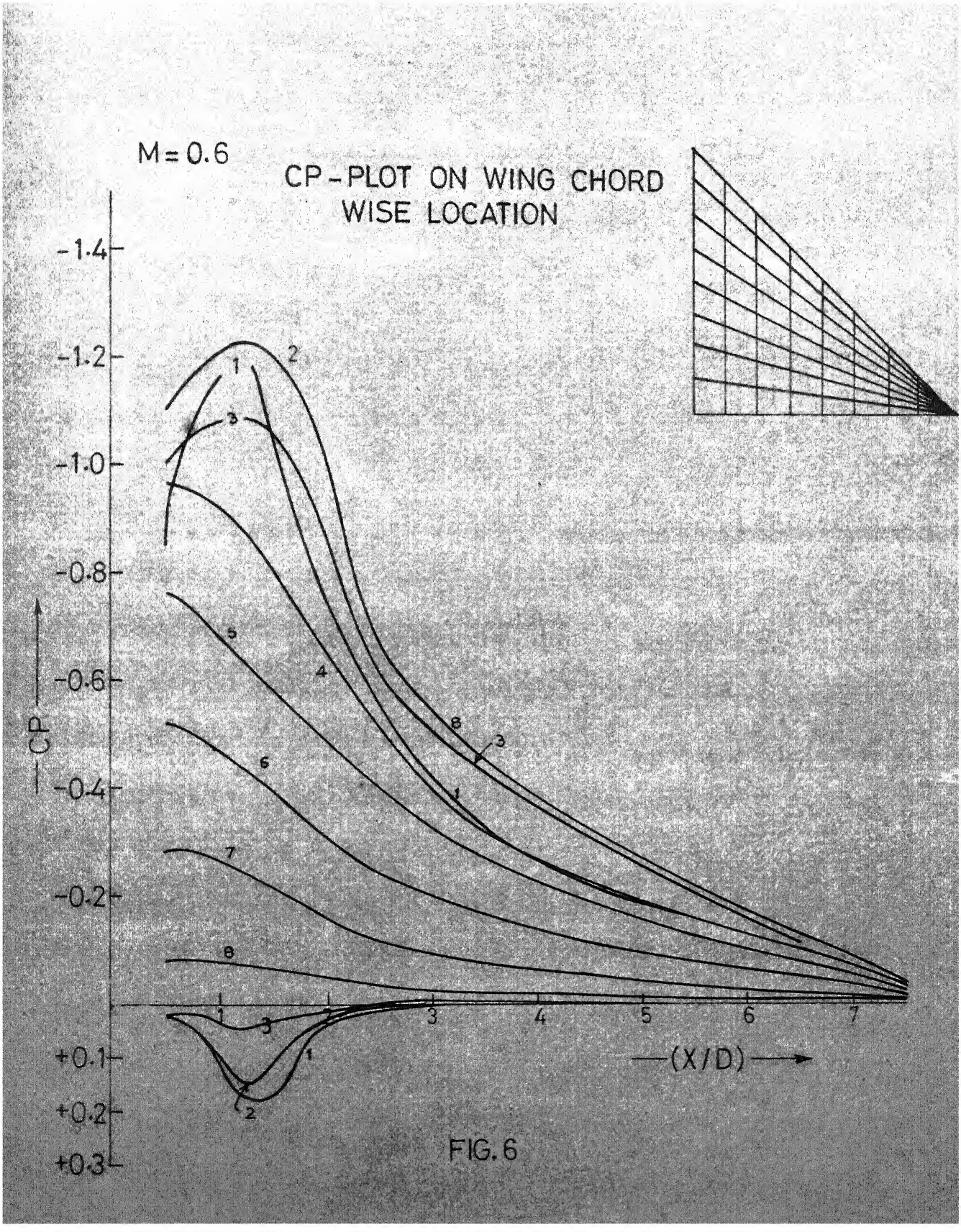
M = 0.6
CP - PLOT ON WING CHORD WISE LOCATION
-1.4
-1.2
-1.0
-0.8
-0.6
-0.4
-0.2
+0.1
+0.2
+0.3
CP
(X/D)
1
2
3
4
5
6
7
8

FIG. 6

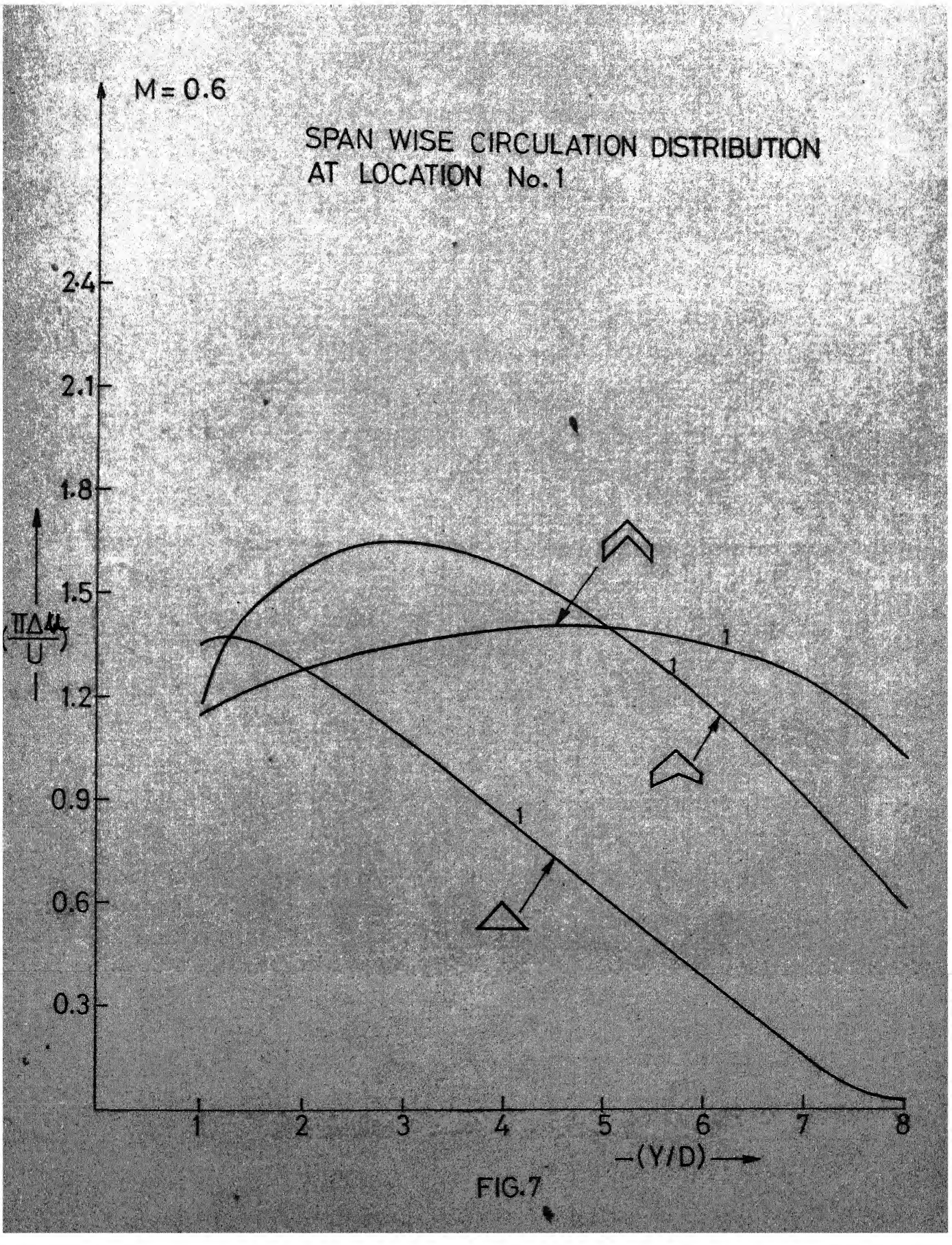
M = 0.6
SPAN WISE CIRCULATION DISTRIBUTION
AT LOCATION No. 1
2·4
2.1
1.8
1.5
1.2
0.9
0.6
0.3
1
2
3
4
5
6
7
8
—(Y/D)—
1
1
1

FIG.7

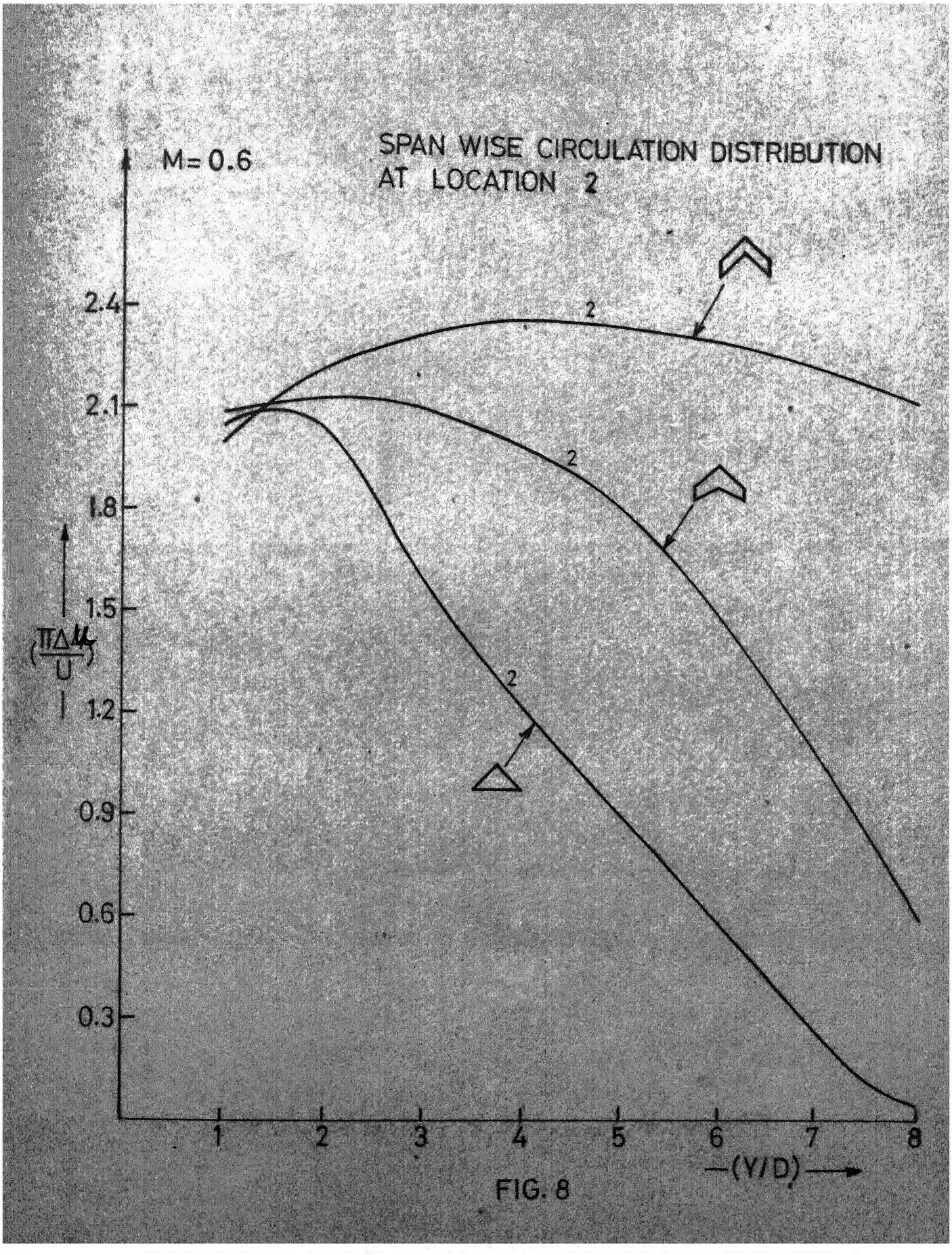
M= 0.6
SPAN WISE CIRCULATION DISTRIBUTION
AT LOCATION 2
2.4
2.1
1.8
1.5
1.2
0.9
0.6
0.3
$(\frac{\pi\Delta u}{U})$
2
2
2
1
2
3
4
5
6
7
8
—(Y/D)—

FIG. 8

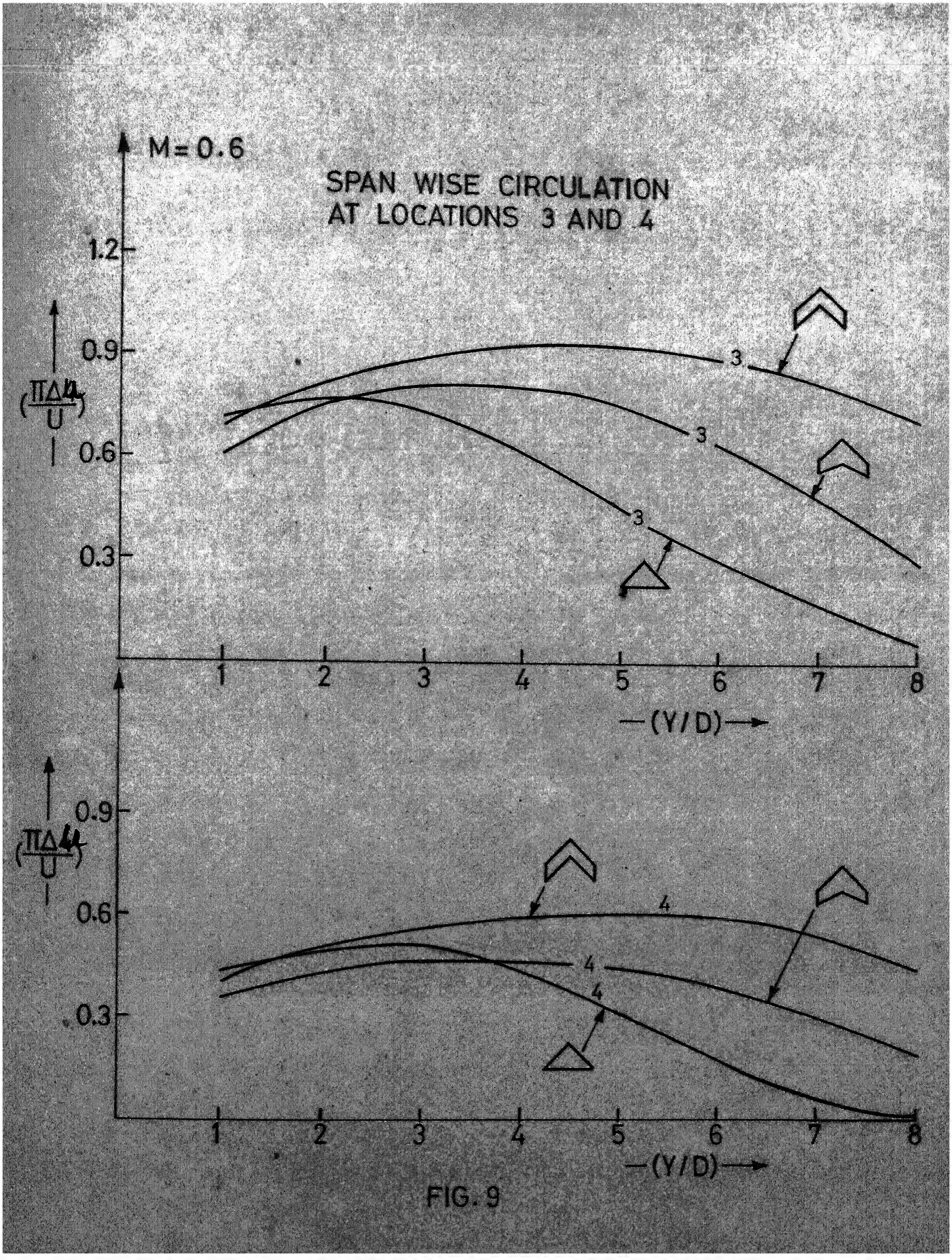
M=0.6
SPAN WISE CIRCULATION
AT LOCATIONS 3 AND 4
1.2
0.9
0.6
0.3
(ΠΔu/U)
3
3
3
1
2
3
4
5
6
7
8
—(Y/D)→
0.9
0.6
0.3
(ΠΔu/U)
4
4
4
1
2
3
4
5
6
7
8
—(Y/D)→

FIG. 9

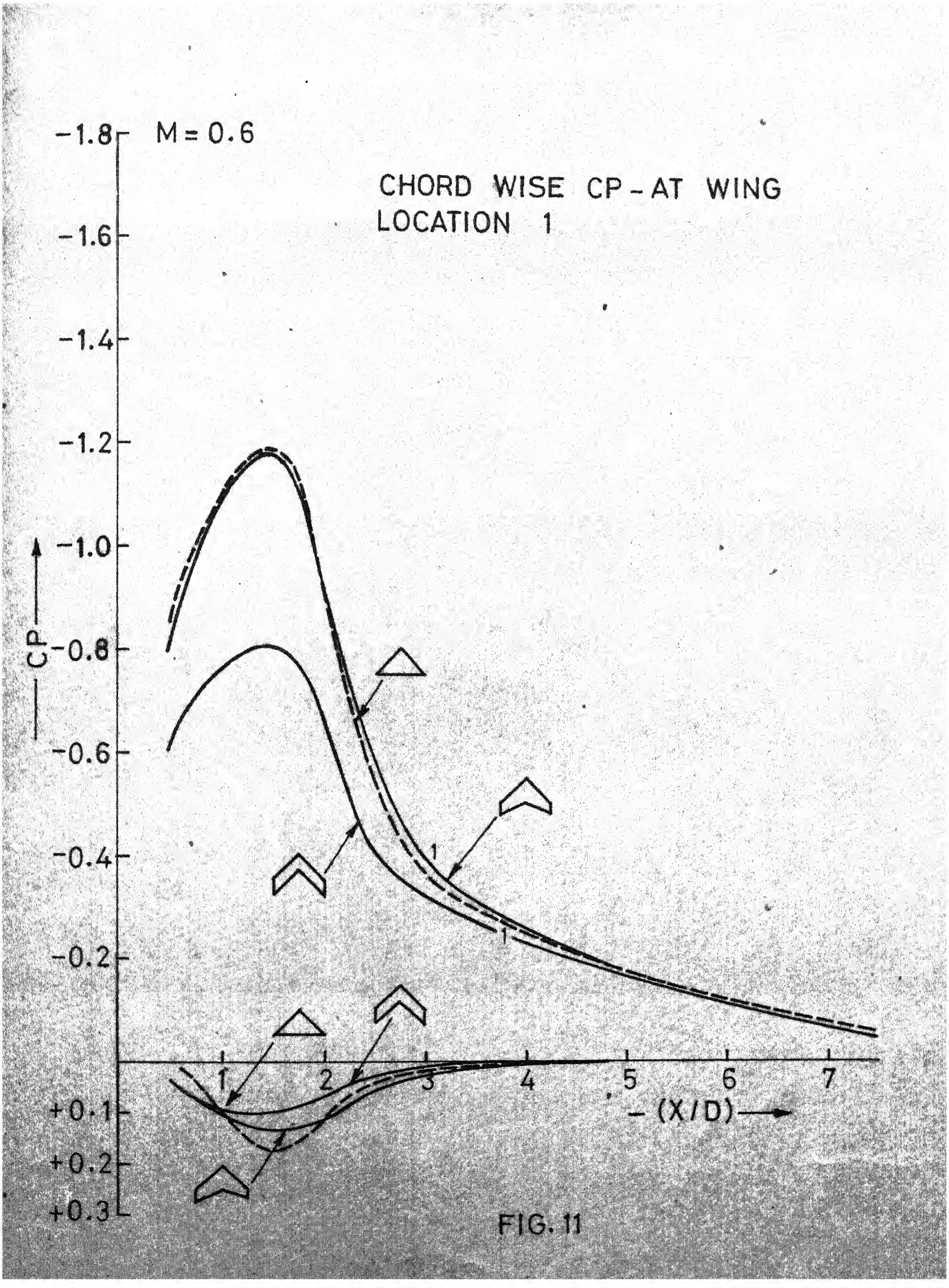
M = 0.6
CHORD WISE CP - AT WING
LOCATION 1
-1.8
-1.6
-1.4
-1.2
-1.0
-0.8
-0.6
-0.4
-0.2
+0.1
+0.2
+0.3
CP
1
2
3
4
5
6
7
- (X/D)

FIG. 11

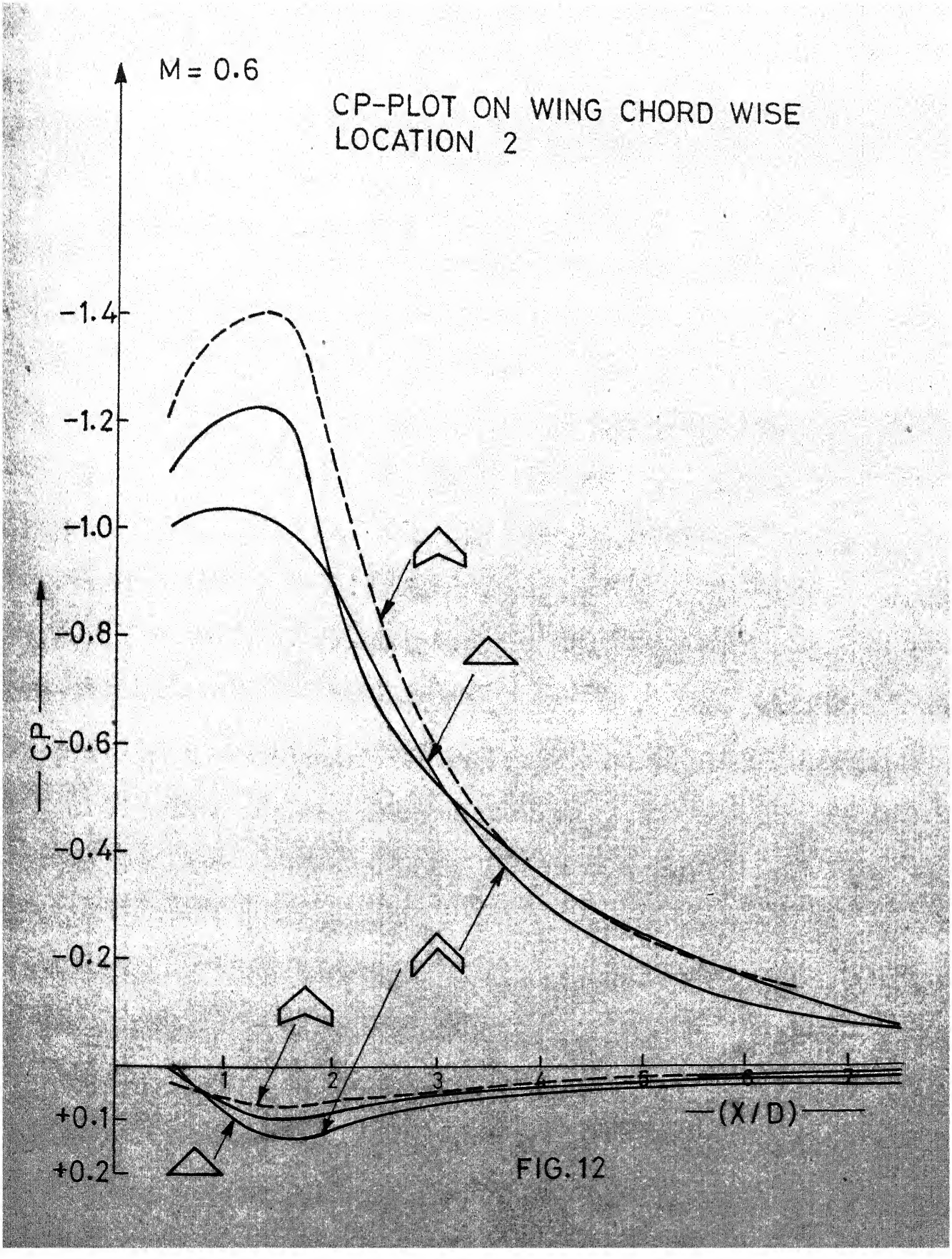
M = 0.6
CP-PLOT ON WING CHORD WISE
LOCATION 2
-1.4
-1.2
-1.0
-0.8
-0.6
-0.4
-0.2
+0.1
+0.2
CP
1
2
3
4
5
6
7
—(X/D)—

FIG.12

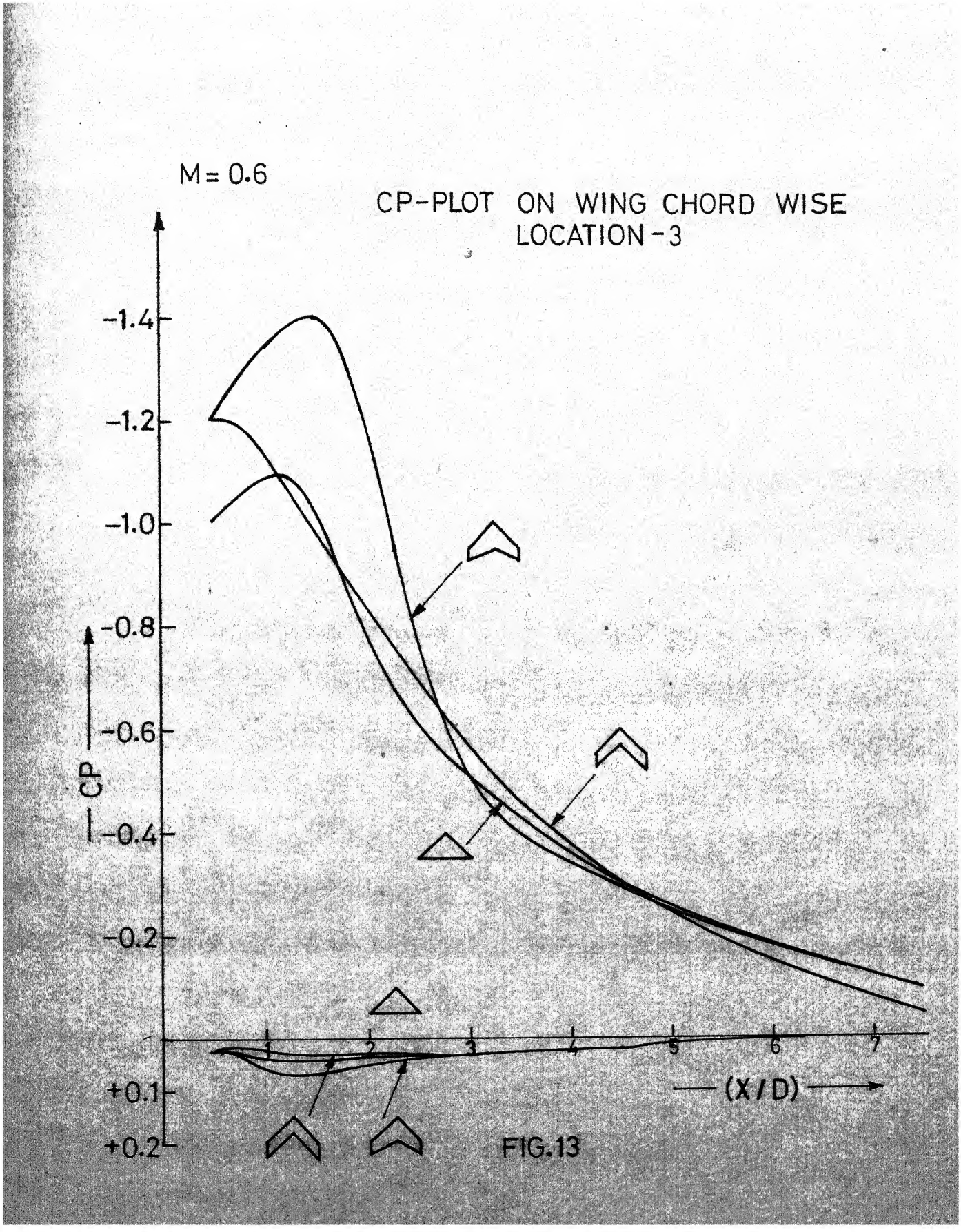
M = 0.6
CP-PLOT ON WING CHORD WISE
LOCATION - 3
-1.4
-1.2
-1.0
-0.8
-0.6
-0.4
-0.2
+0.1
+0.2
CP
1
2
3
4
5
6
7
(X / D)

FIG.13

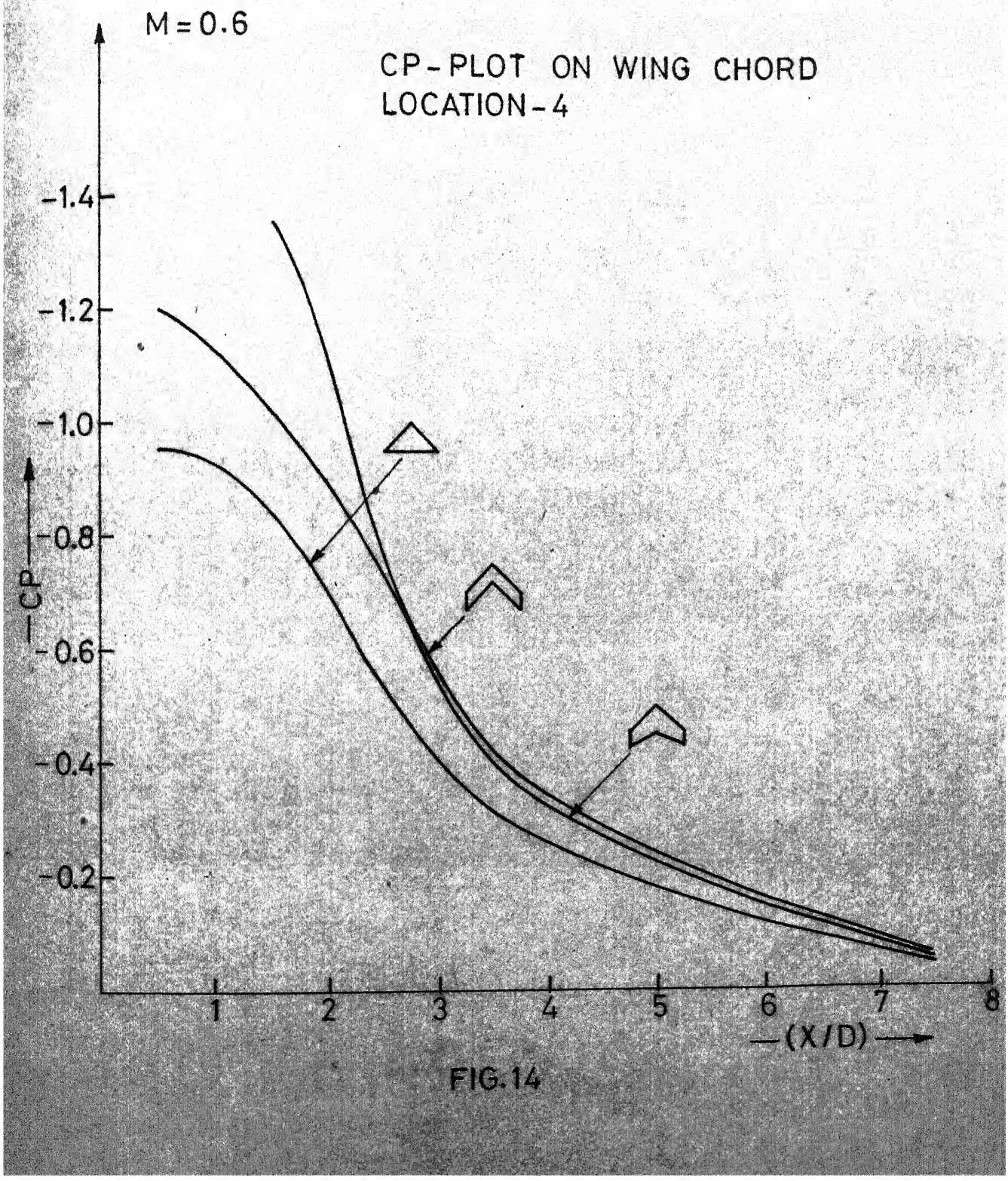
M = 0.6
CP - PLOT ON WING CHORD
LOCATION - 4
-1.4
-1.2
-1.0
-0.8
-0.6
-0.4
-0.2
-Cp
1
2
3
4
5
6
7
8
— (X/D) —

FIG.14

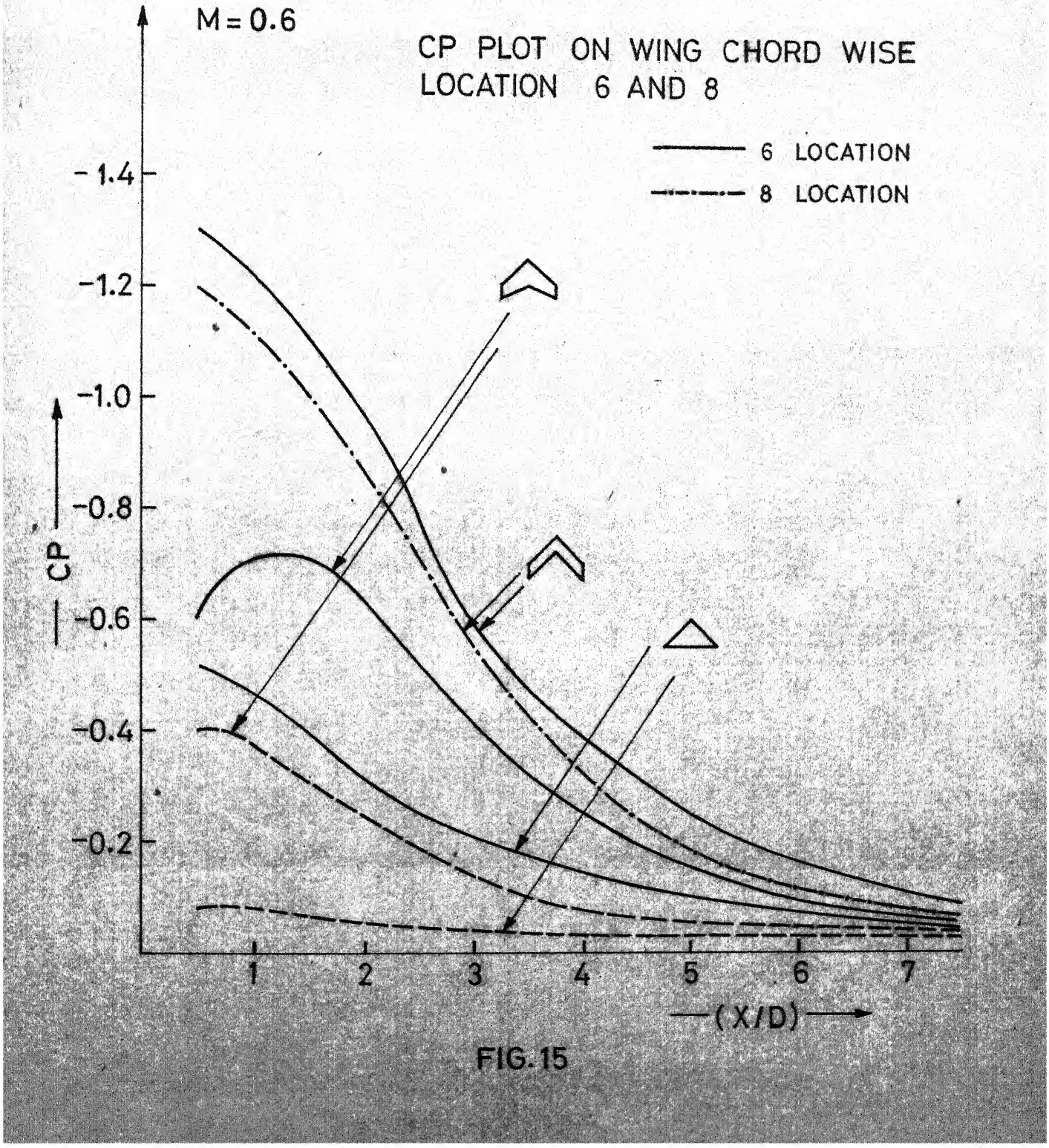
M = 0.6
CP PLOT ON WING CHORD WISE
LOCATION 6 AND 8
6 LOCATION
8 LOCATION
-1.4
-1.2
-1.0
-0.8
-0.6
-0.4
-0.2
CP
1
2
3
4
5
6
7
(X/D)

FIG. 15

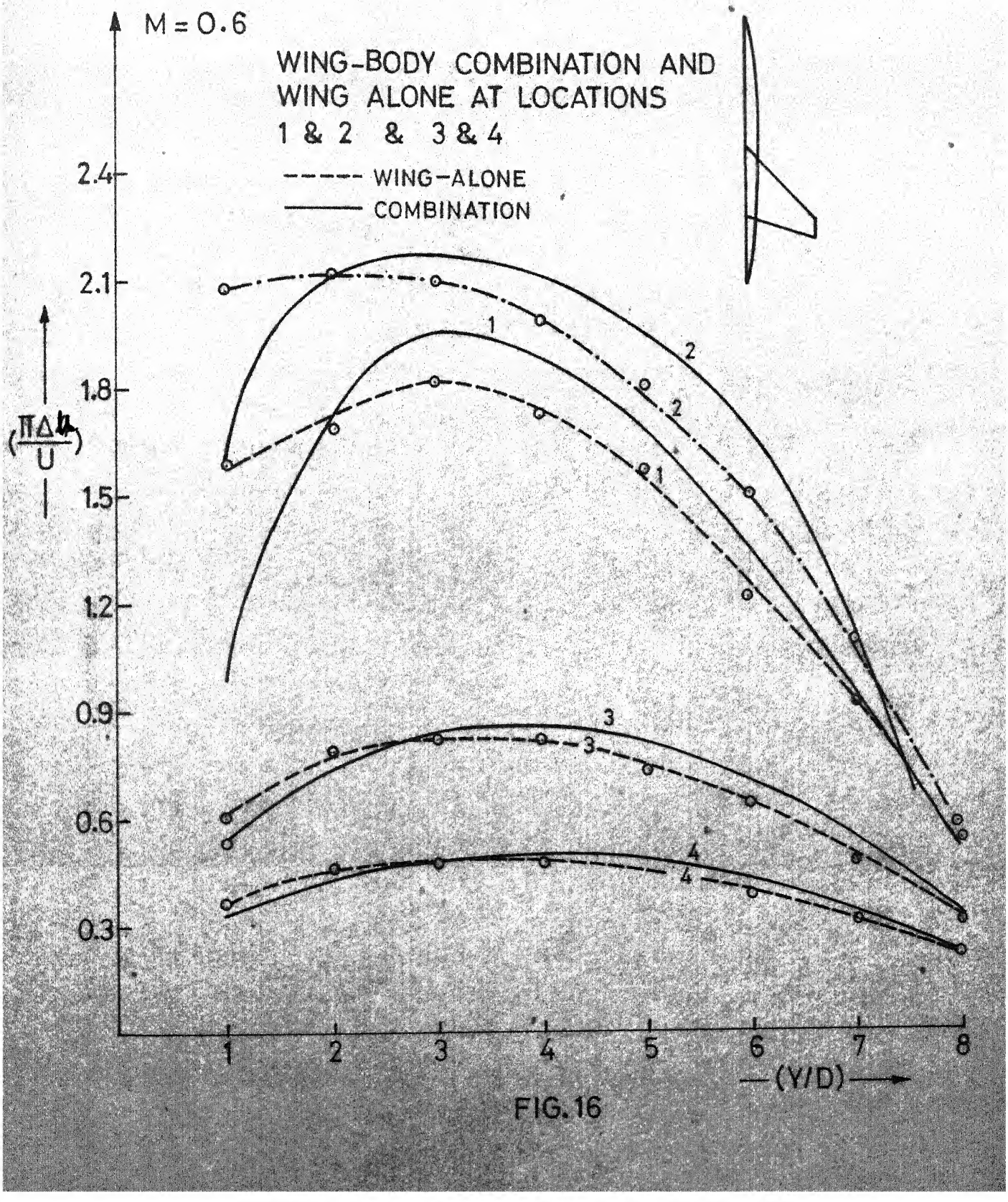
M = 0.6
WING-BODY COMBINATION AND
WING ALONE AT LOCATIONS
1 & 2 & 3 & 4
WING-ALONE
COMBINATION
2.4
2.1
1.8
1.5
1.2
0.9
0.6
0.3
(ΠΔh/U)
1
2
3
4
5
6
7
8
(Y/D)

FIG. 16

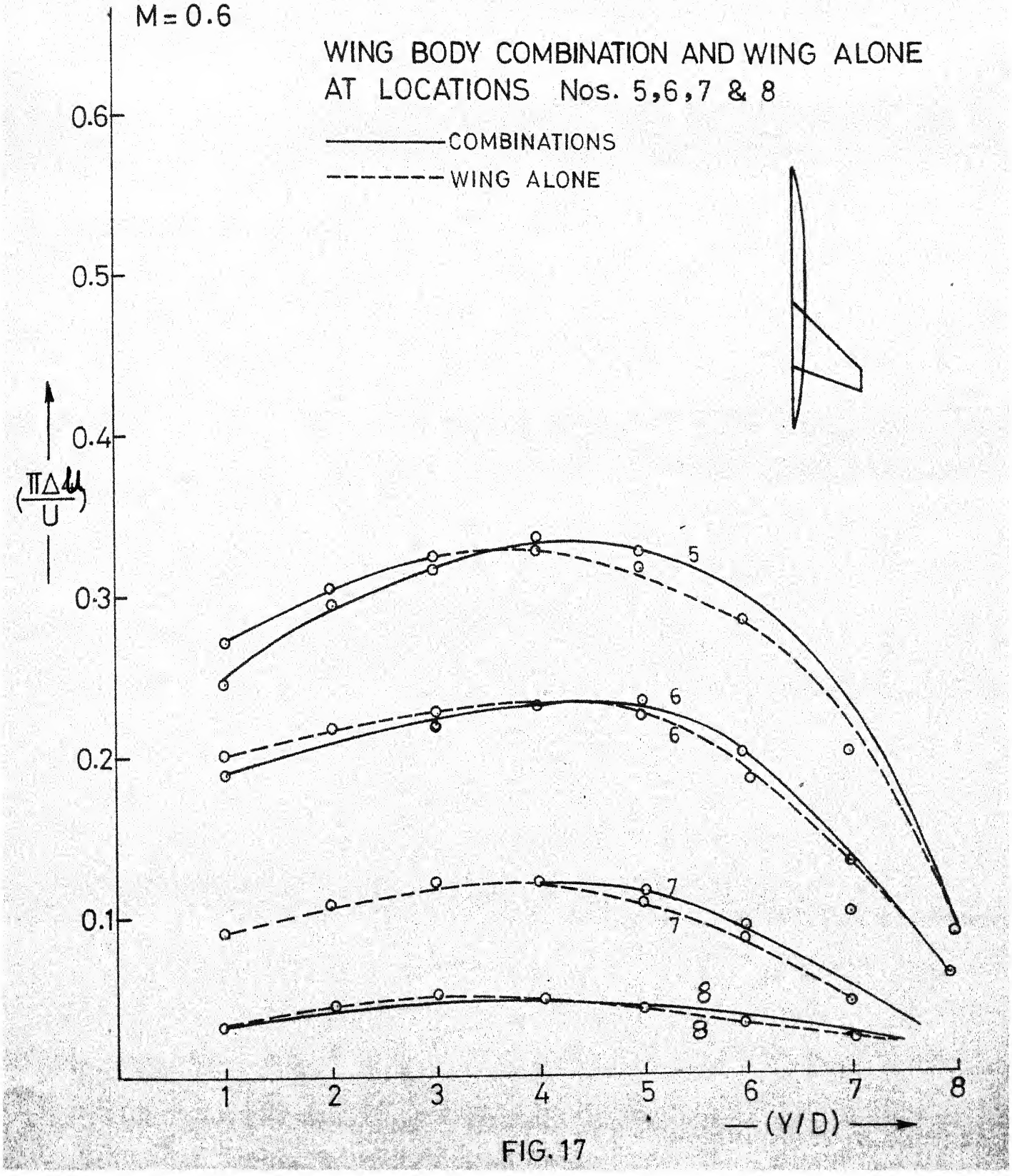
M = 0.6
WING BODY COMBINATION AND WING ALONE
AT LOCATIONS Nos. 5,6,7 & 8
COMBINATIONS
WING ALONE
0.6
0.5
0.4
0.3
0.2
0.1
(πΔu/U)
5
6
6
7
7
8
8
1
2
3
4
5
6
7
8
(Y/D)

FIG. 17

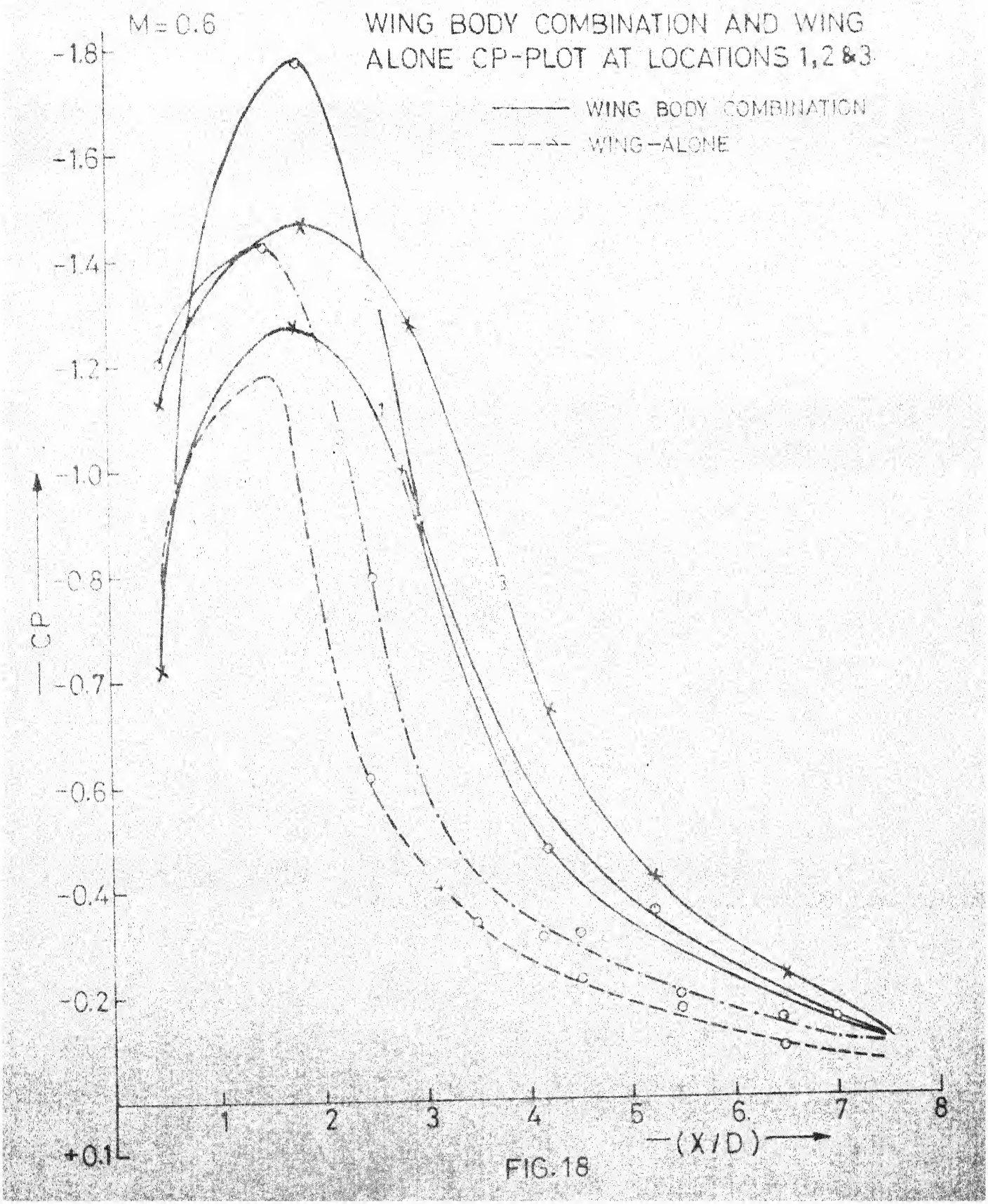
M = 0.6
WING BODY COMBINATION AND WING ALONE CP-PLOT AT LOCATIONS 1, 2 & 3
WING BODY COMBINATION
WING-ALONE
-1.8
-1.6
-1.4
-1.2
-1.0
-0.8
-0.7
-0.6
-0.4
-0.2
+0.1
CP
1
2
3
4
5
6
7
8
—(X/D)—

FIG. 18

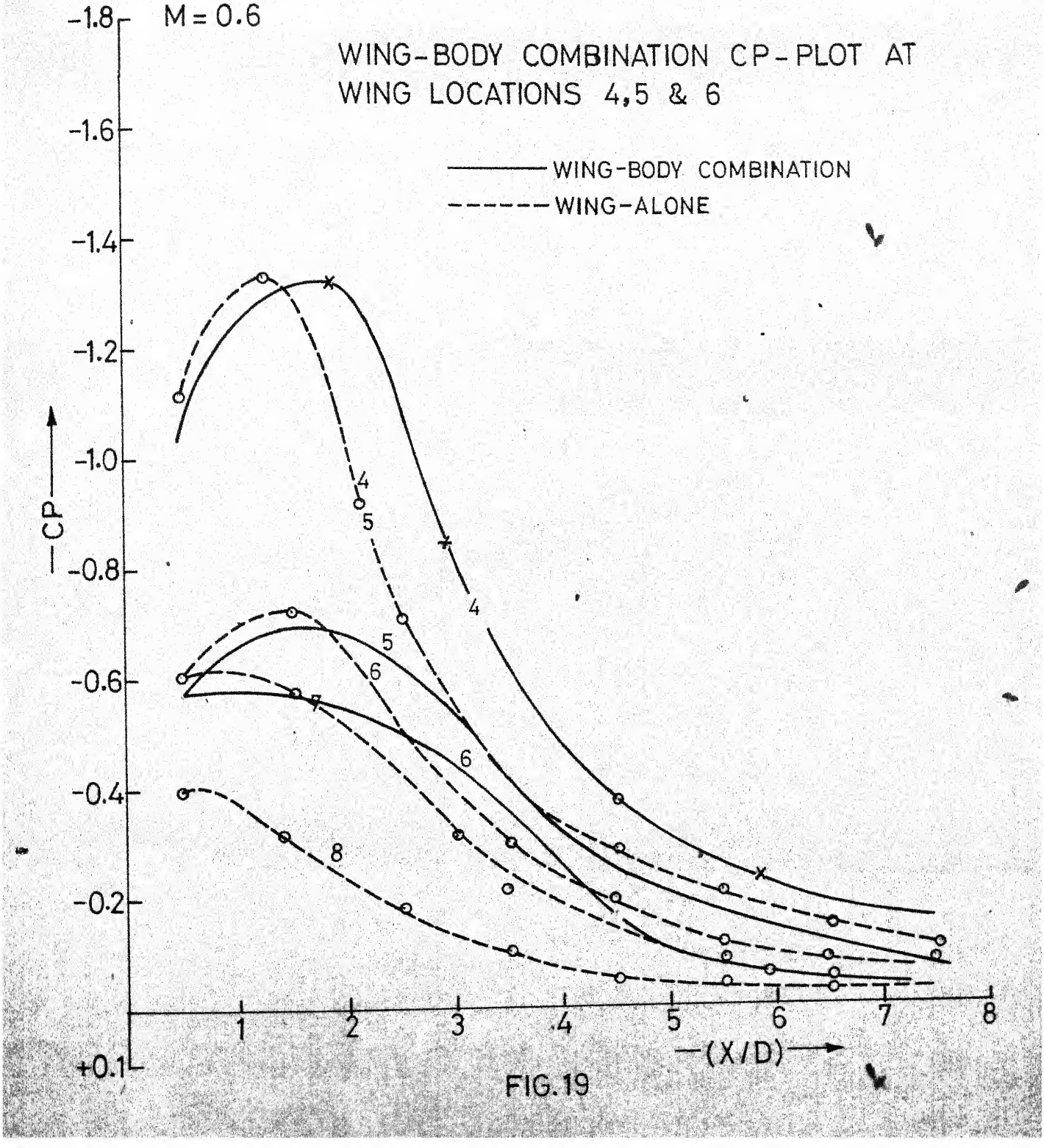
M = 0.6
WING-BODY COMBINATION CP-PLOT AT
WING LOCATIONS 4,5 & 6
WING-BODY COMBINATION
WING-ALONE
-CP
-1.8
-1.6
-1.4
-1.2
-1.0
-0.8
-0.6
-0.4
-0.2
+0.1
4
5
4
5
6
6
8
1
2
3
4
5
6
7
8
(X/D)

FIG. 19

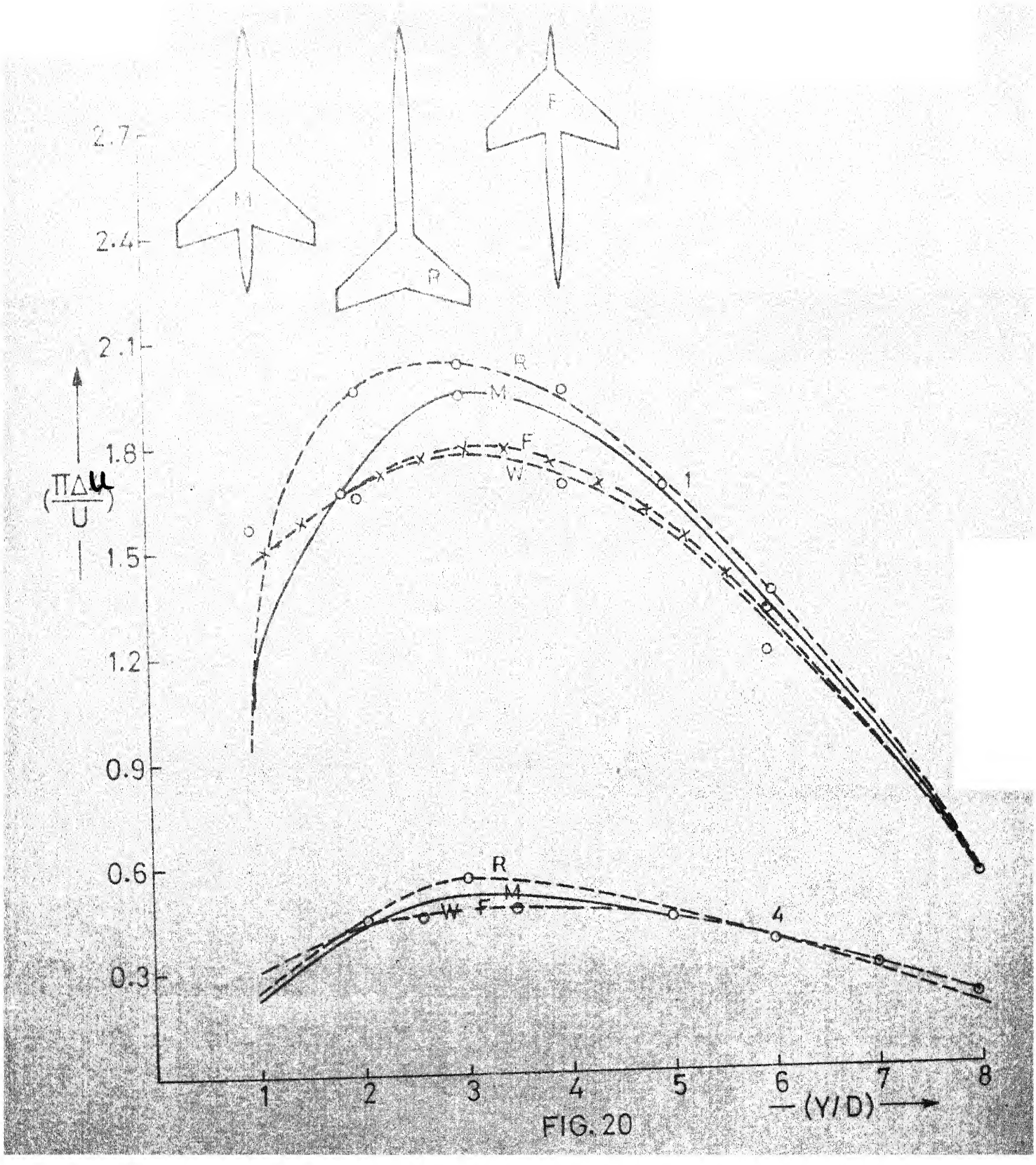

FIG. 20

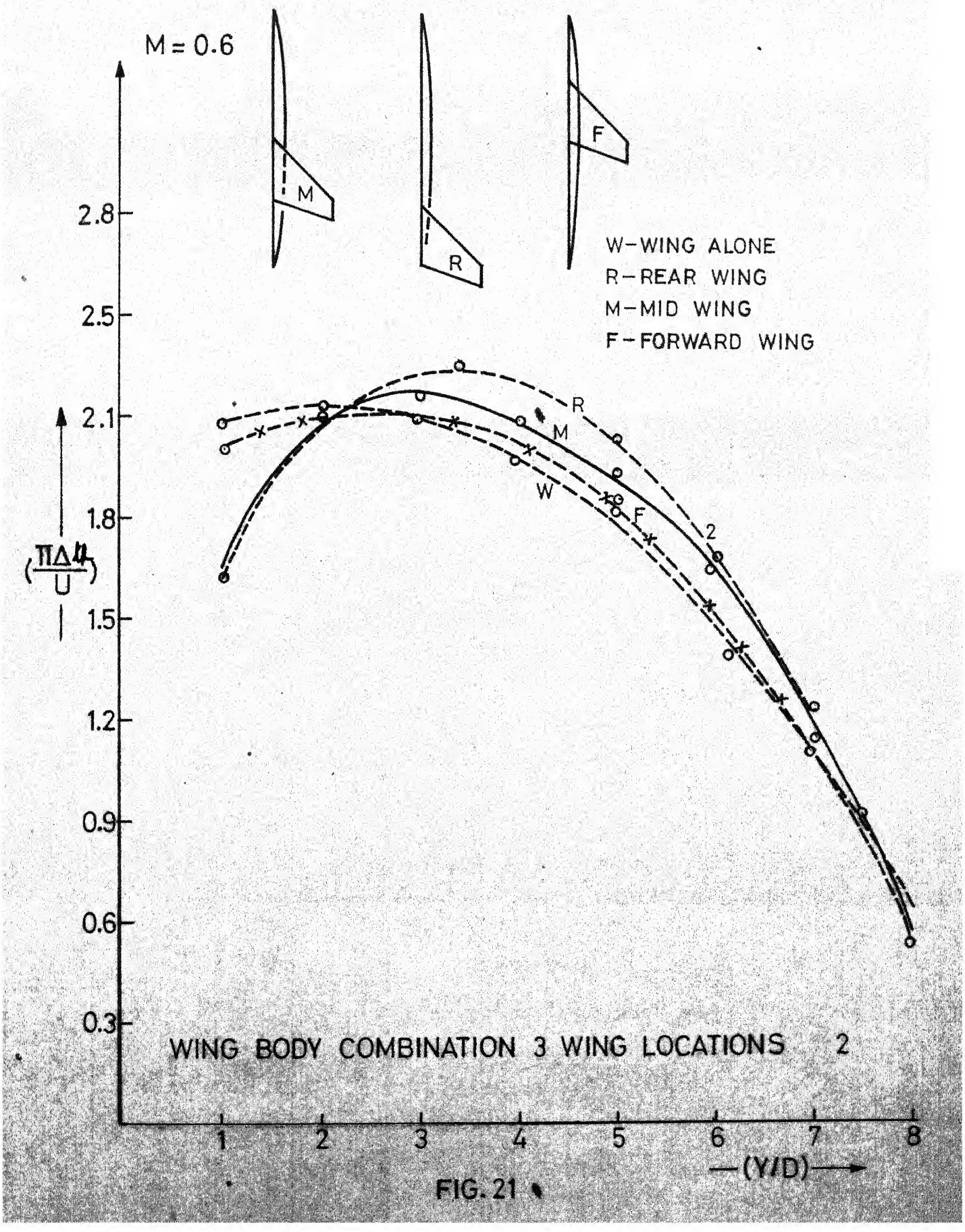
M = 0.6
M
R
F
W-WING ALONE
R-REAR WING
M-MID WING
F-FORWARD WING
2.8
2.5
2.1
1.8
1.5
1.2
0.9
0.6
0.3
(πΔμ/U)
R
M
W
F
2
1
2
3
4
5
6
7
8
—(Y/D)—
WING BODY COMBINATION 3 WING LOCATIONS 2

FIG. 21

M = 0.6

WING BODY COMBINATION 3 WING LOCATIONS
CP-PLOT AT CHORD 1 & 2

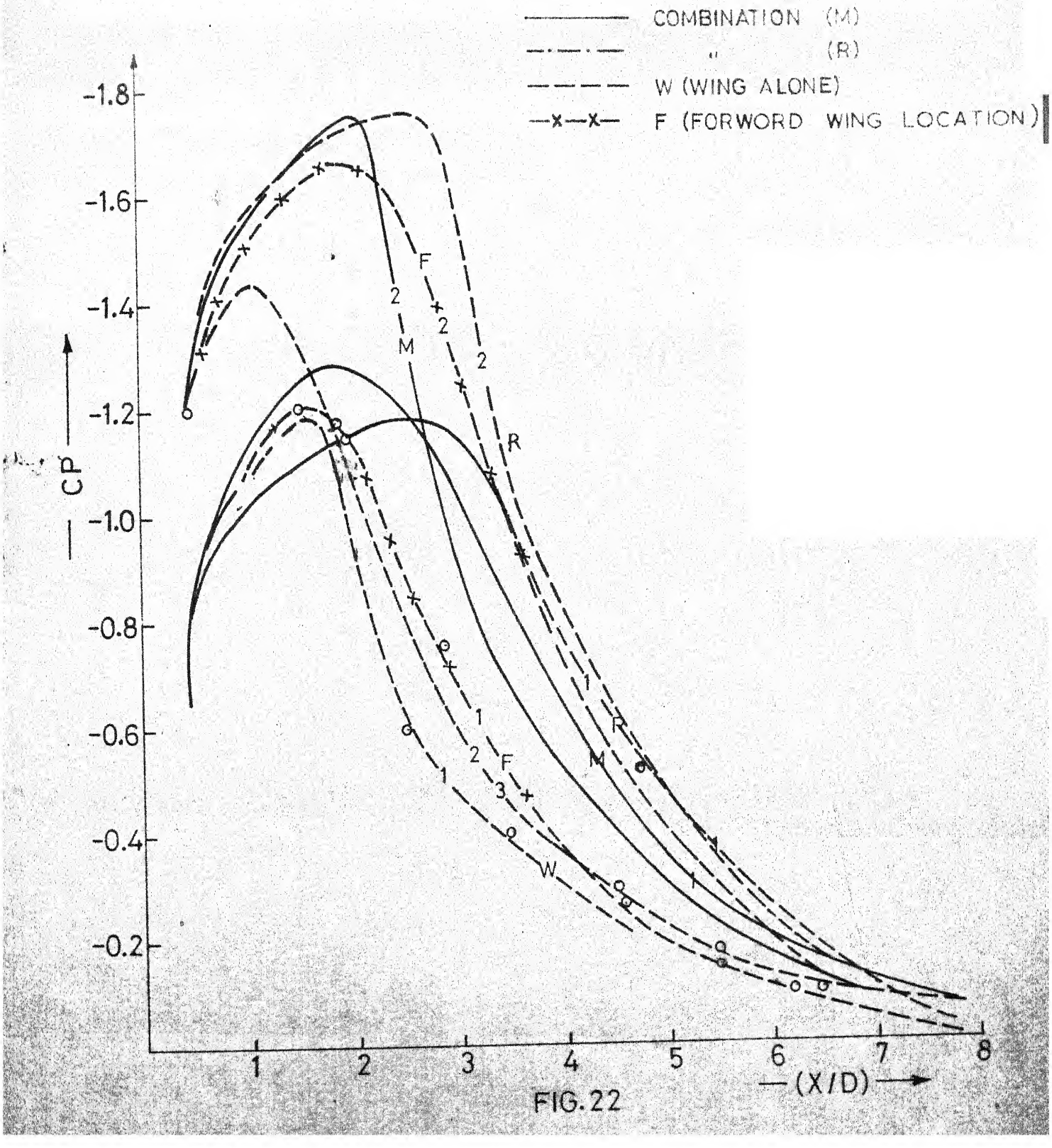

FIG. 22

M = 0.6 W_B COMBINATION

3 WING LOCATIONS

AT CHORD_5

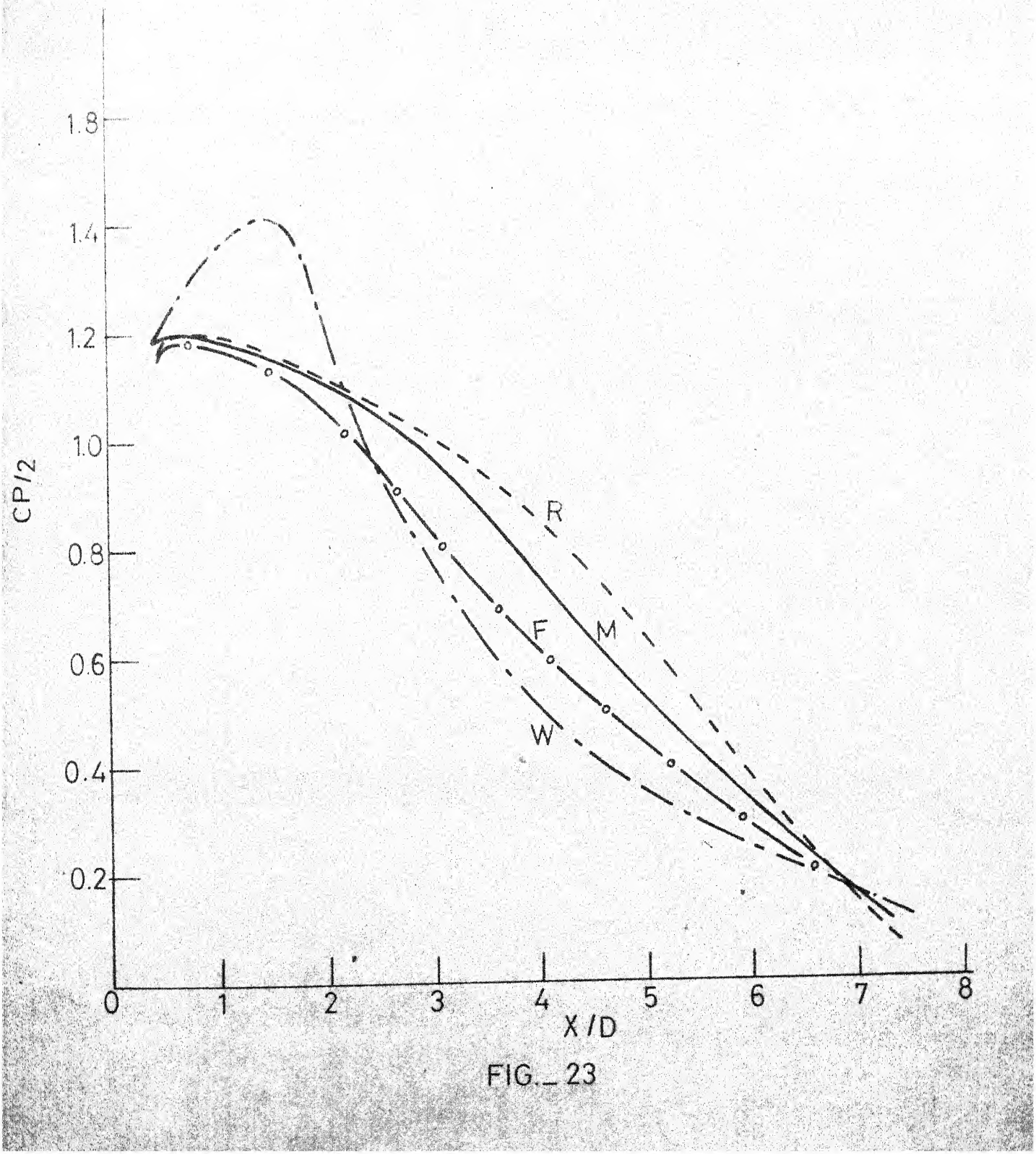

FIG._23

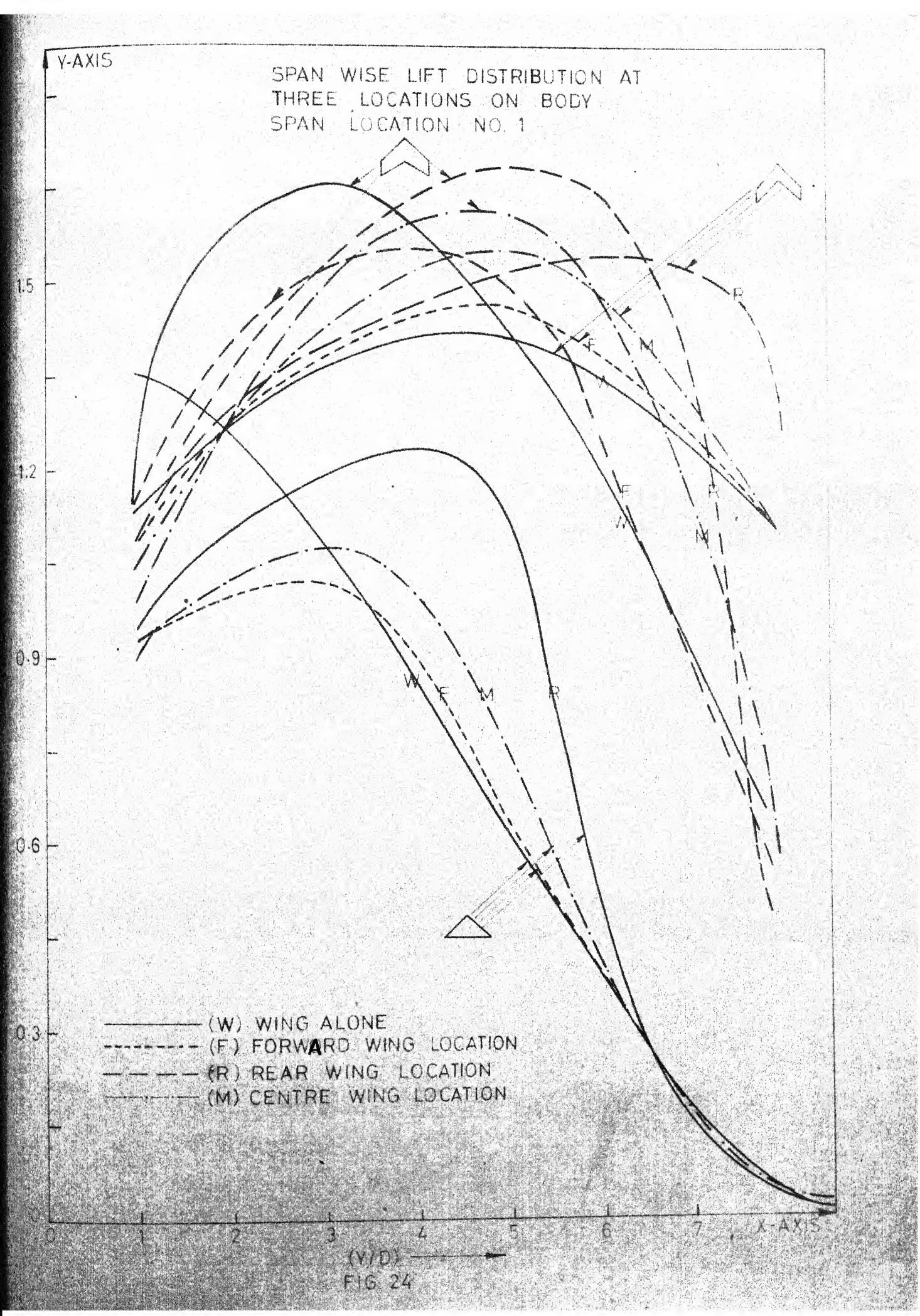
Y-AXIS
SPAN WISE LIFT DISTRIBUTION AT
THREE LOCATIONS ON BODY
SPAN LOCATION NO. 1
1.5
1.2
0.9
0.6
0.3
0
W
F
M
R
(W) WING ALONE
(F) FORWARD WING LOCATION
(R) REAR WING LOCATION
(M) CENTRE WING LOCATION
0
1
2
3
4
5
6
7
X-AXIS
(X/D)

FIG. 24

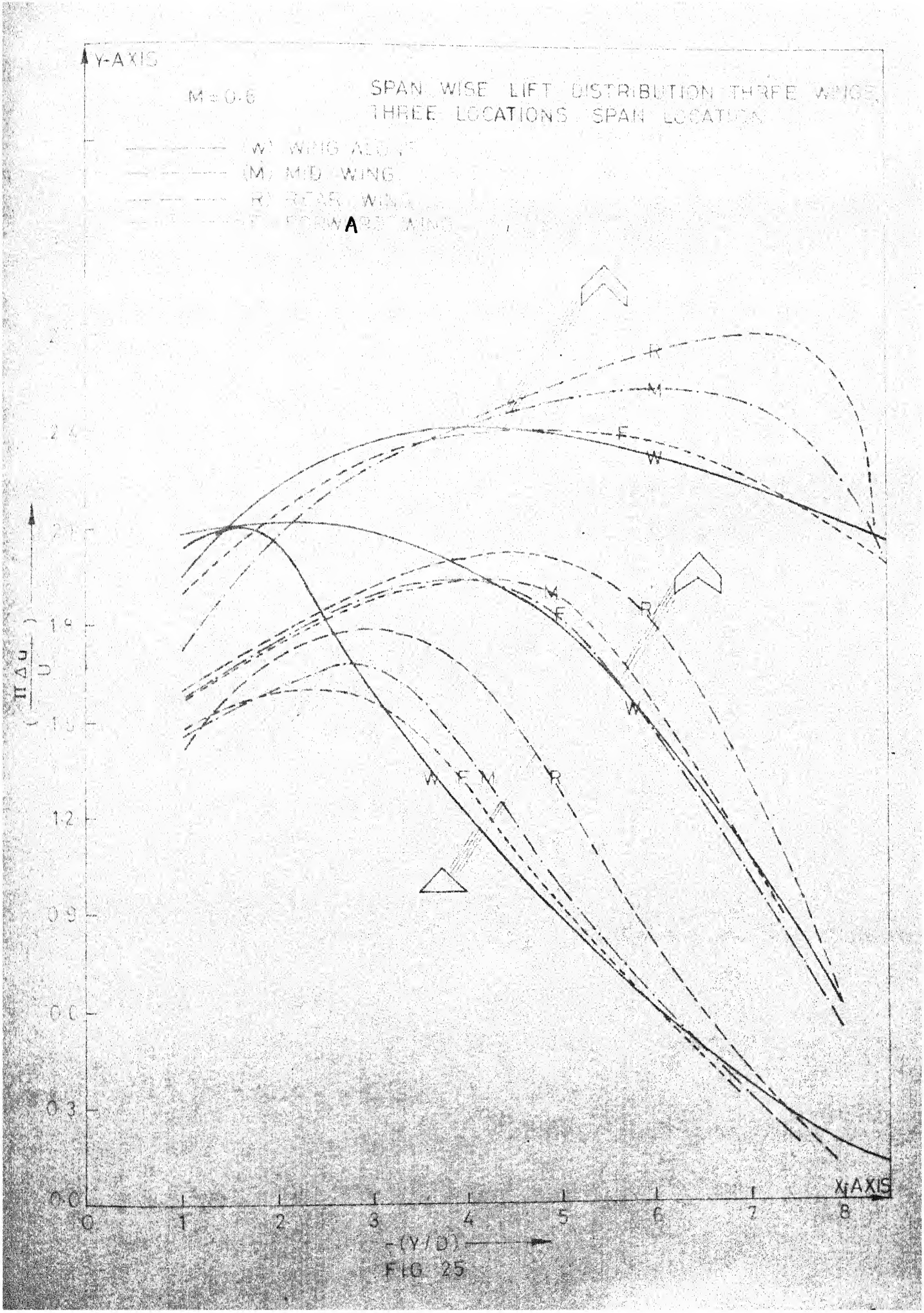
Y-AXIS
M = 0·6
SPAN WISE LIFT DISTRIBUTION THREE WINGS
THREE LOCATIONS SPAN LOCATIONS
(W) WING ALONE
(M) MID WING
(R) REAR WING
(F) FORWARD WING
A
W
M
F
R
2·4
2·1
1·8
1·5
1·2
0·9
0·6
0·3
0·0
0
1
2
3
4
5
6
7
8
X-AXIS
-(Y/D)

FIG 25

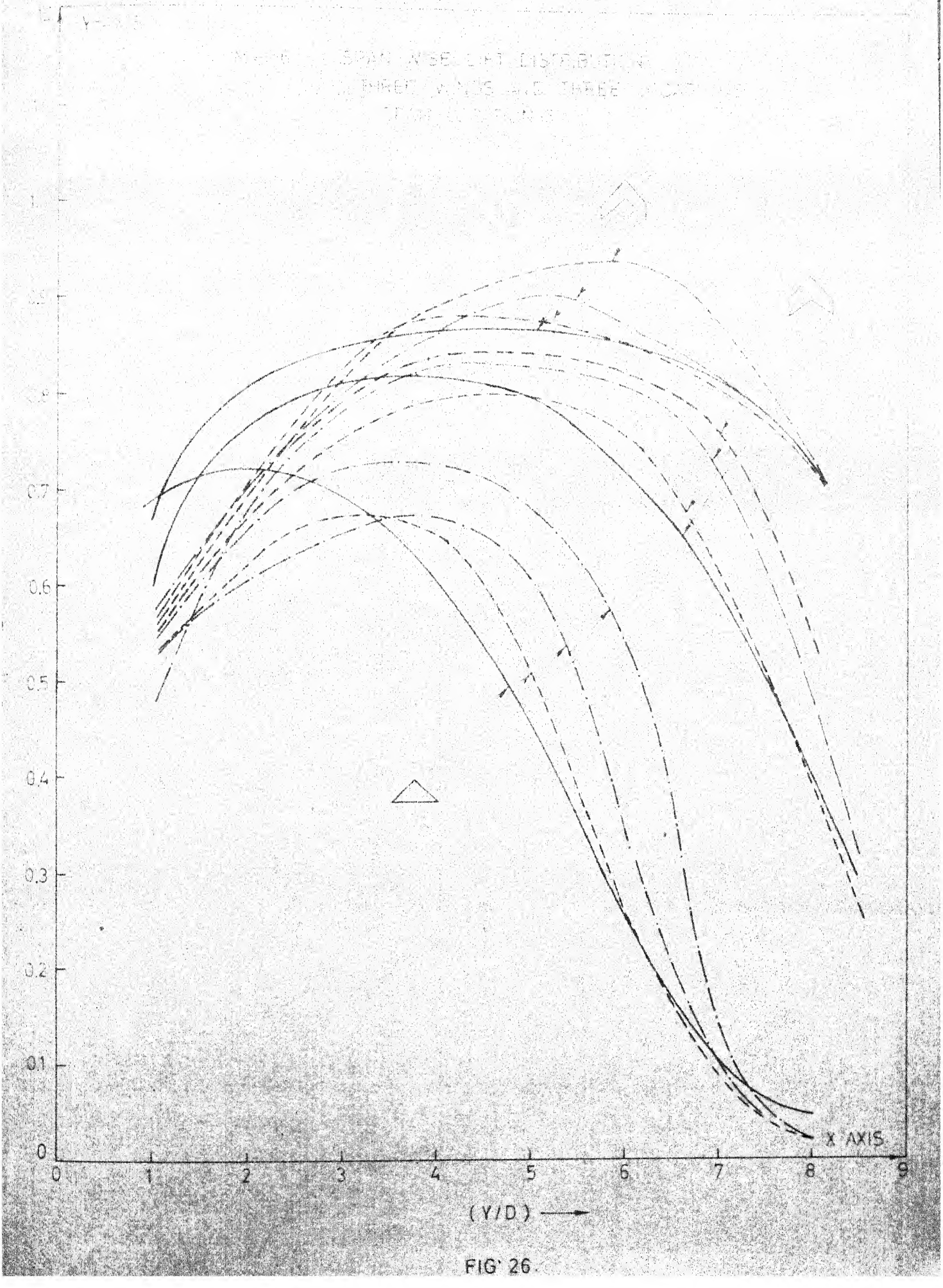

FIG' 26

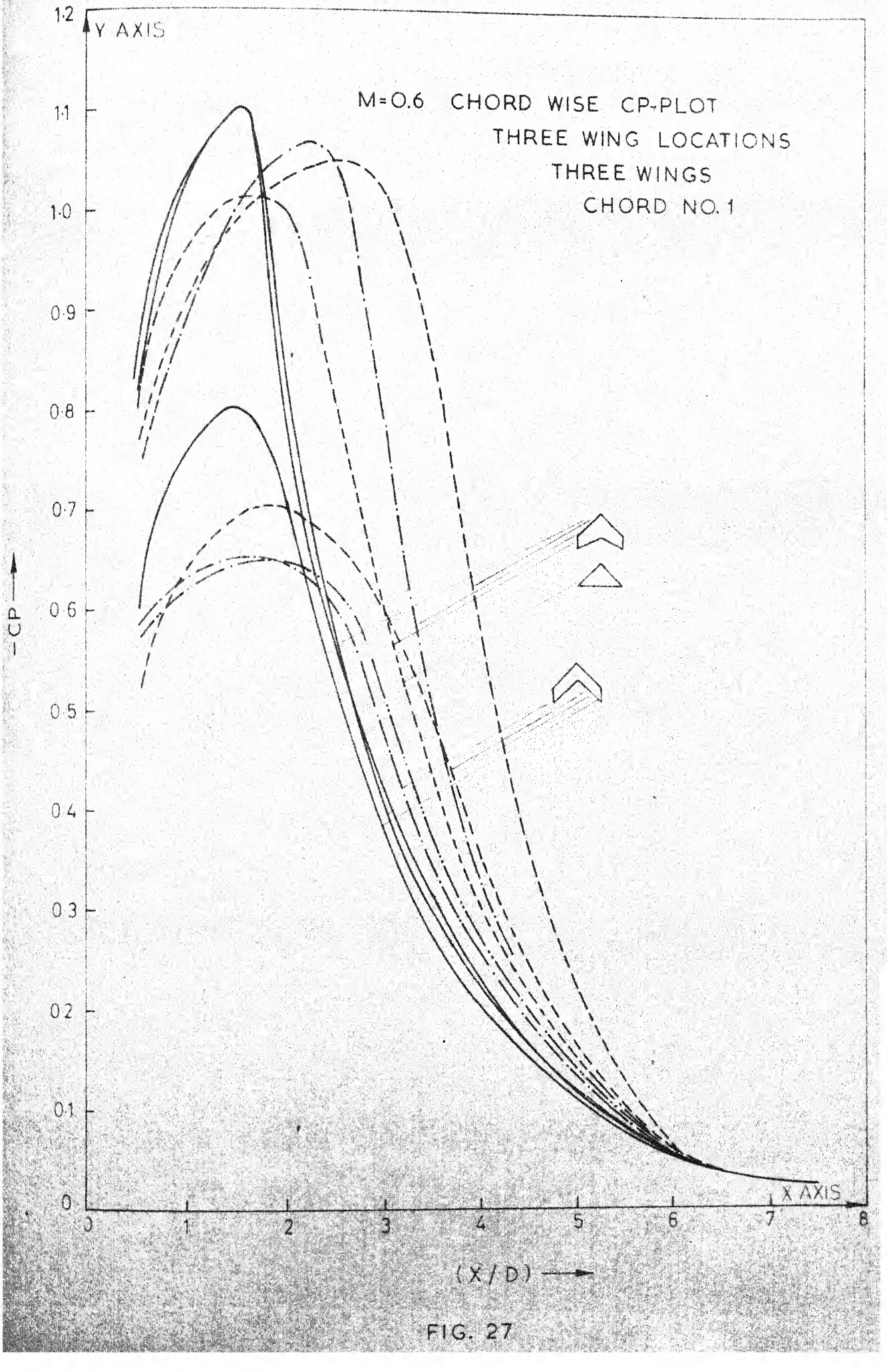
Y AXIS
M=0.6 CHORD WISE CP-PLOT
THREE WING LOCATIONS
THREE WINGS
CHORD NO. 1
1·2
1·1
1·0
0·9
0·8
0·7
0·6
0·5
0·4
0·3
0·2
0·1
0
-CP
X AXIS
0
1
2
3
4
5
6
7
8
(X/D)

FIG. 27

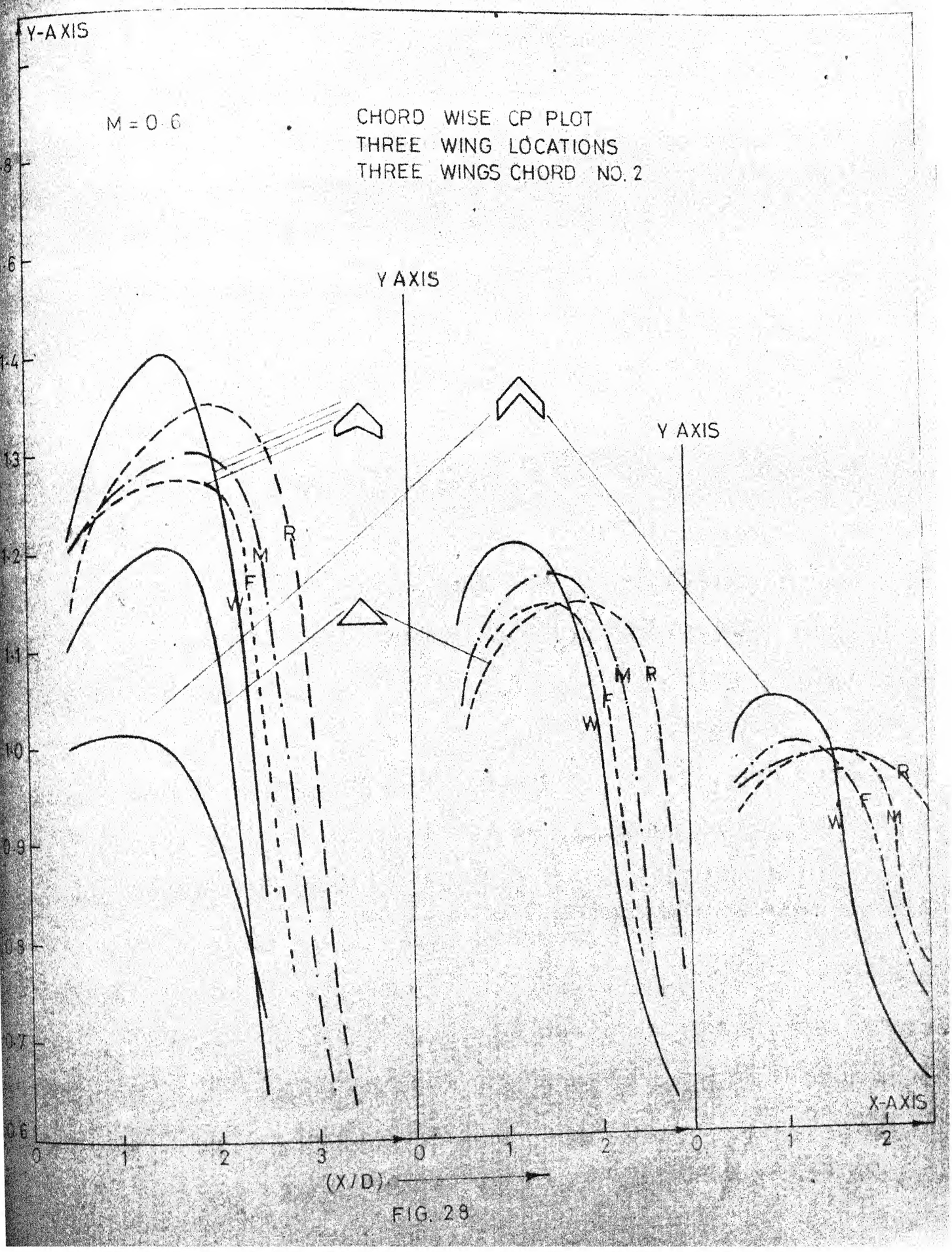
Y-AXIS
M = 0·6
CHORD WISE CP PLOT
THREE WING LOCATIONS
THREE WINGS CHORD NO. 2
1·8
1·6
1·4
1·3
1·2
1·1
1·0
0·9
0·8
0·7
0·6
Y AXIS
Y AXIS
R
M
F
W
M R
F
W
R
F
M
W
X-AXIS
0
1
2
3
0
1
2
0
1
2
(X/D)

FIG. 28

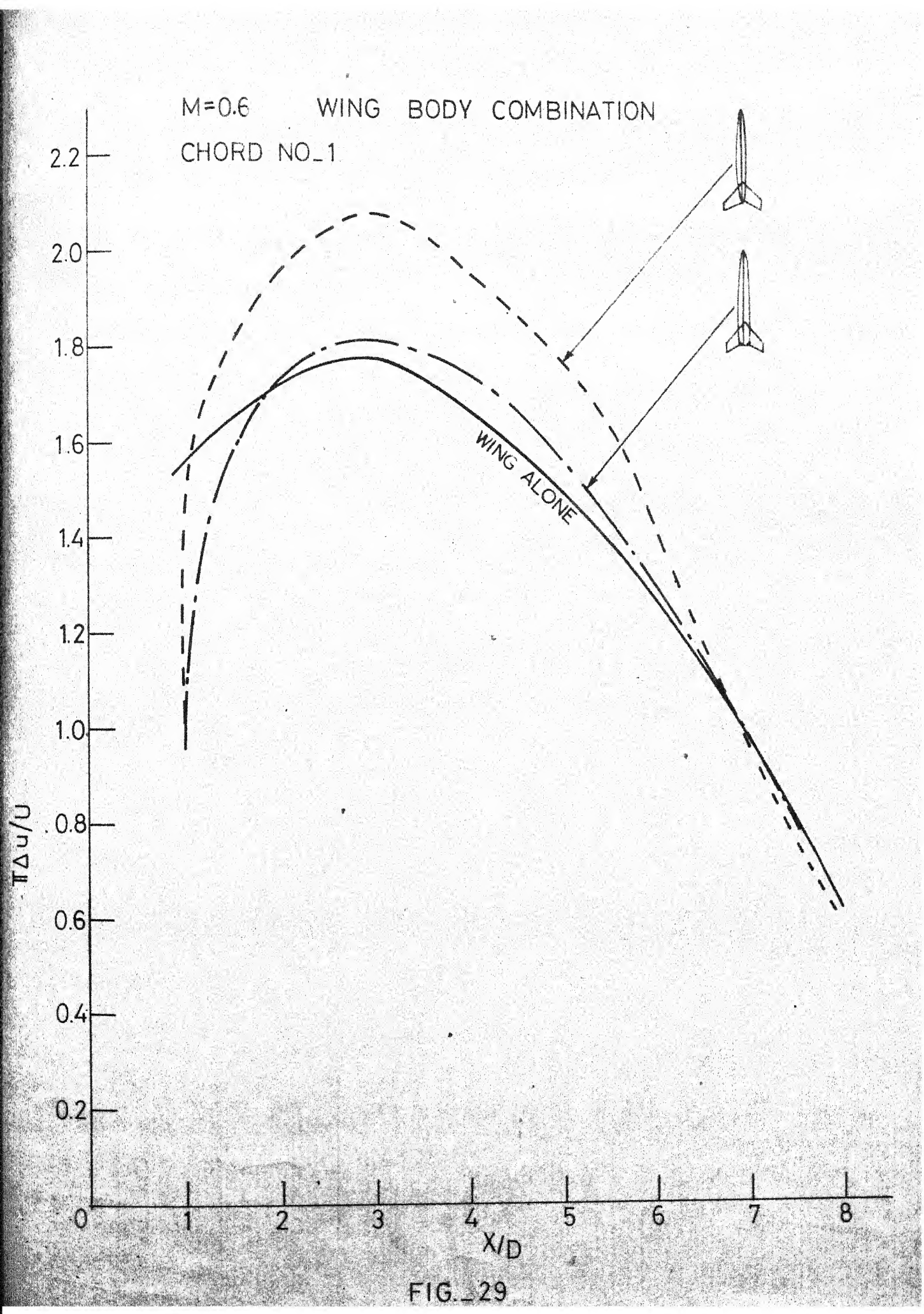
M=0.6 WING BODY COMBINATION
CHORD NO_1
2.2
2.0
1.8
1.6
1.4
1.2
1.0
0.8
0.6
0.4
0.2
0
1
2
3
4
5
6
7
8
X/D
T Δu/U
WING ALONE

FIG._29

M = 0.6 W–B COMBINATION

CHORD LOCATION _ 2

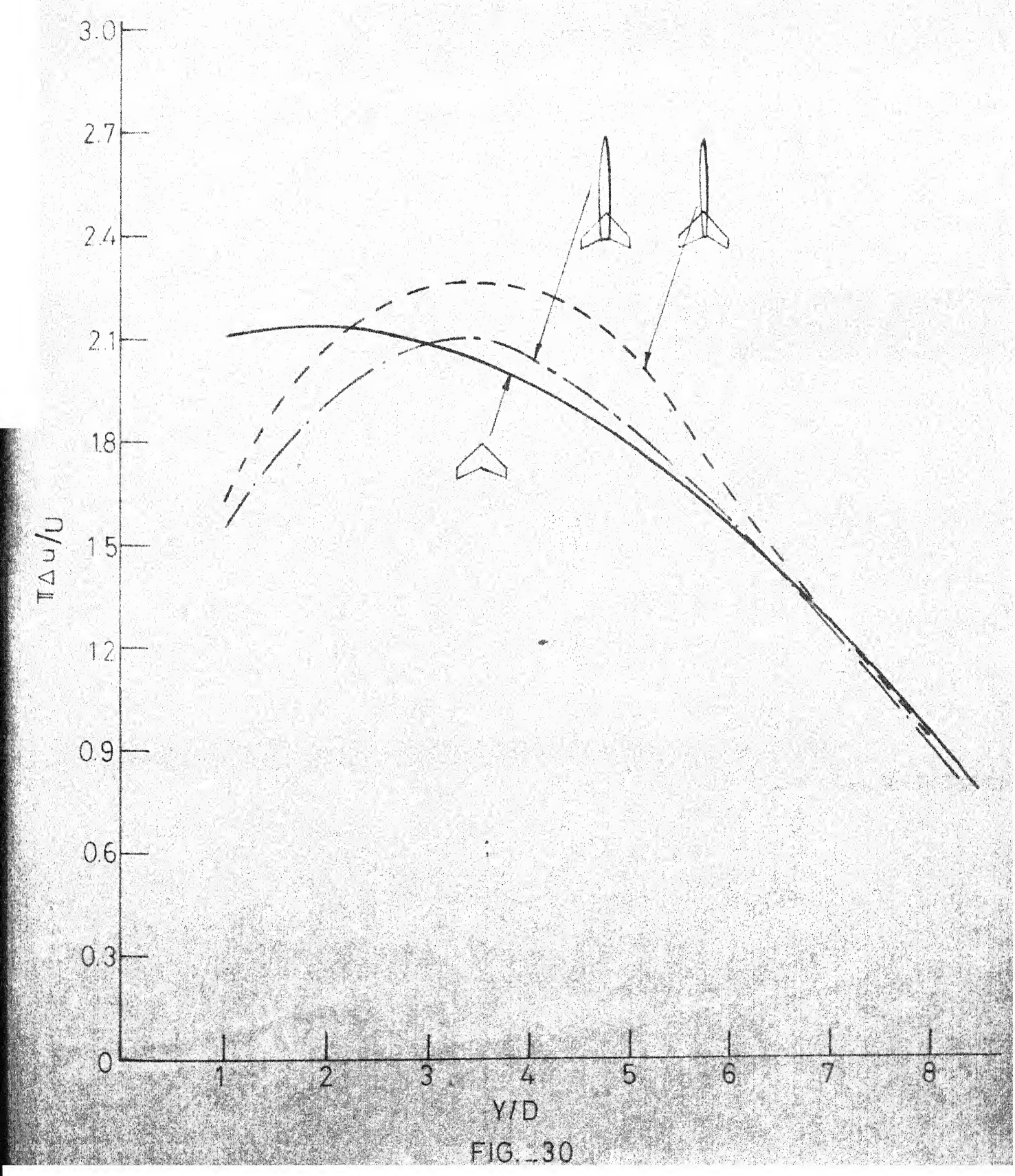

FIG._30

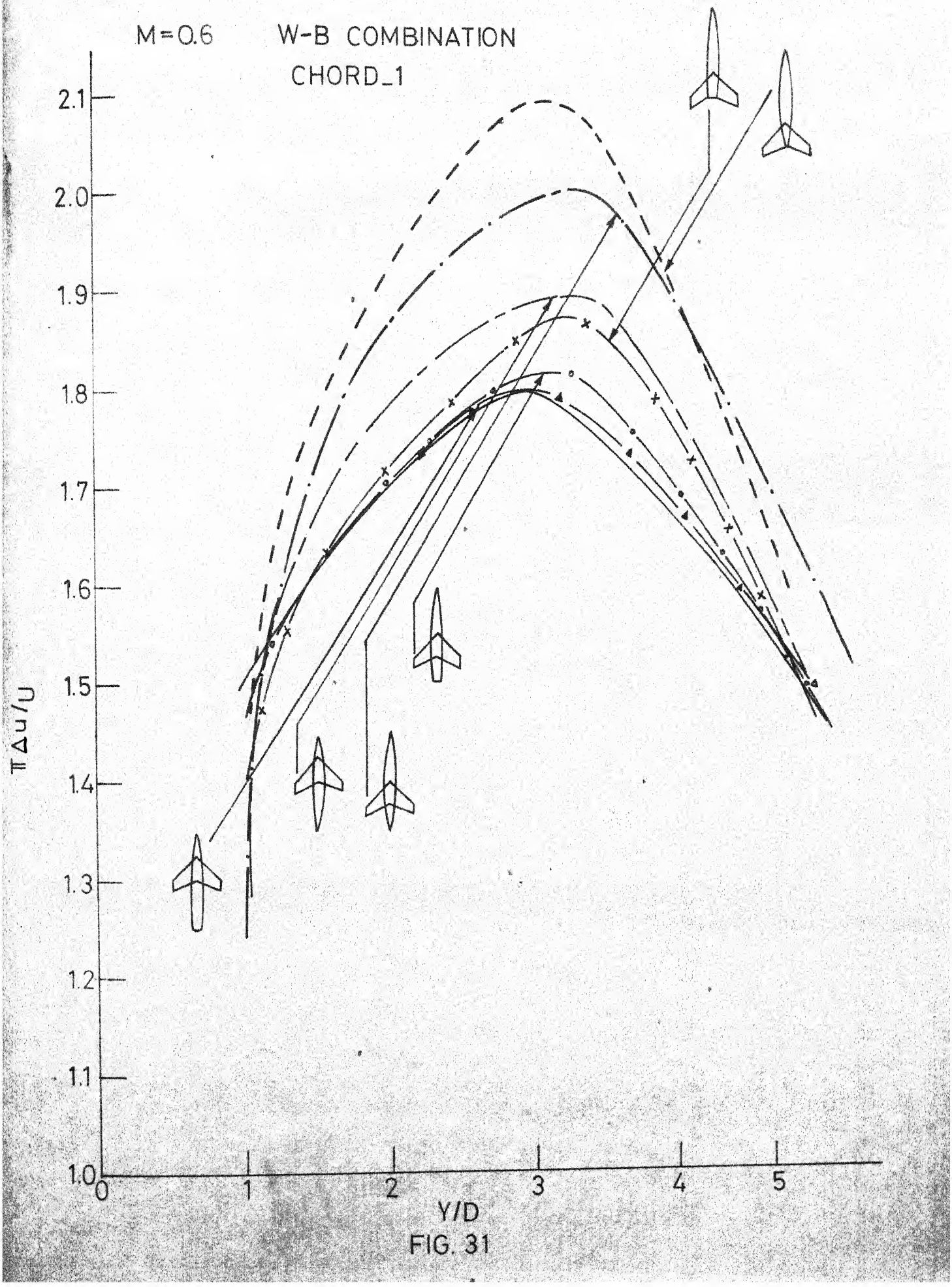
M=0.6
W-B COMBINATION
CHORD_1
2.1
2.0
1.9
1.8
1.7
1.6
1.5
1.4
1.3
1.2
1.1
1.0
0
1
2
3
4
5
Y/D
$\pi\Delta u/U$

FIG. 31

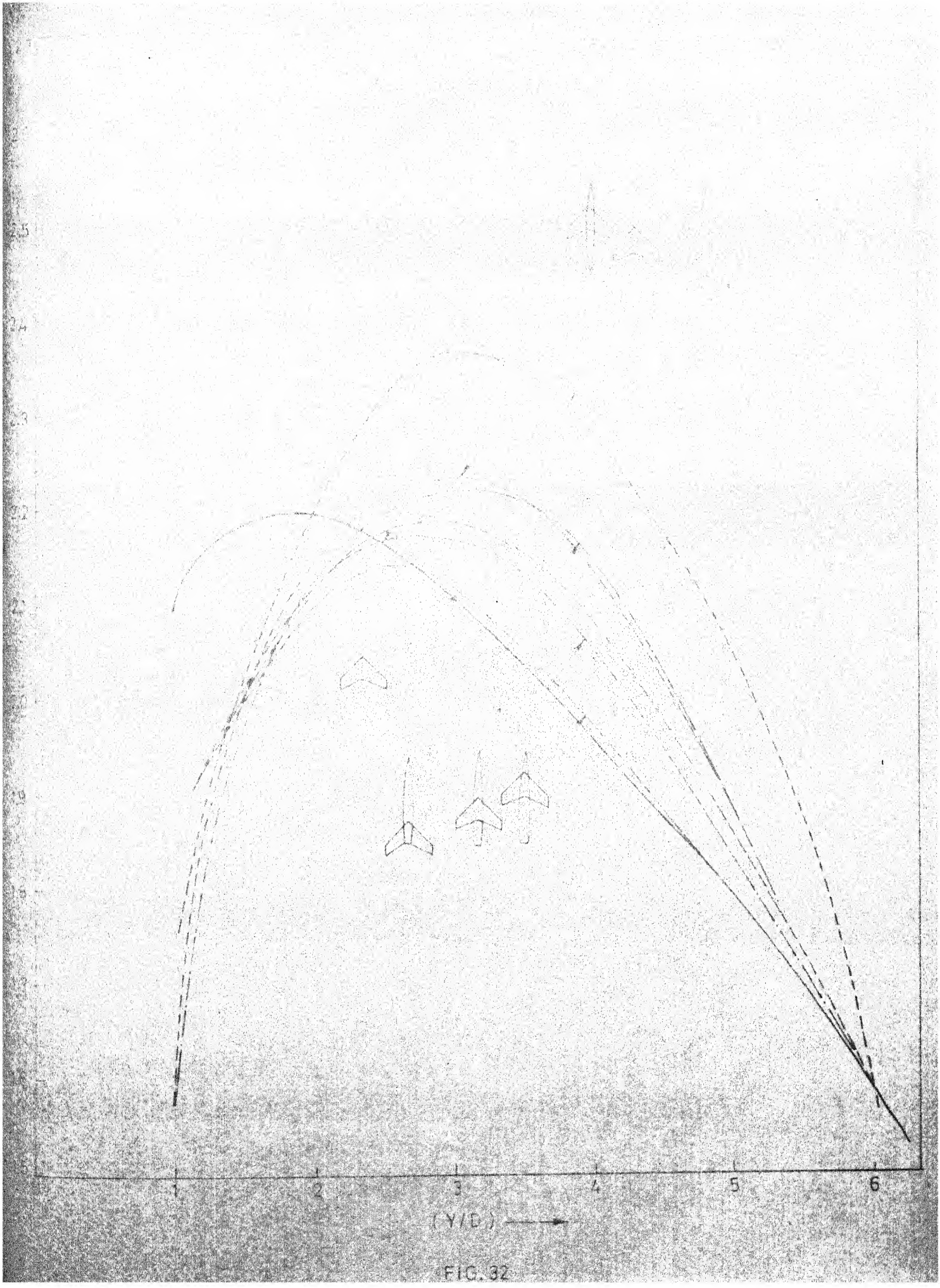

FIG. 32

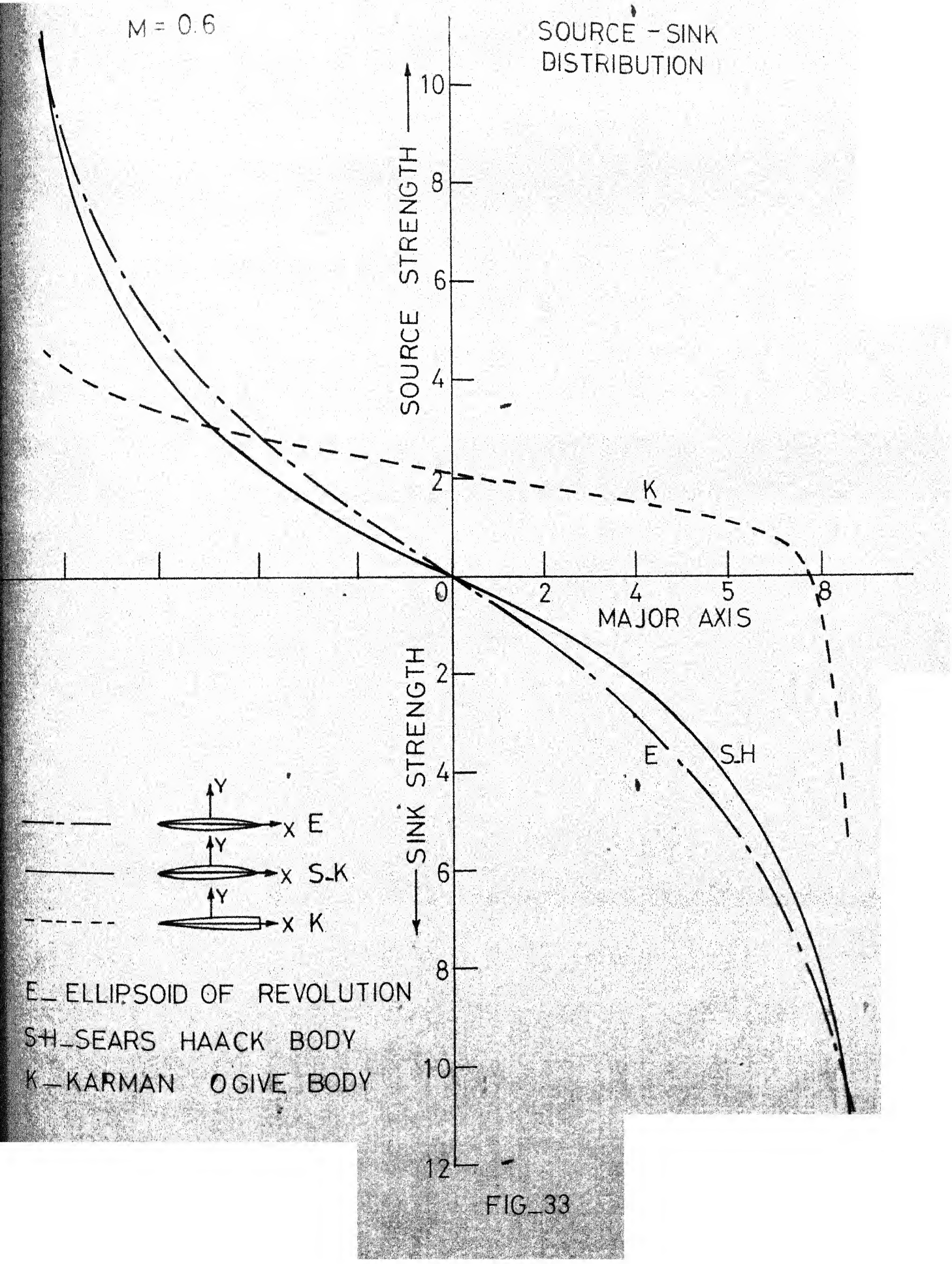
M = 0.6
SOURCE - SINK DISTRIBUTION
SOURCE STRENGTH
SINK STRENGTH
10
8
6
4
2
0
2
4
5
8
MAJOR AXIS
K
E
S.H
Y
X E
Y
X S.K
Y
X K
E_ ELLIPSOID OF REVOLUTION
S.H_SEARS HAACK BODY
K_KARMAN OGIVE BODY

FIG_33

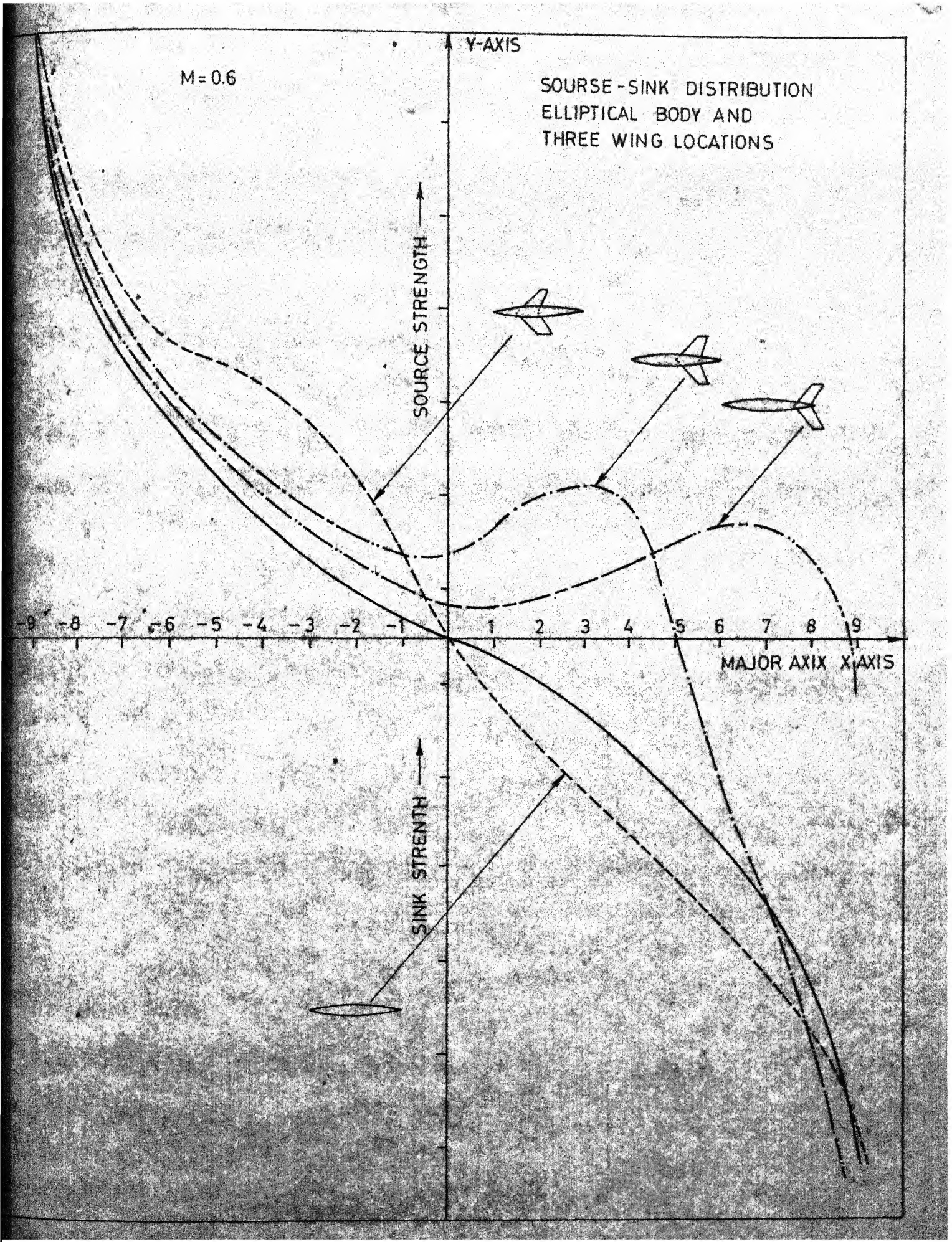
Y-AXIS
M = 0.6
SOURSE - SINK DISTRIBUTION
ELLIPTICAL BODY AND
THREE WING LOCATIONS
SOURCE STRENGTH
SINK STRENTH
-9 -8 -7 -6 -5 -4 -3 -2 -1
1 2 3 4 5 6 7 8 9
MAJOR AXIX X AXIS

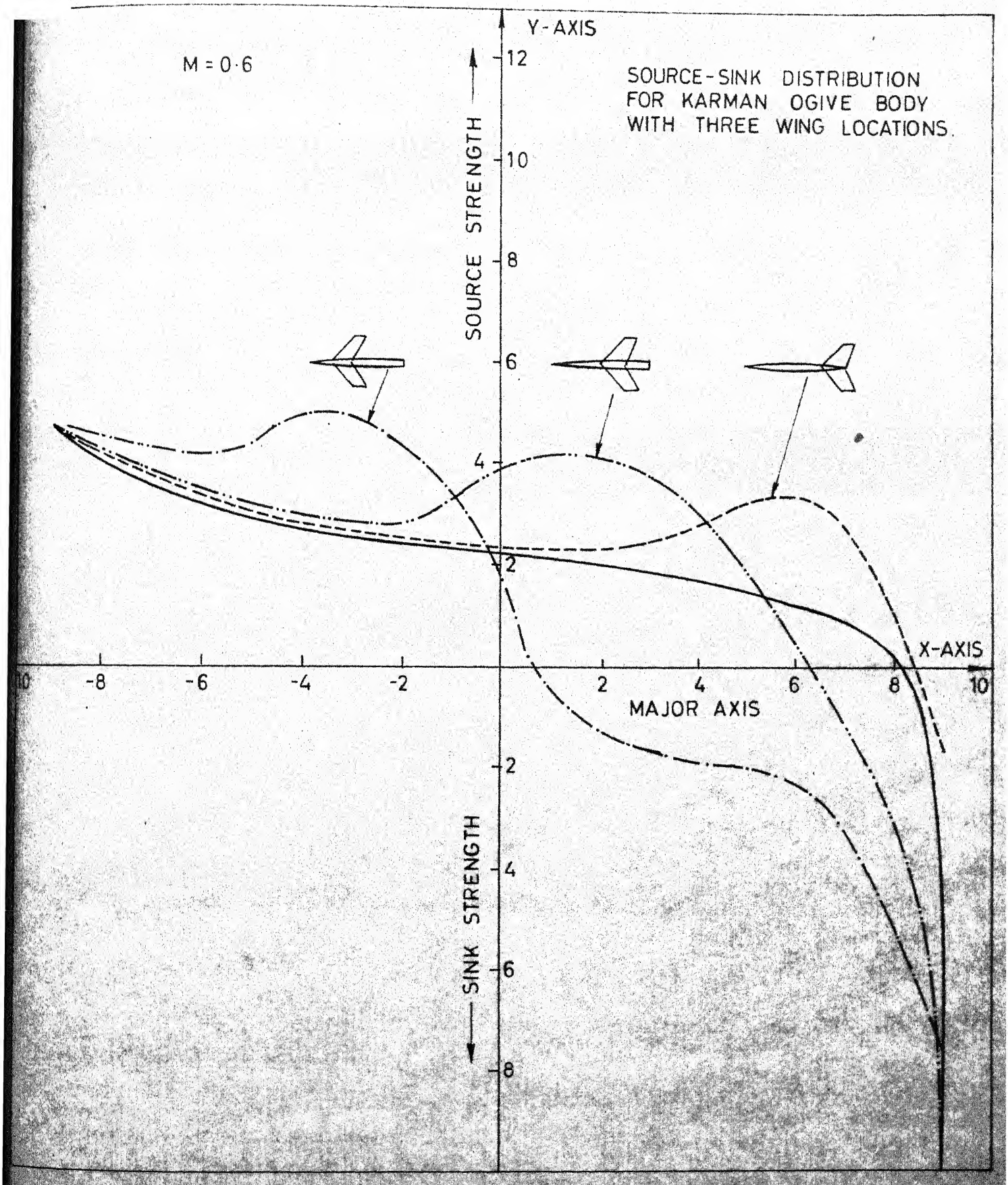
M = 0·6
SOURCE-SINK DISTRIBUTION
FOR KARMAN OGIVE BODY
WITH THREE WING LOCATIONS.
Y-AXIS
SOURCE STRENGTH
SINK STRENGTH
X-AXIS
MAJOR AXIS
12
10
8
6
4
2
-2
-4
-6
-8
-10
-8
-6
-4
-2
2
4
6
8
10

FIG. 35

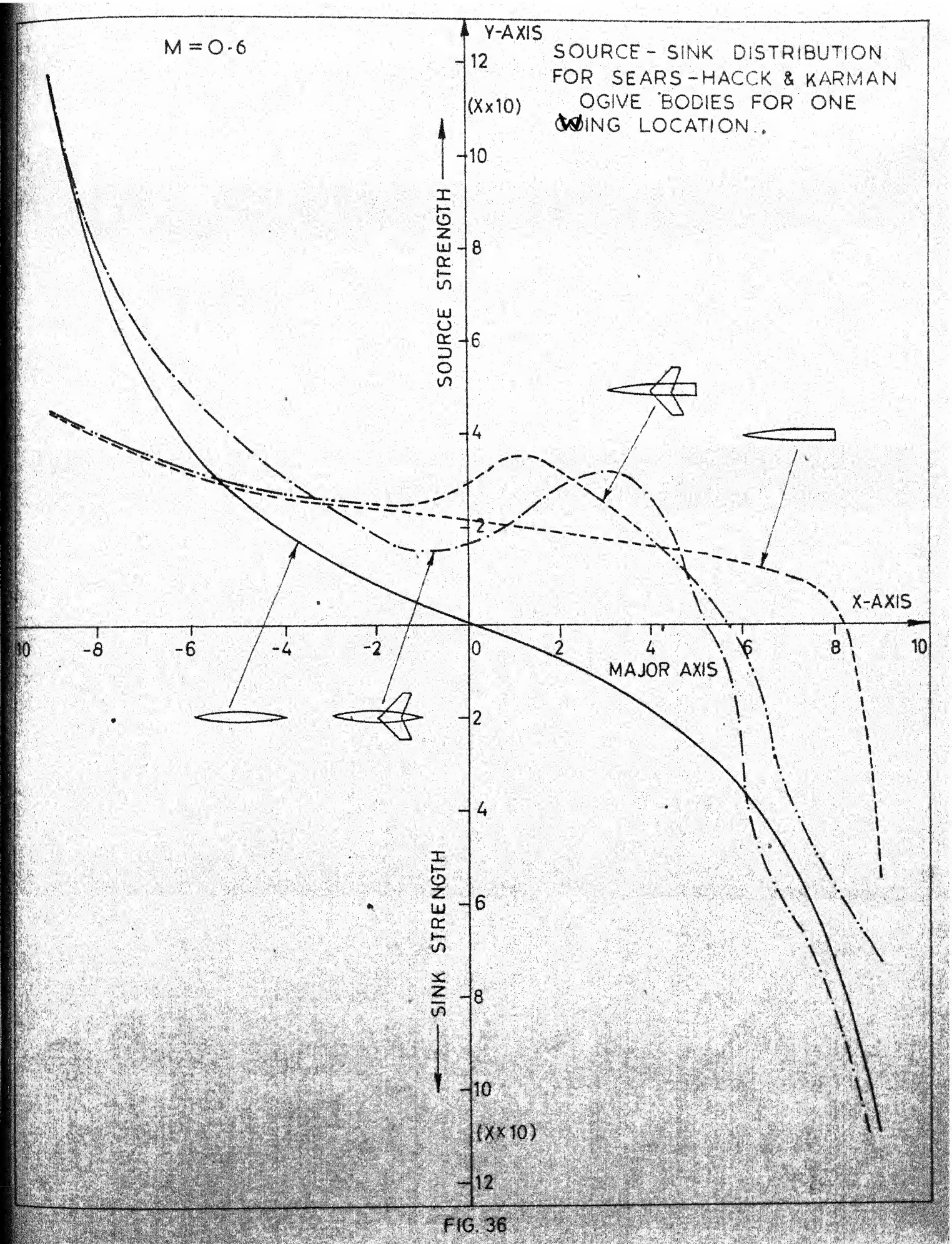
M = O·6
Y-AXIS
SOURCE - SINK DISTRIBUTION FOR SEARS-HACCK & KARMAN OGIVE BODIES FOR ONE WING LOCATION.
(X×10)
SOURCE STRENGTH
SINK STRENGTH
X-AXIS
MAJOR AXIS
12
10
8
6
4
2
0
-8
-6
-4
-2
2
4
6
8
10

FIG. 36

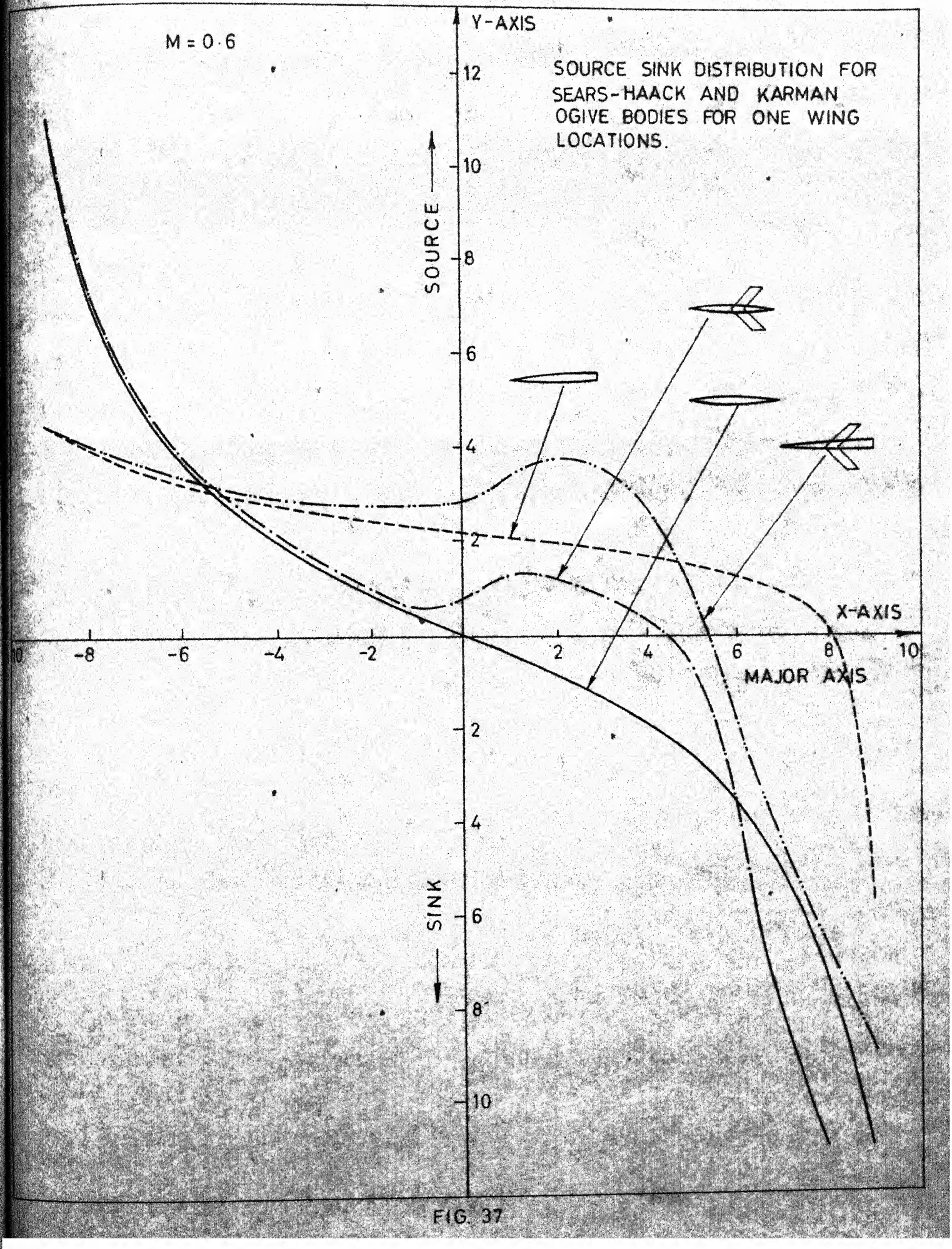
M = 0·6
Y-AXIS
SOURCE SINK DISTRIBUTION FOR SEARS-HAACK AND KARMAN OGIVE BODIES FOR ONE WING LOCATIONS.
SOURCE
SINK
X-AXIS
MAJOR AXIS
12
10
8
6
4
2
-8
-6
-4
-2
2
4
6
8
10

FIG. 37

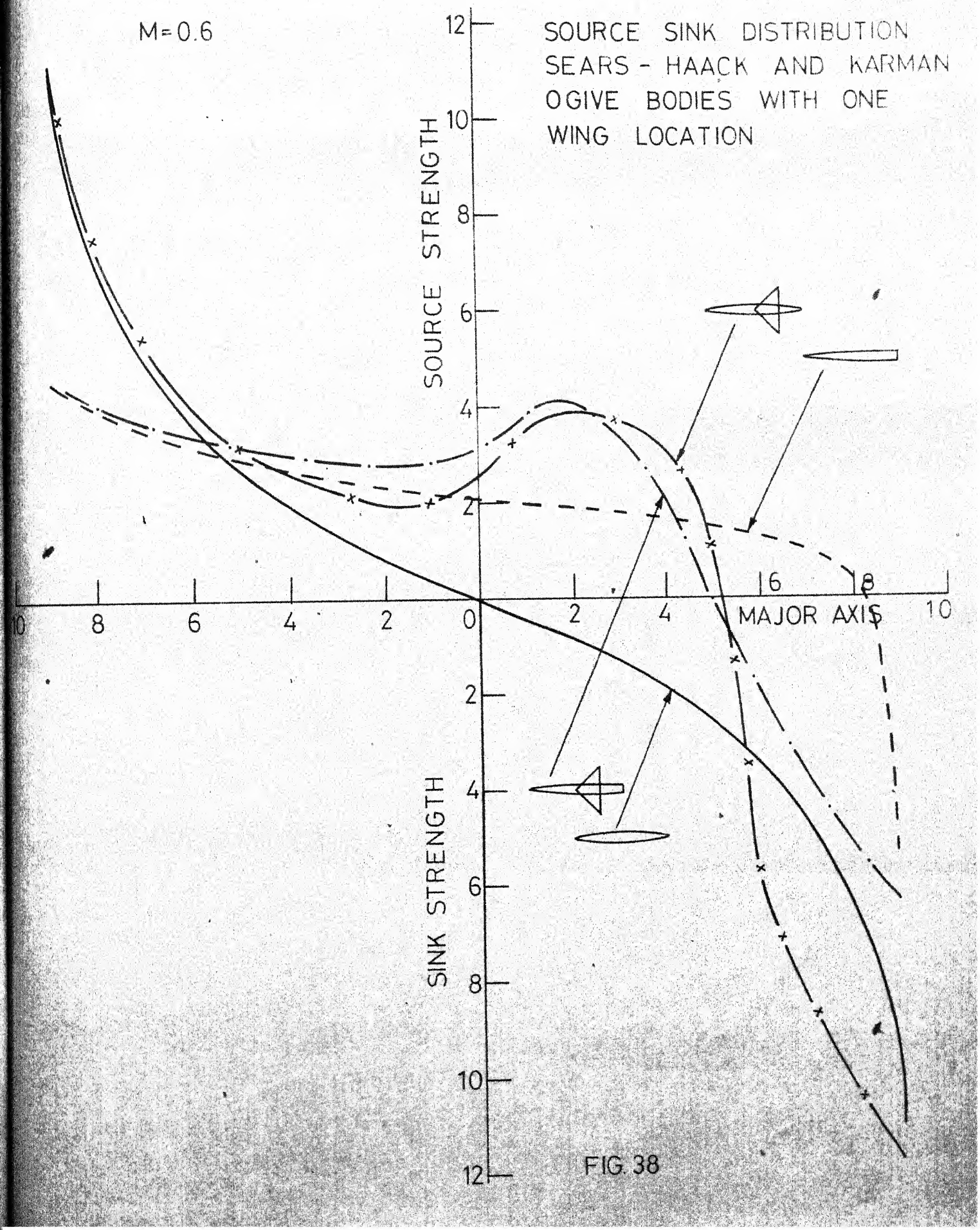
M=0.6
SOURCE SINK DISTRIBUTION
SEARS - HAACK AND KARMAN
OGIVE BODIES WITH ONE
WING LOCATION
SOURCE STRENGTH
SINK STRENGTH
MAJOR AXIS
12
10
8
6
4
2
0
2
4
6
8
10
12

FIG. 38

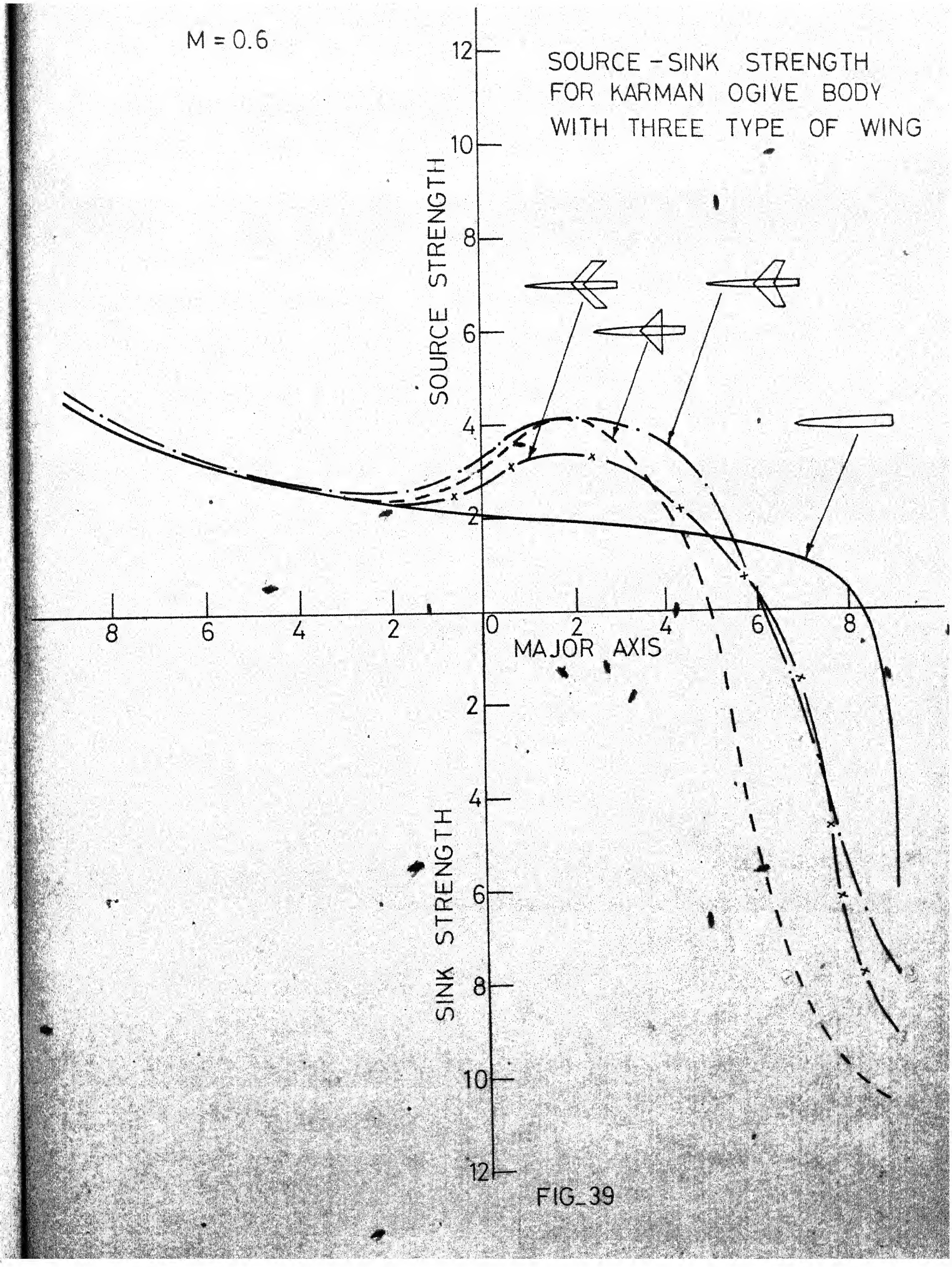
M = 0.6
SOURCE - SINK STRENGTH
FOR KARMAN OGIVE BODY
WITH THREE TYPE OF WING
SOURCE STRENGTH
SINK STRENGTH
MAJOR AXIS
12
10
8
6
4
2
0
2
4
6
8

FIG_39

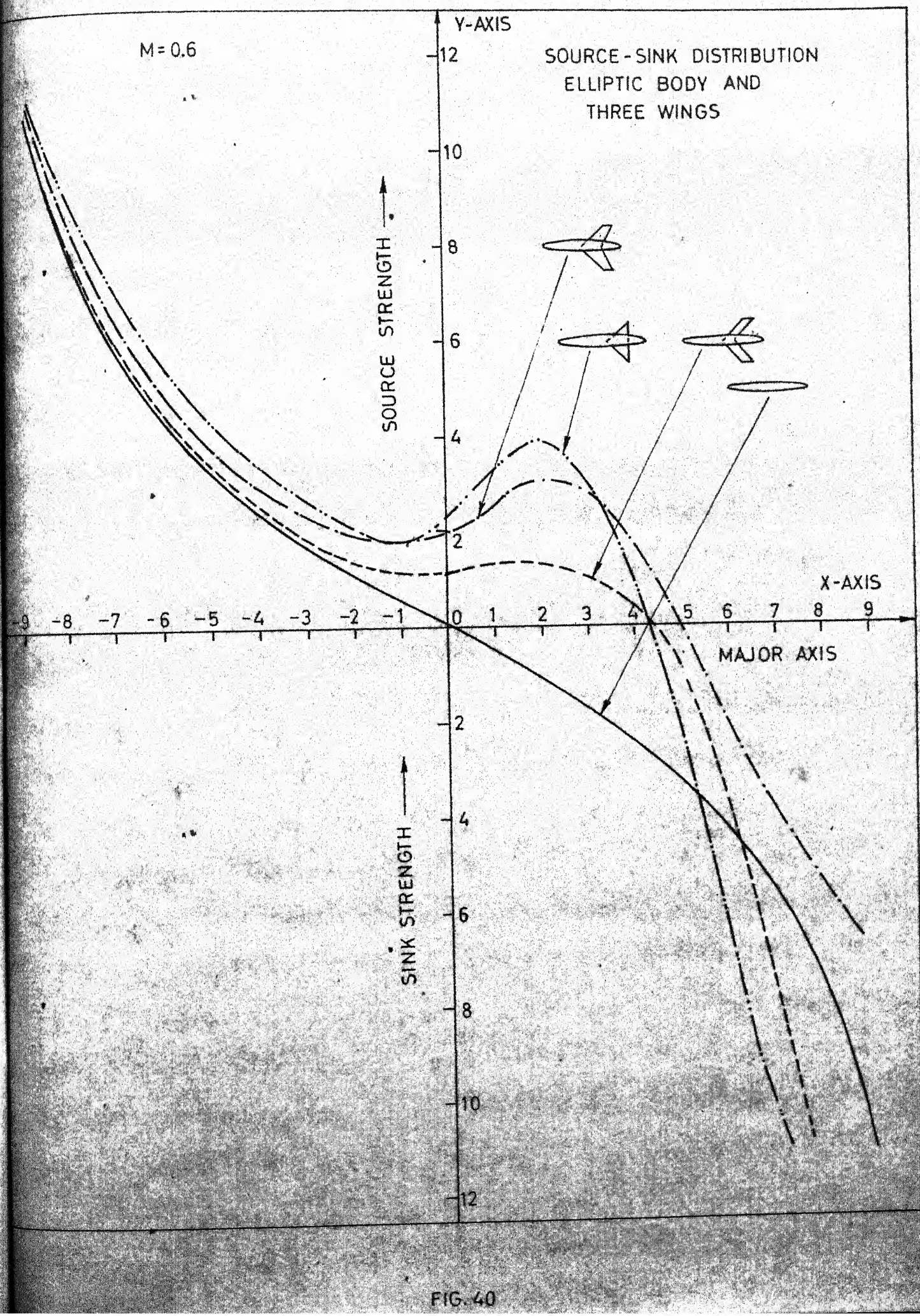
M = 0.6
SOURCE - SINK DISTRIBUTION
ELLIPTIC BODY AND
THREE WINGS
Y-AXIS
X-AXIS
MAJOR AXIS
SOURCE STRENGTH
SINK STRENGTH
12
10
8
6
4
2
-9 -8 -7 -6 -5 -4 -3 -2 -1 0 1 2 3 4 5 6 7 8 9

FIG. 40

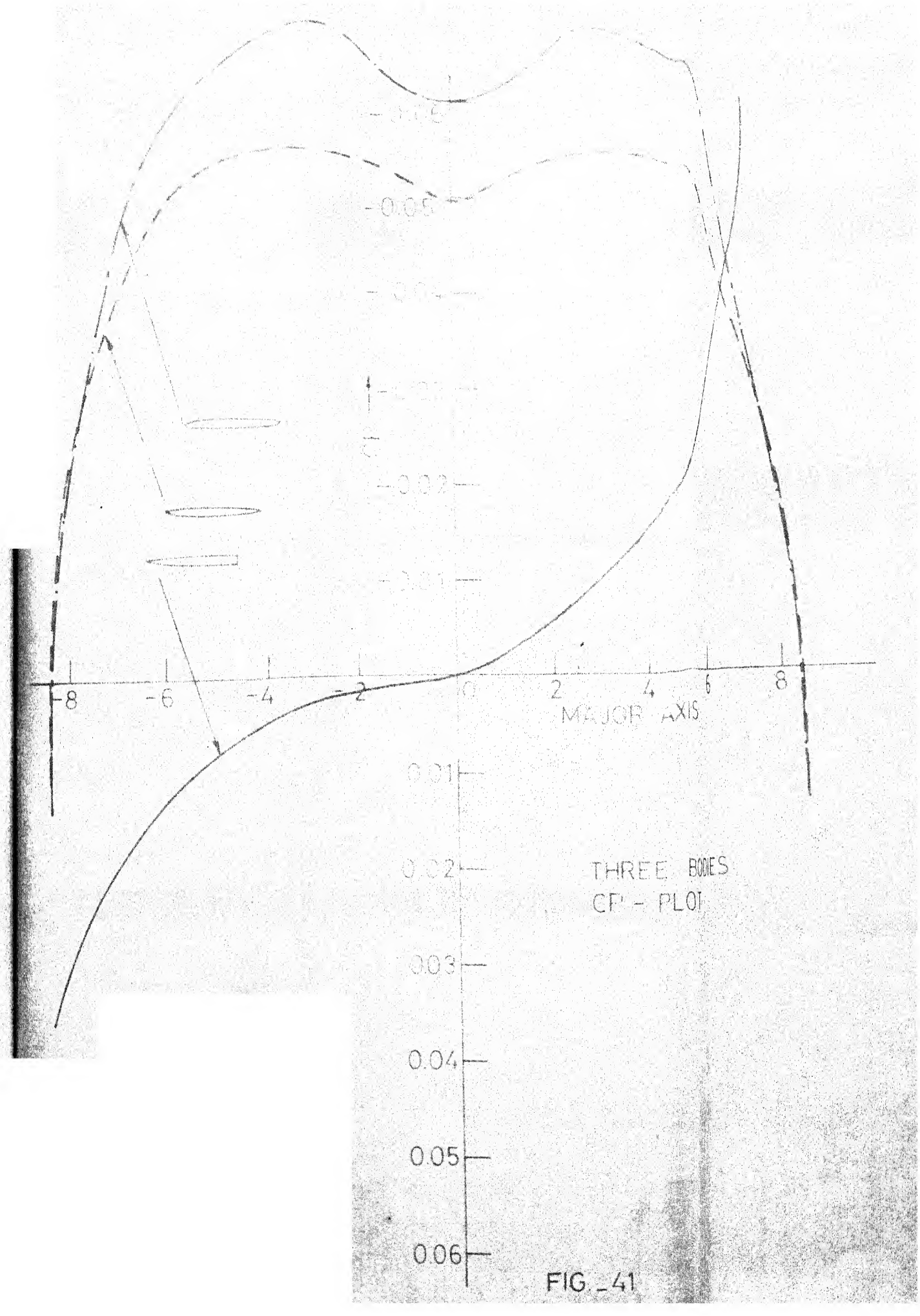
-0.05
-0.02
-8
-6
-4
-2
0
2
4
6
8
MAJOR AXIS
0.01
0.02
0.03
0.04
0.05
0.06
THREE BODIES
CP - PLOT

FIG. - 41

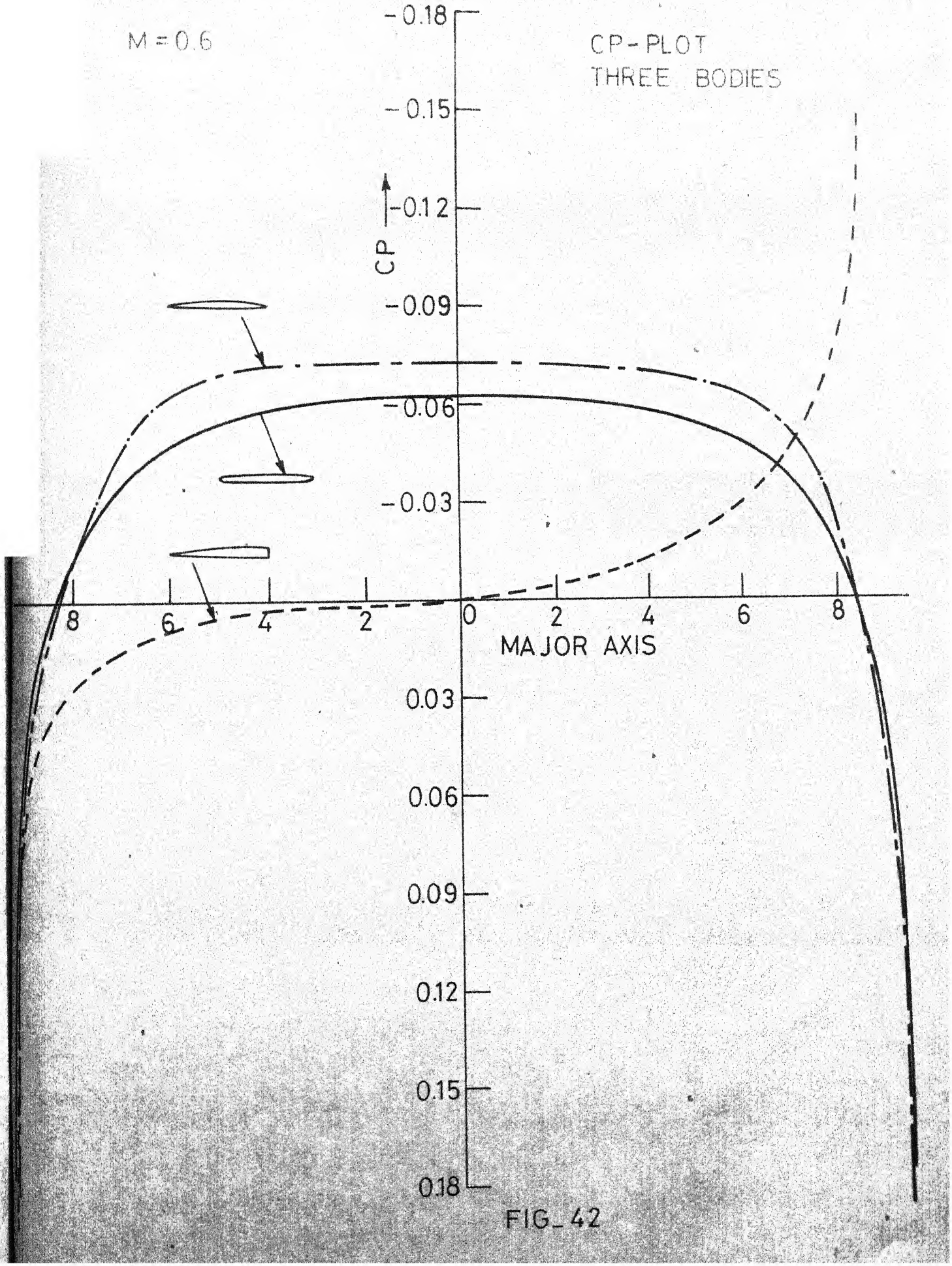
M = 0.6
CP - PLOT
THREE BODIES
-0.18
-0.15
-0.12
-0.09
-0.06
-0.03
CP
8
6
4
2
0
2
4
6
8
MAJOR AXIS
0.03
0.06
0.09
0.12
0.15
0.18

FIG_42

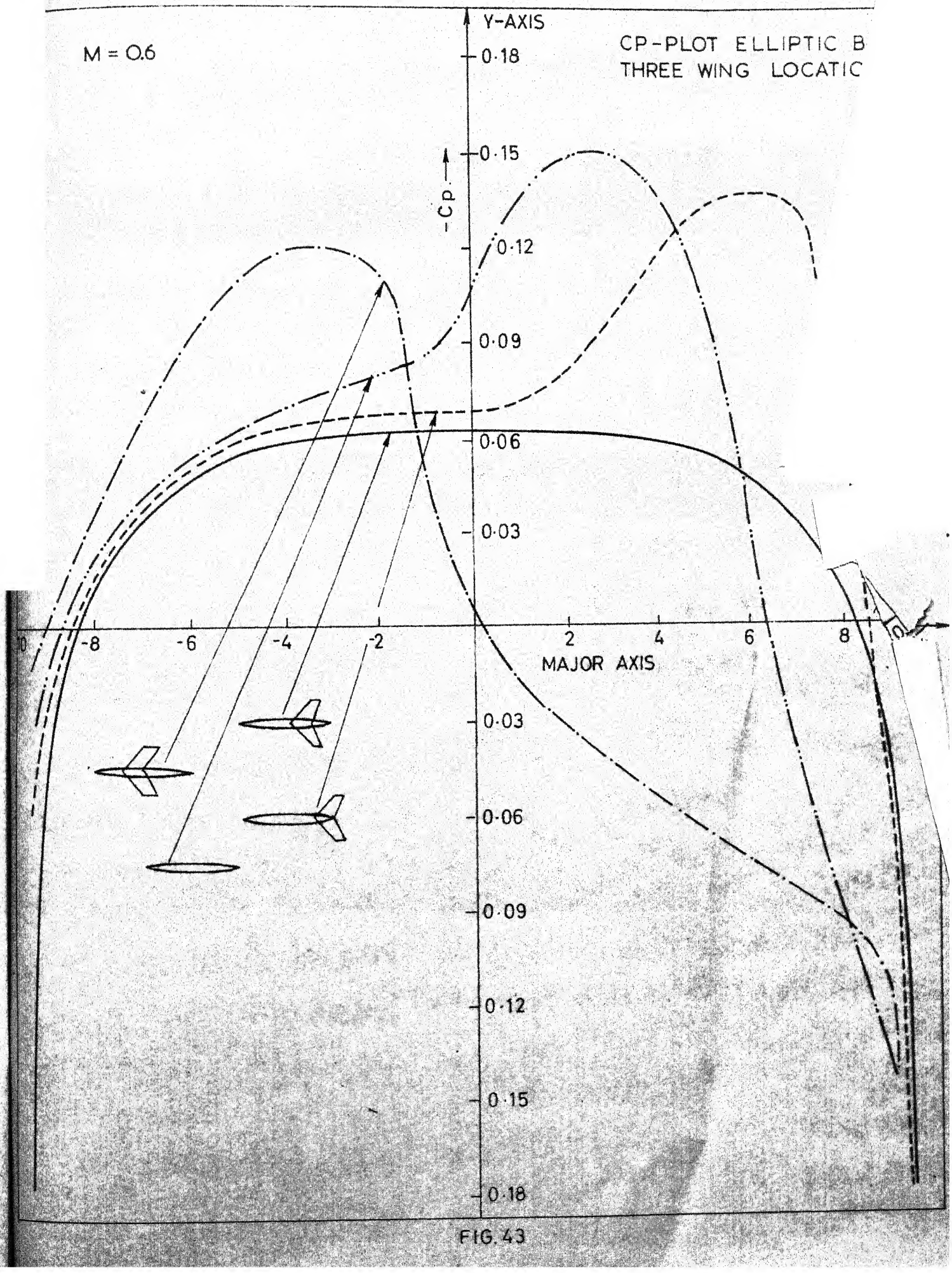
M = 0.6
CP-PLOT ELLIPTIC B
THREE WING LOCATIC
Y-AXIS
0·18
0·15
0·12
0·09
0·06
0·03
-Cp
10
-8
-6
-4
-2
2
4
6
8
MAJOR AXIS
0·03
0·06
0·09
0·12
0·15
0·18

FIG. 43

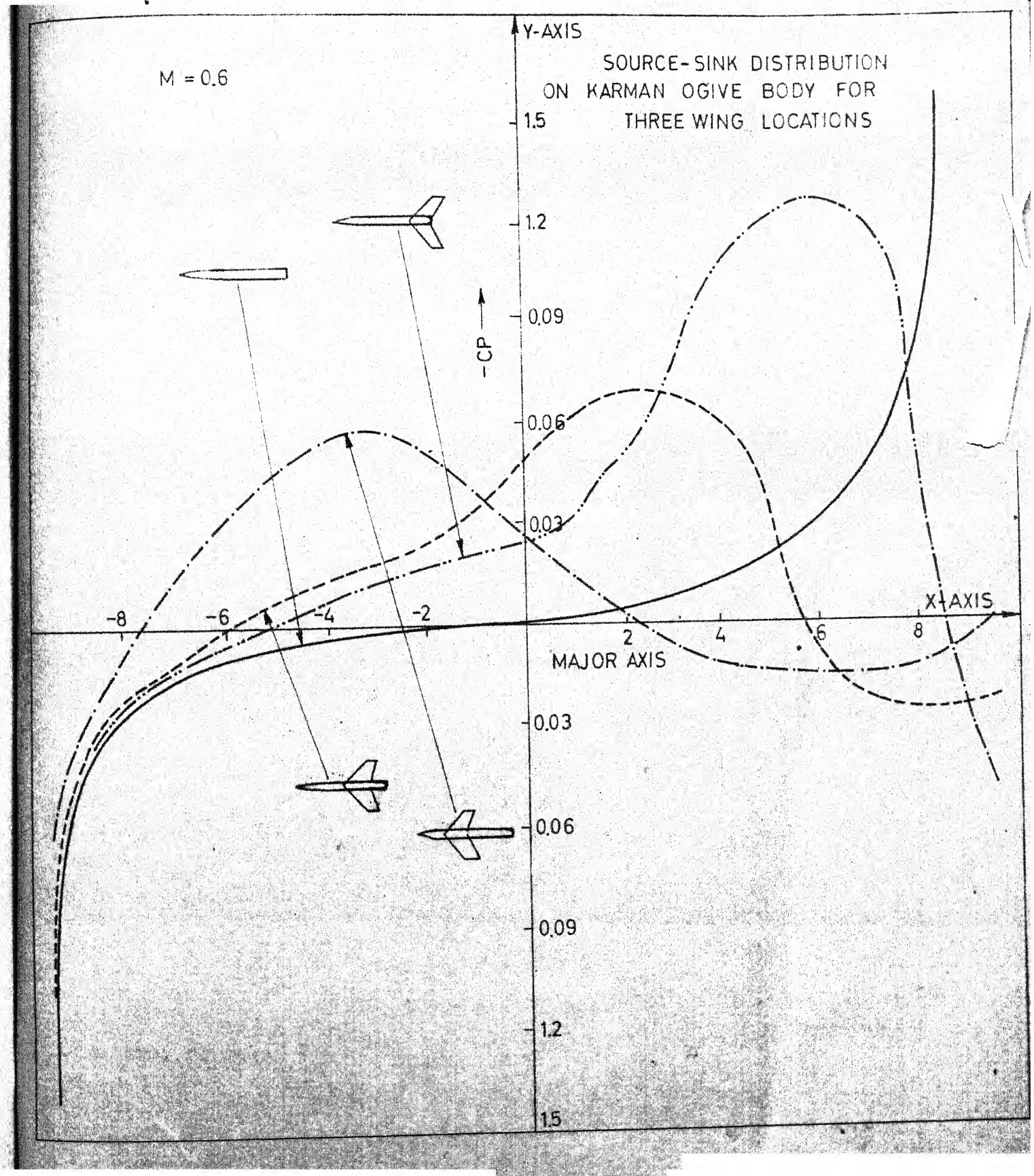
M = 0.6
Y-AXIS
SOURCE-SINK DISTRIBUTION
ON KARMAN OGIVE BODY FOR
THREE WING LOCATIONS
1.5
1.2
0.09
-CP
0.06
0.03
X-AXIS
-8
-6
-4
-2
2
4
6
8
MAJOR AXIS
0.03
0.06
0.09
1.2
1.5

FIG 44

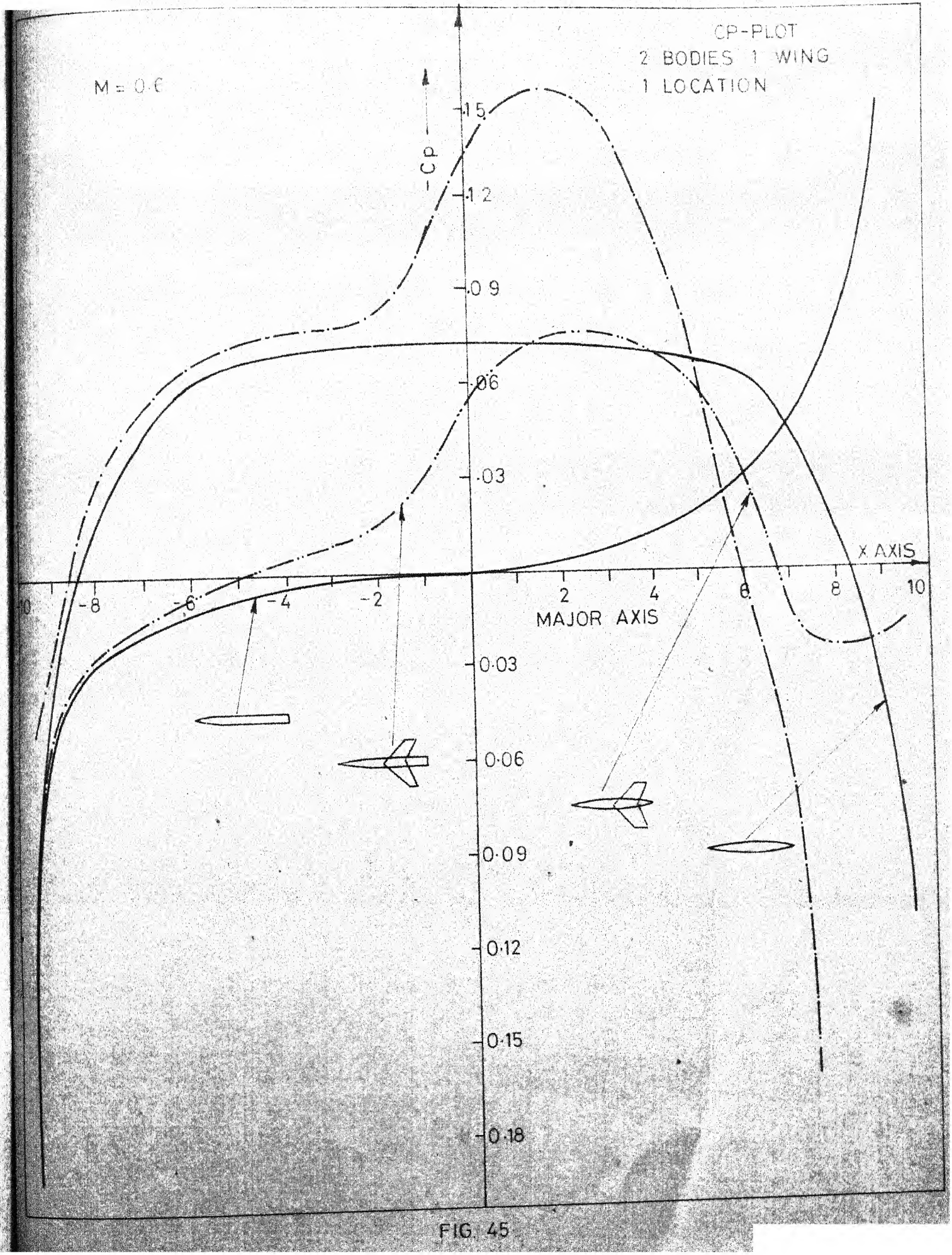
CP-PLOT
2 BODIES 1 WING
1 LOCATION
M = 0.6
-Cp
1.5
1.2
0.9
.06
.03
X AXIS
-10
-8
-6
-4
-2
2
4
6
8
10
MAJOR AXIS
0.03
0.06
0.09
0.12
0.15
0.18

FIG. 45

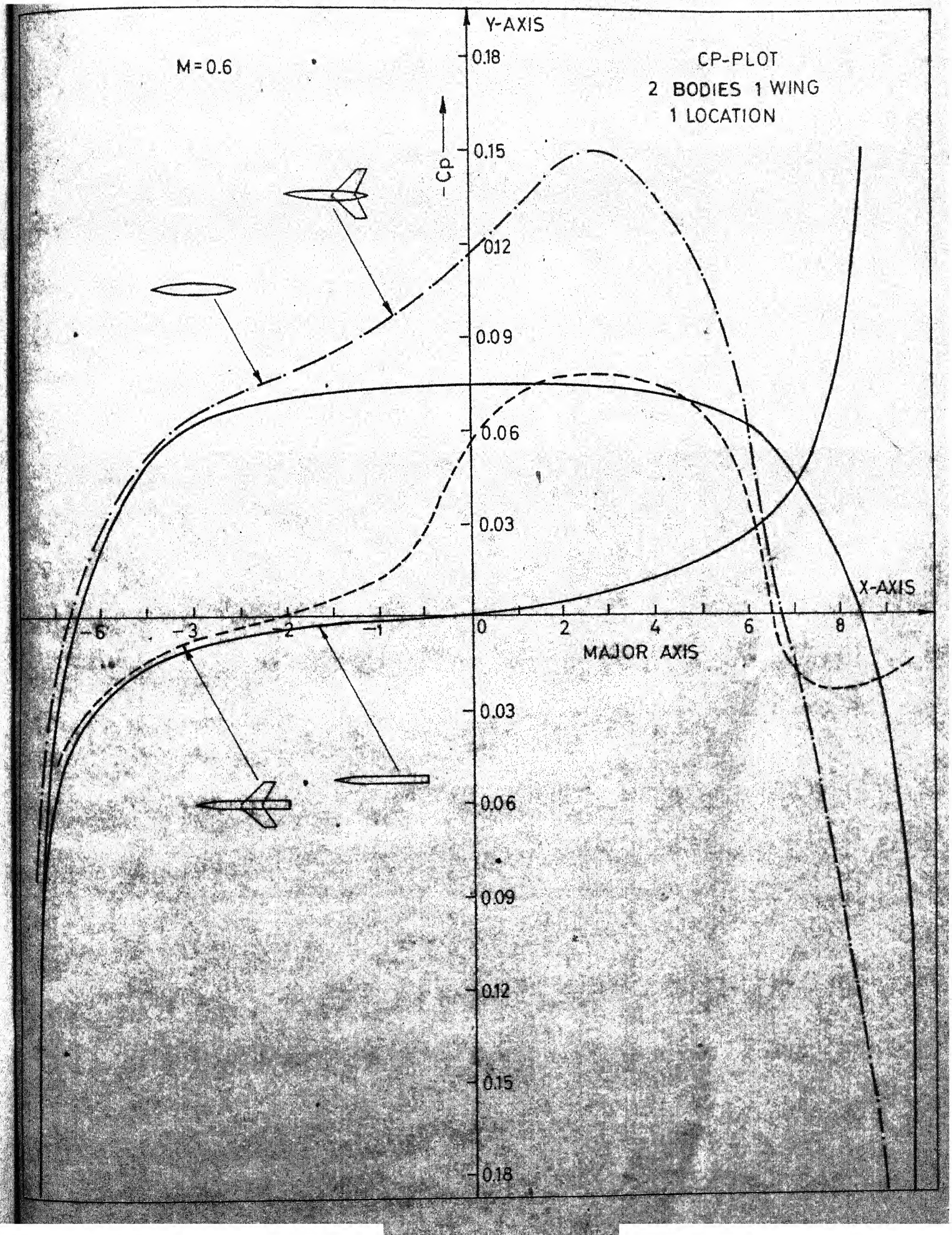
M = 0.6
CP-PLOT
2 BODIES 1 WING
1 LOCATION
Y-AXIS
X-AXIS
MAJOR AXIS
-Cp
0.18
0.15
0.12
0.09
0.06
0.03
0.03
0.06
0.09
0.12
0.15
0.18
-6
-3
-2
-1
0
2
4
6
8

FIG 46

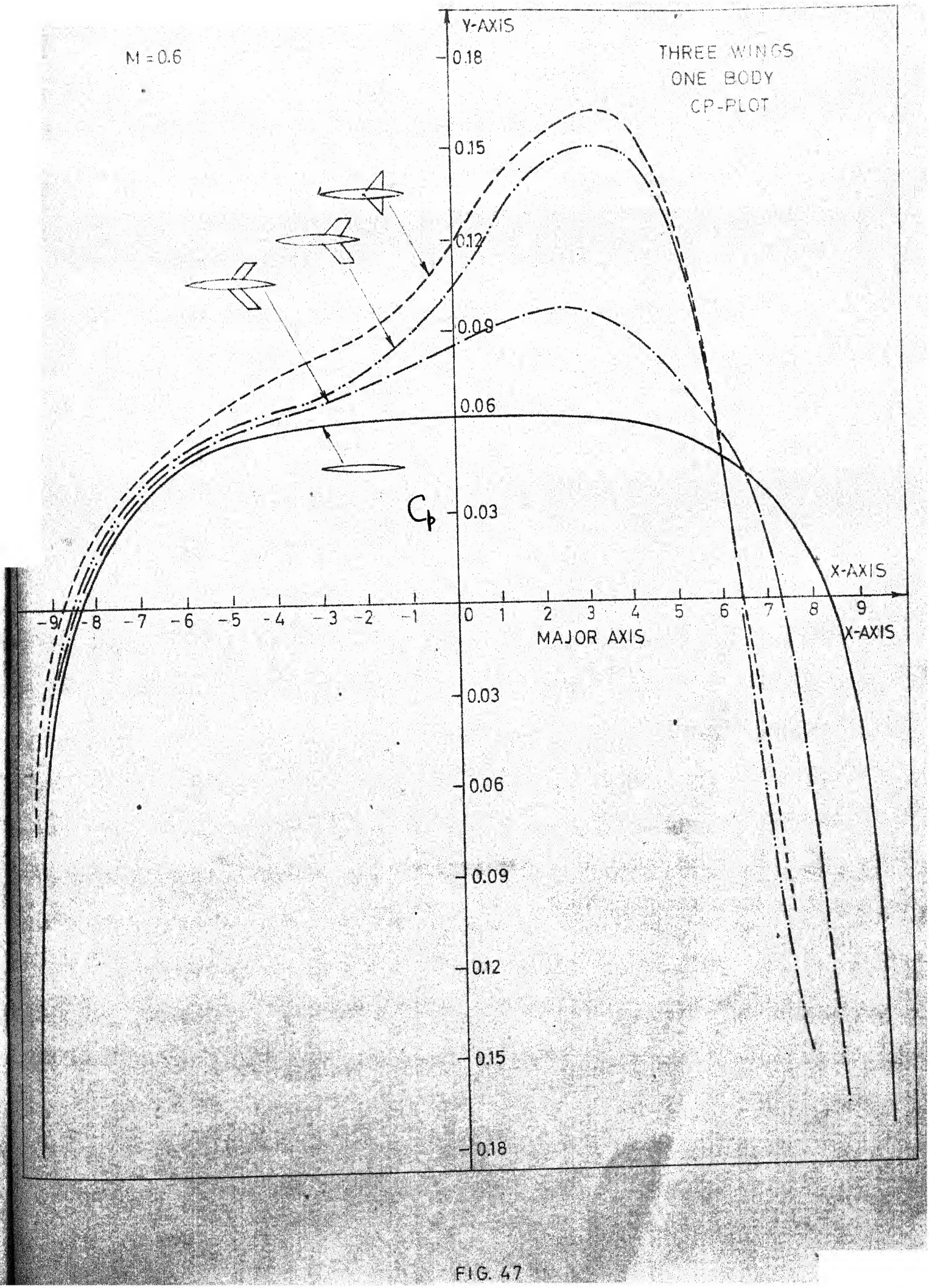
M = 0.6
THREE WINGS
ONE BODY
CP-PLOT
Y-AXIS
0.18
0.15
0.12
0.09
0.06
0.03
C_p
X-AXIS
-9 -8 -7 -6 -5 -4 -3 -2 -1 0 1 2 3 4 5 6 7 8 9
MAJOR AXIS
X-AXIS
0.03
0.06
0.09
0.12
0.15
0.18

FIG. 47

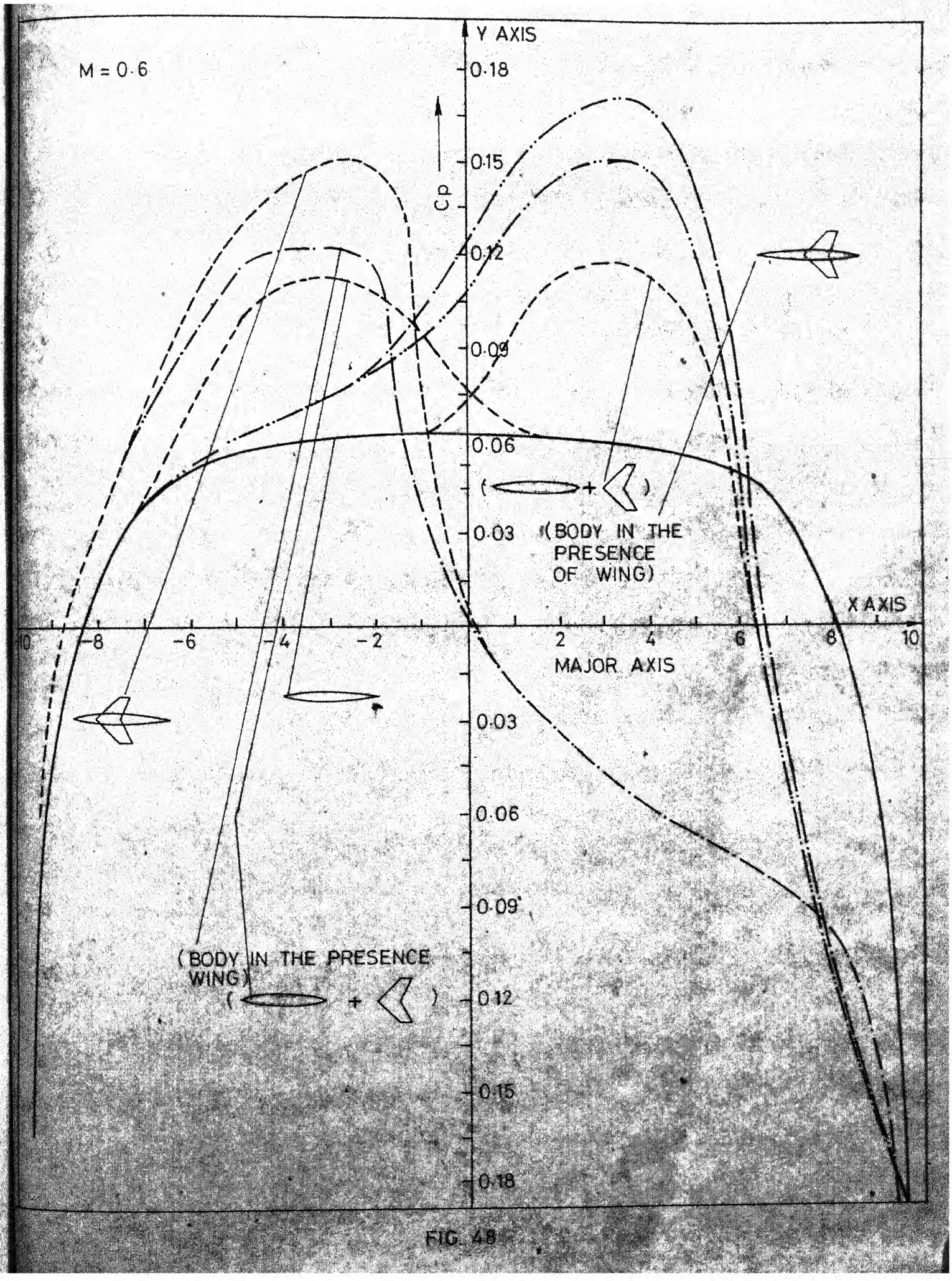
M = 0·6
Y AXIS
0·18
0·15
Cp
0·12
0·09
0·06
0·03
(BODY IN THE PRESENCE OF WING)
X AXIS
-8
-6
-4
-2
2
4
6
8
10
MAJOR AXIS
0·03
0·06
0·09
0·12
0·15
0·18
(BODY IN THE PRESENCE WING)

FIG. 48

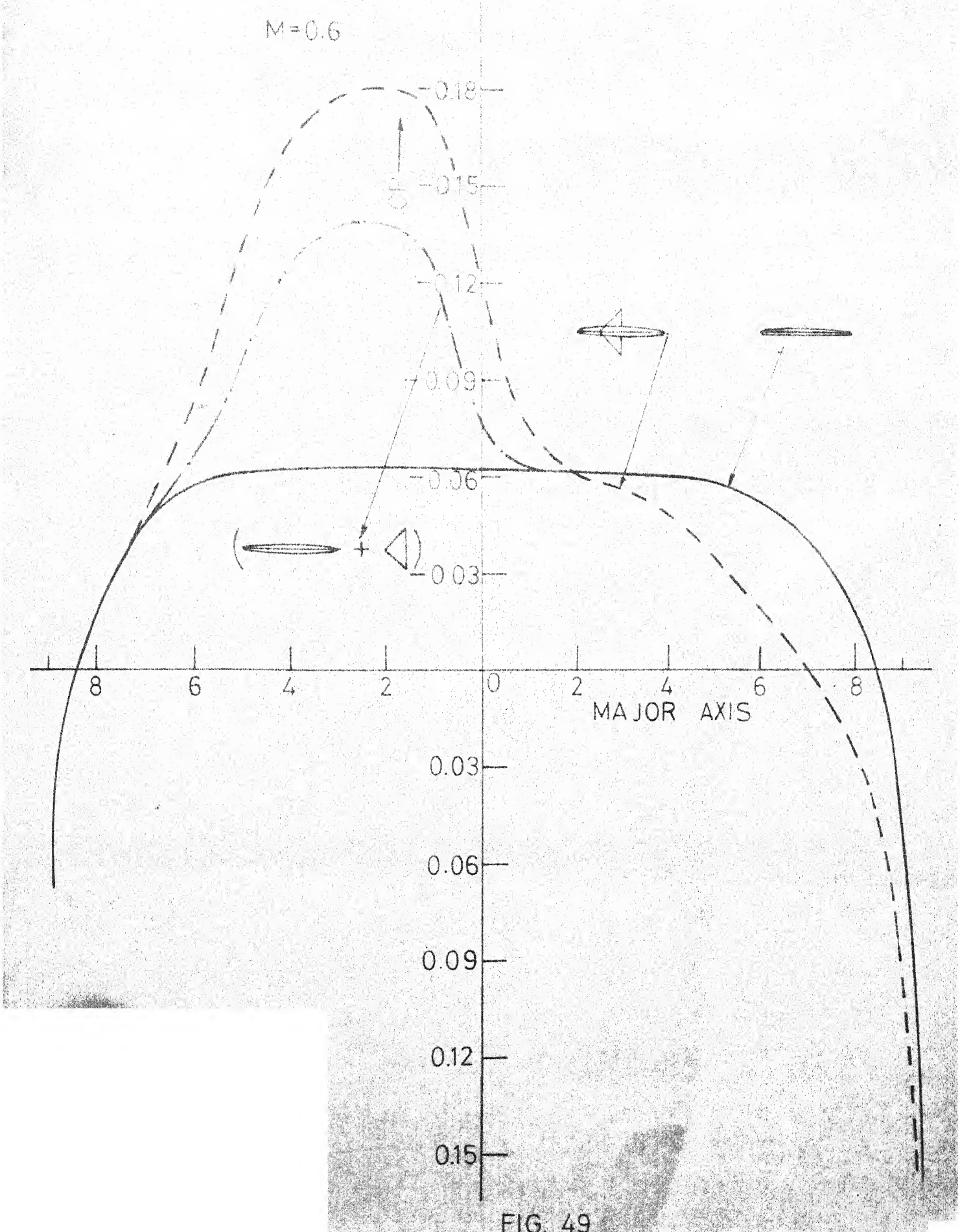
M=0.6
0.18
0.15
0.12
0.09
0.06
0.03
8
6
4
2
0
2
4
6
8
MAJOR AXIS
0.03
0.06
0.09
0.12
0.15

FIG. 49

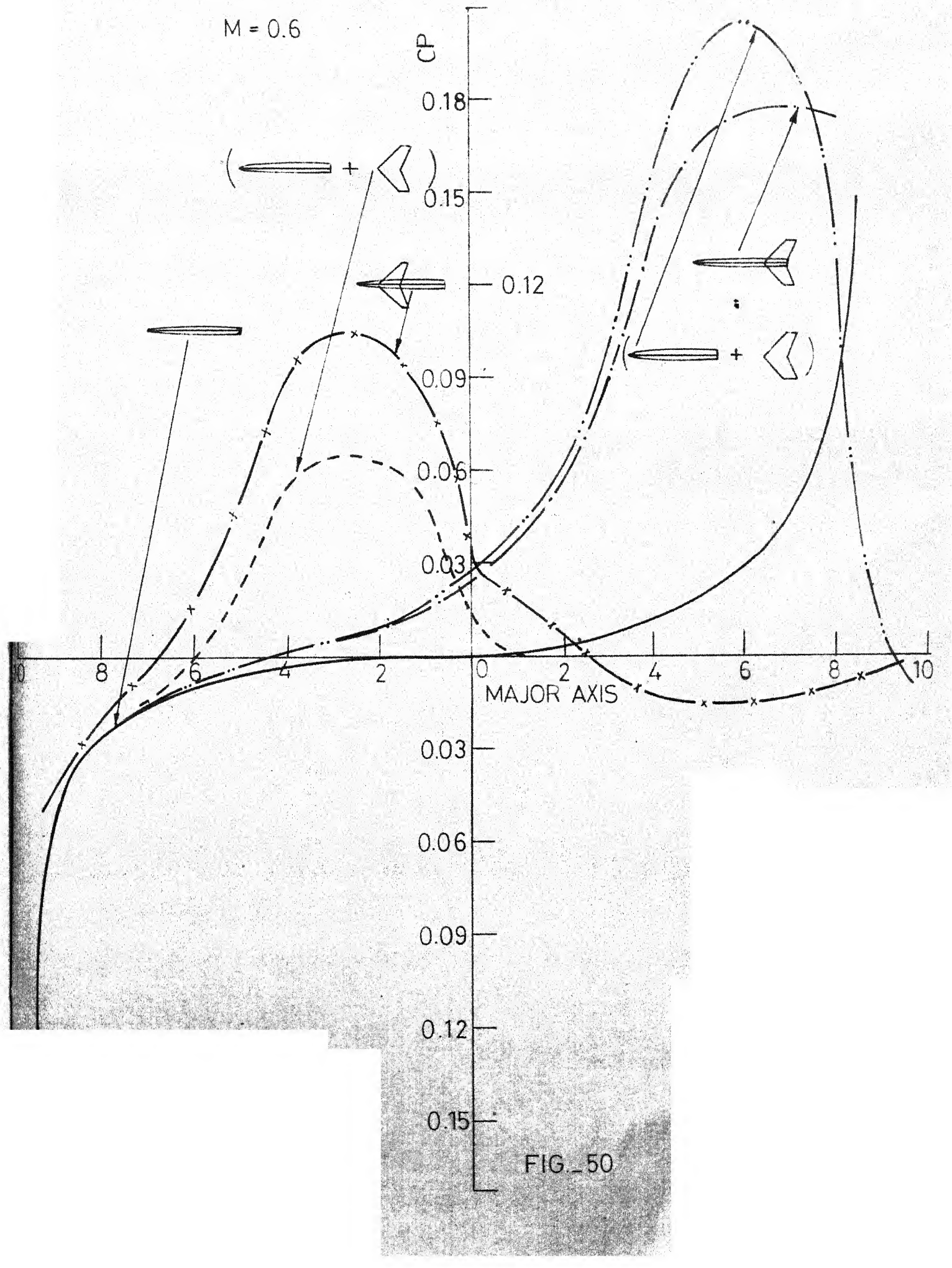
M = 0.6
CP
0.18
0.15
0.12
0.09
0.06
0.03
0.03
0.06
0.09
0.12
0.15
8
6
4
2
0
2
4
6
8
10
MAJOR AXIS

FIG._50

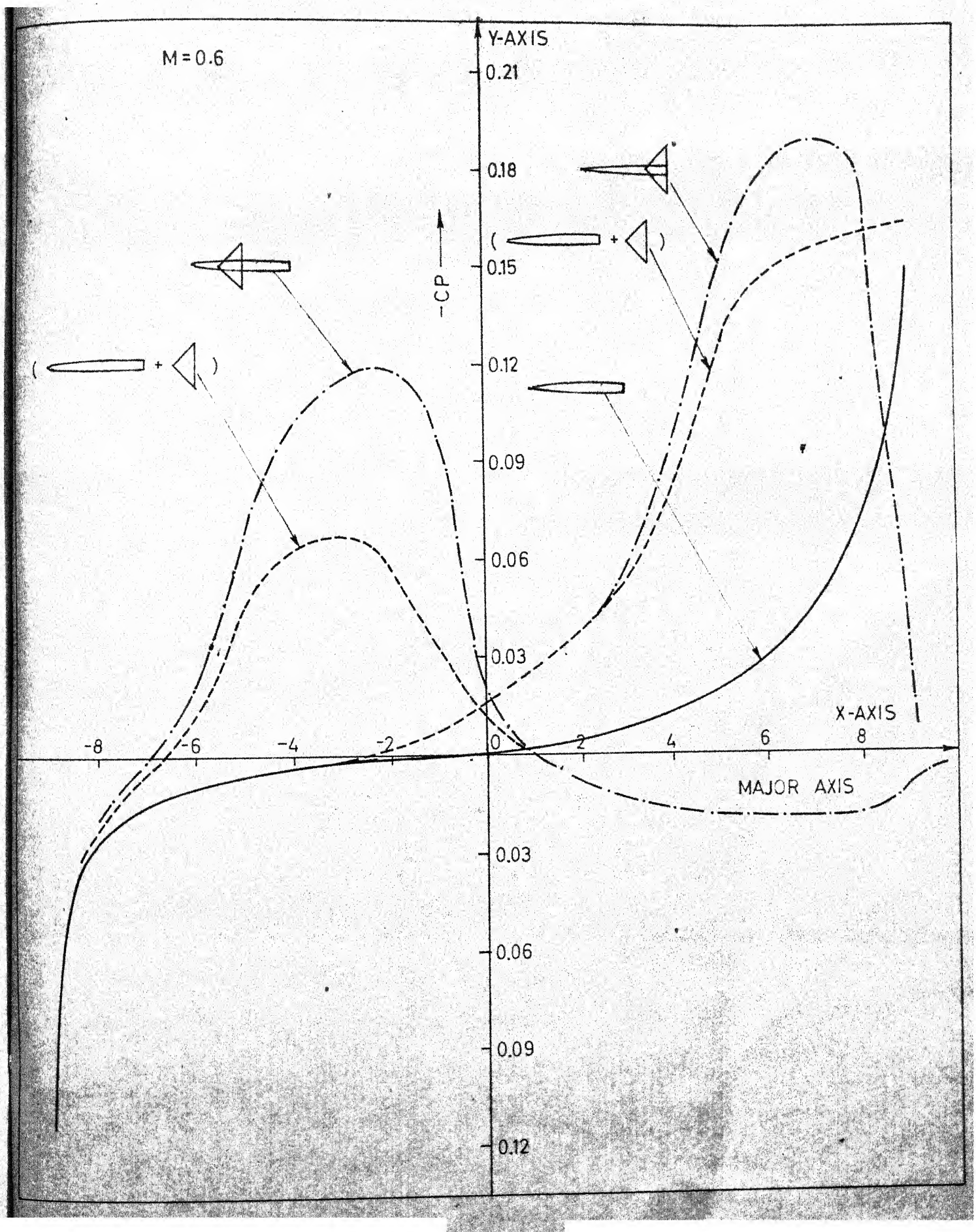
M = 0.6
Y-AXIS
0.21
0.18
0.15
0.12
0.09
0.06
0.03
-CP
(+)
(+)
X-AXIS
-8
-6
-4
-2
0
2
4
6
8
MAJOR AXIS
0.03
0.06
0.09
0.12

FIG. 51

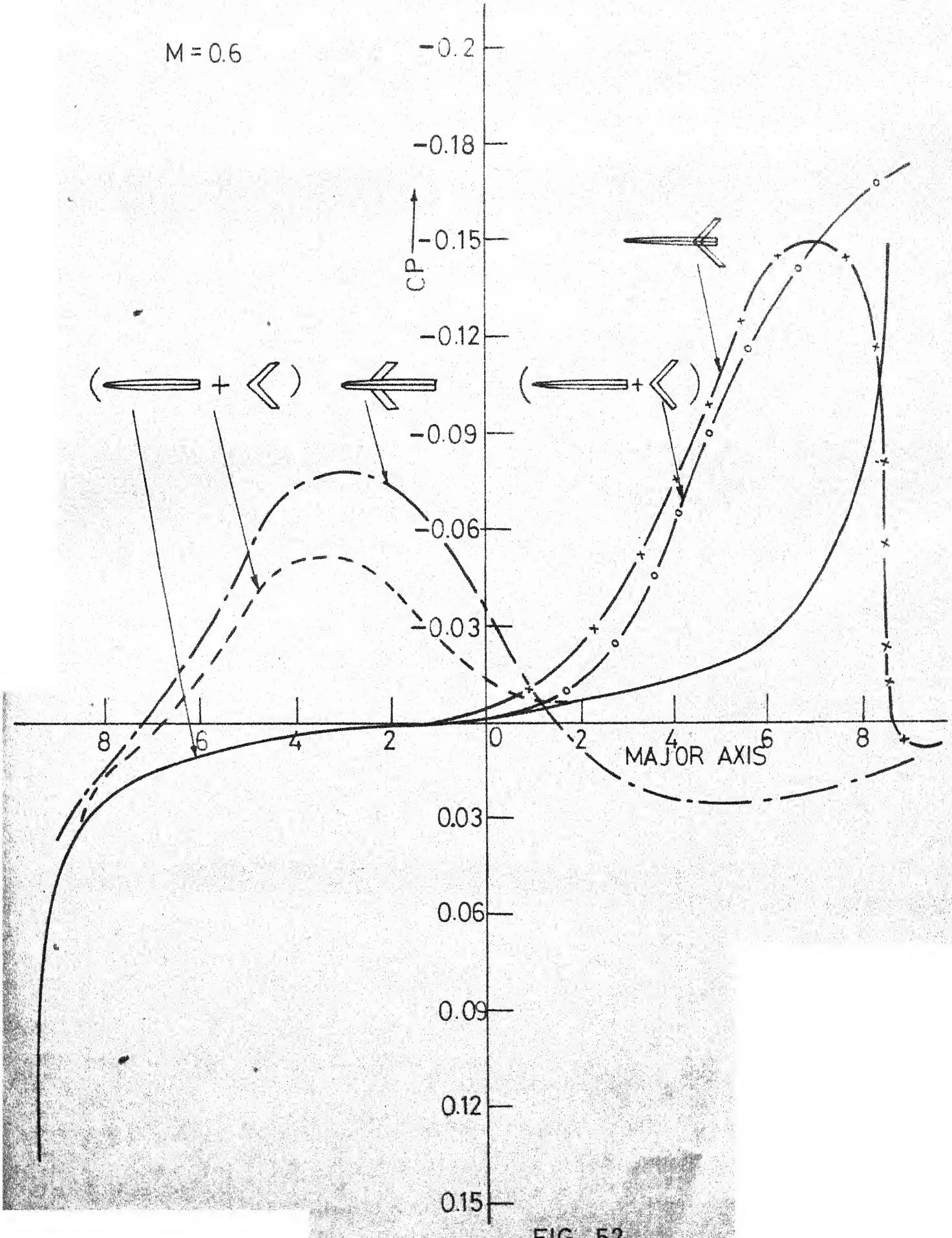
M = 0.6
-0.2
-0.18
-0.15
-0.12
-0.09
-0.06
-0.03
CP
0.03
0.06
0.09
0.12
0.15
8
6
4
2
0
2
4
6
8
MAJOR AXIS

FIG._52

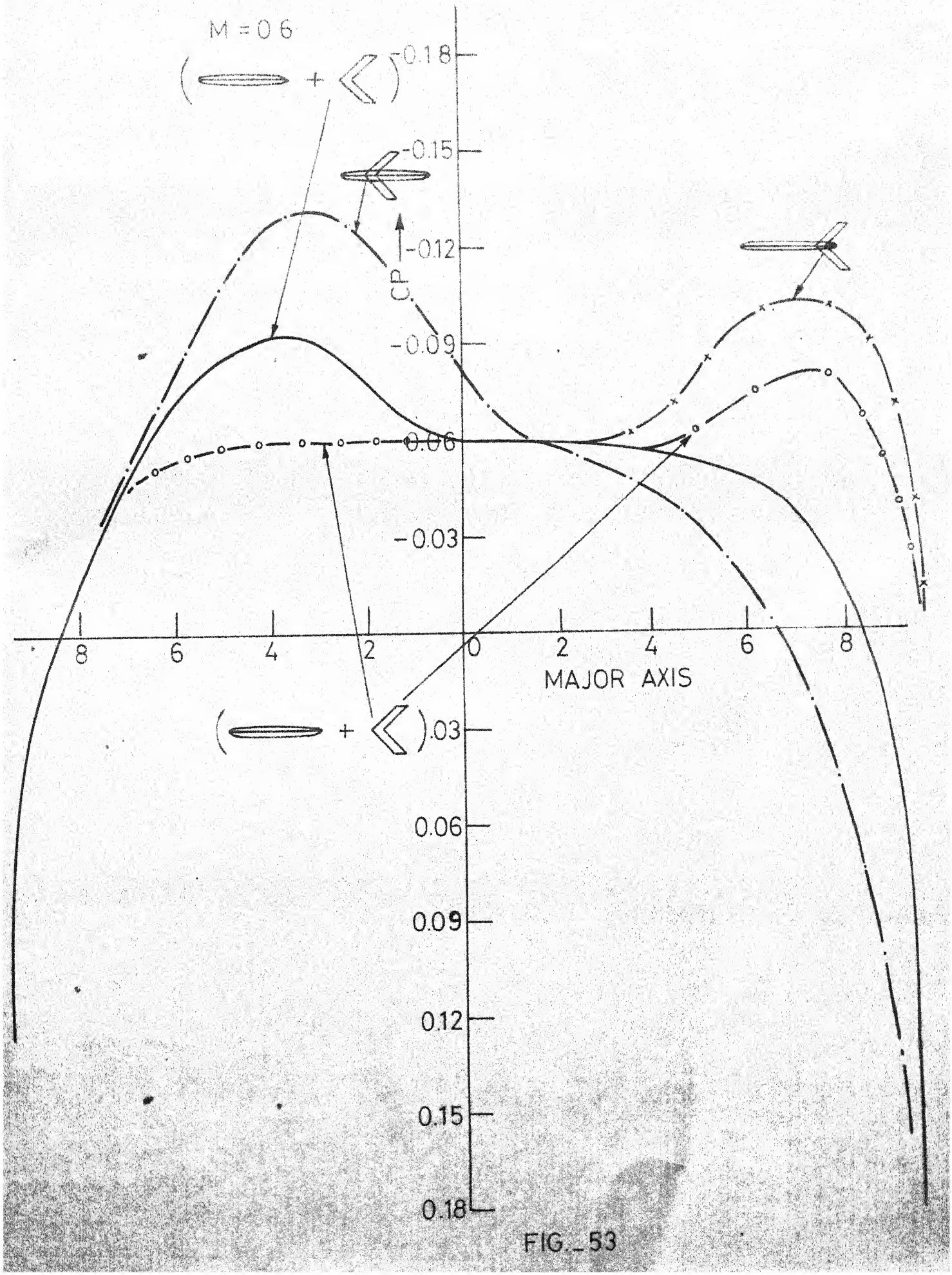
M = 0 6
-0.18
-0.15
-0.12
-0.09
-0.06
-0.03
C_D
8
6
4
2
0
2
4
6
8
MAJOR AXIS
.03
0.06
0.09
0.12
0.15
0.18

FIG._53

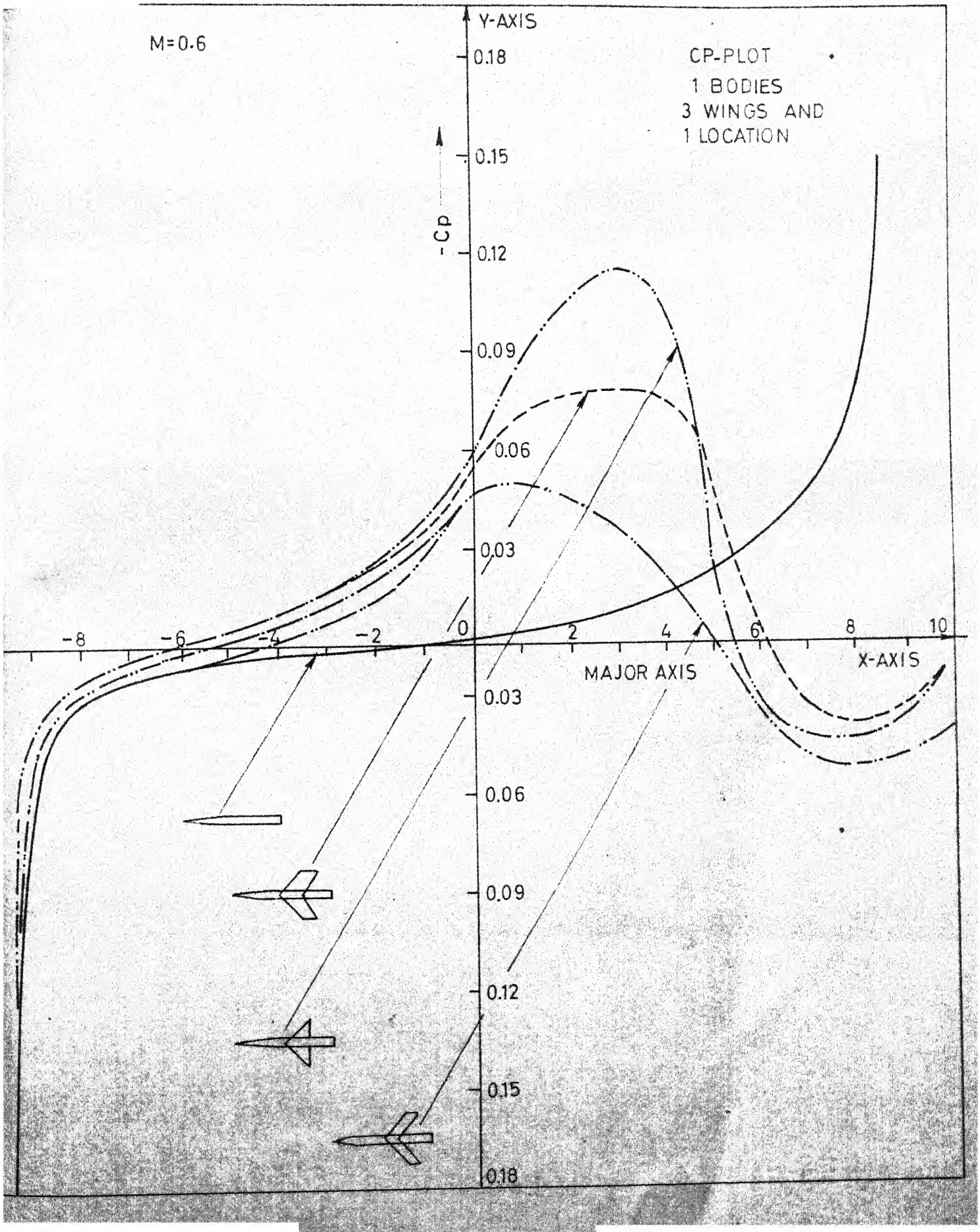
M=0.6
Y-AXIS
CP-PLOT
1 BODIES
3 WINGS AND
1 LOCATION
-Cp
0.18
0.15
0.12
0.09
0.06
0.03
0
0.03
0.06
0.09
0.12
0.15
0.18
-8
-6
-4
-2
2
4
6
8
10
X-AXIS
MAJOR AXIS

FIG. 54

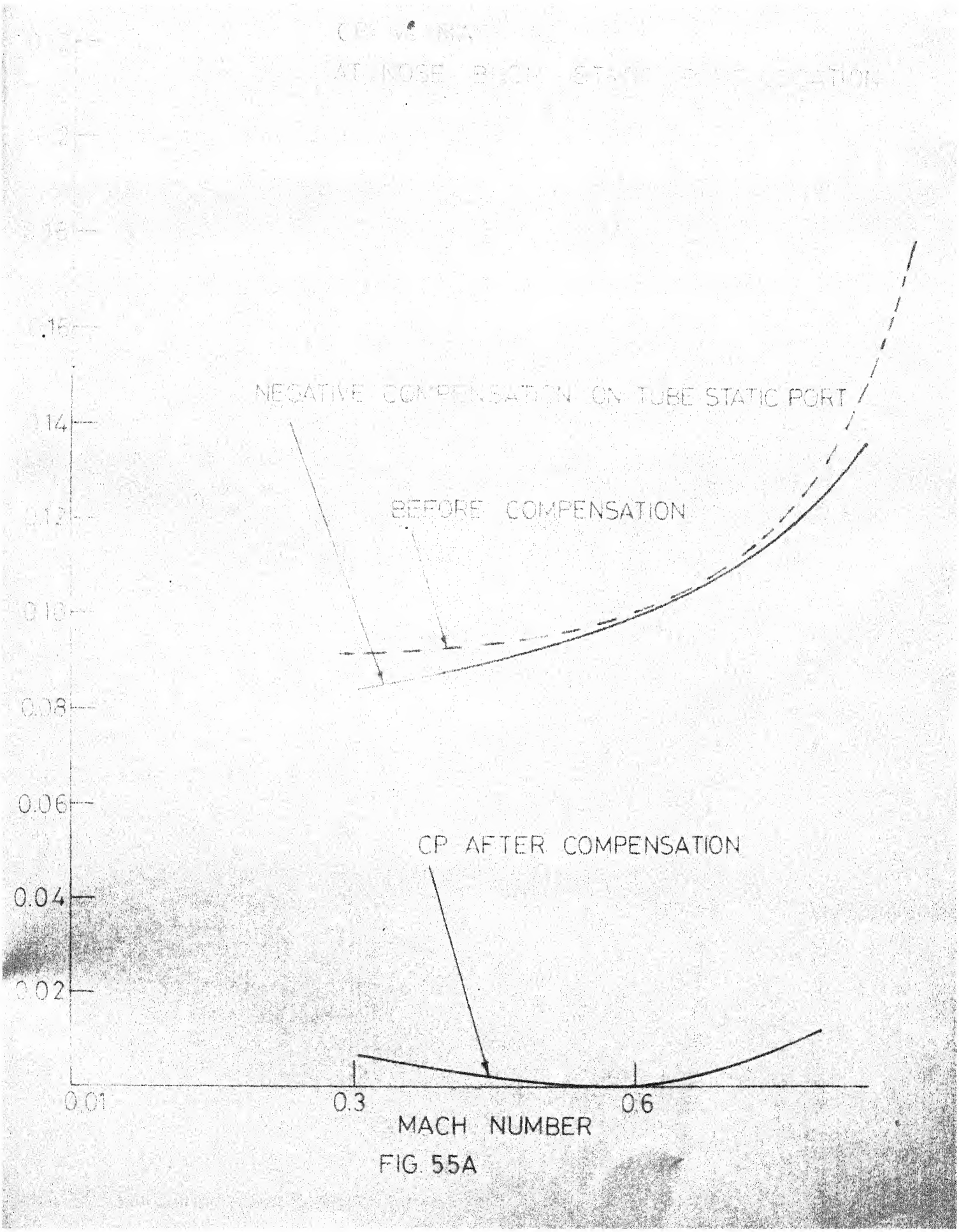
.15
14
12
0.10
0.08
0.06
0.04
0.02
0.01
0.3
0.6
NEGATIVE COMPENSATION ON TUBE STATIC PORT
BEFORE COMPENSATION
CP AFTER COMPENSATION
MACH NUMBER

FIG. 55A

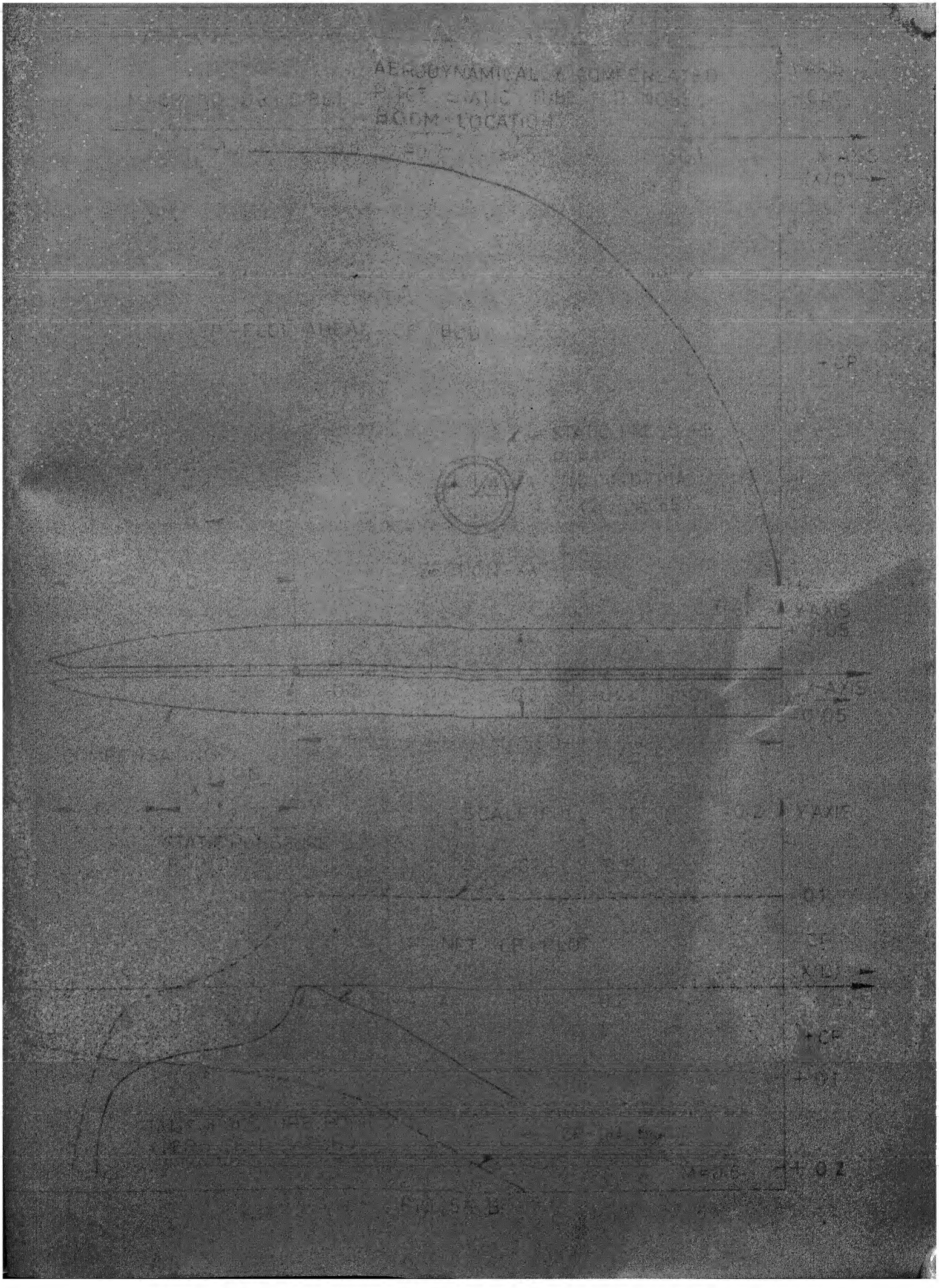

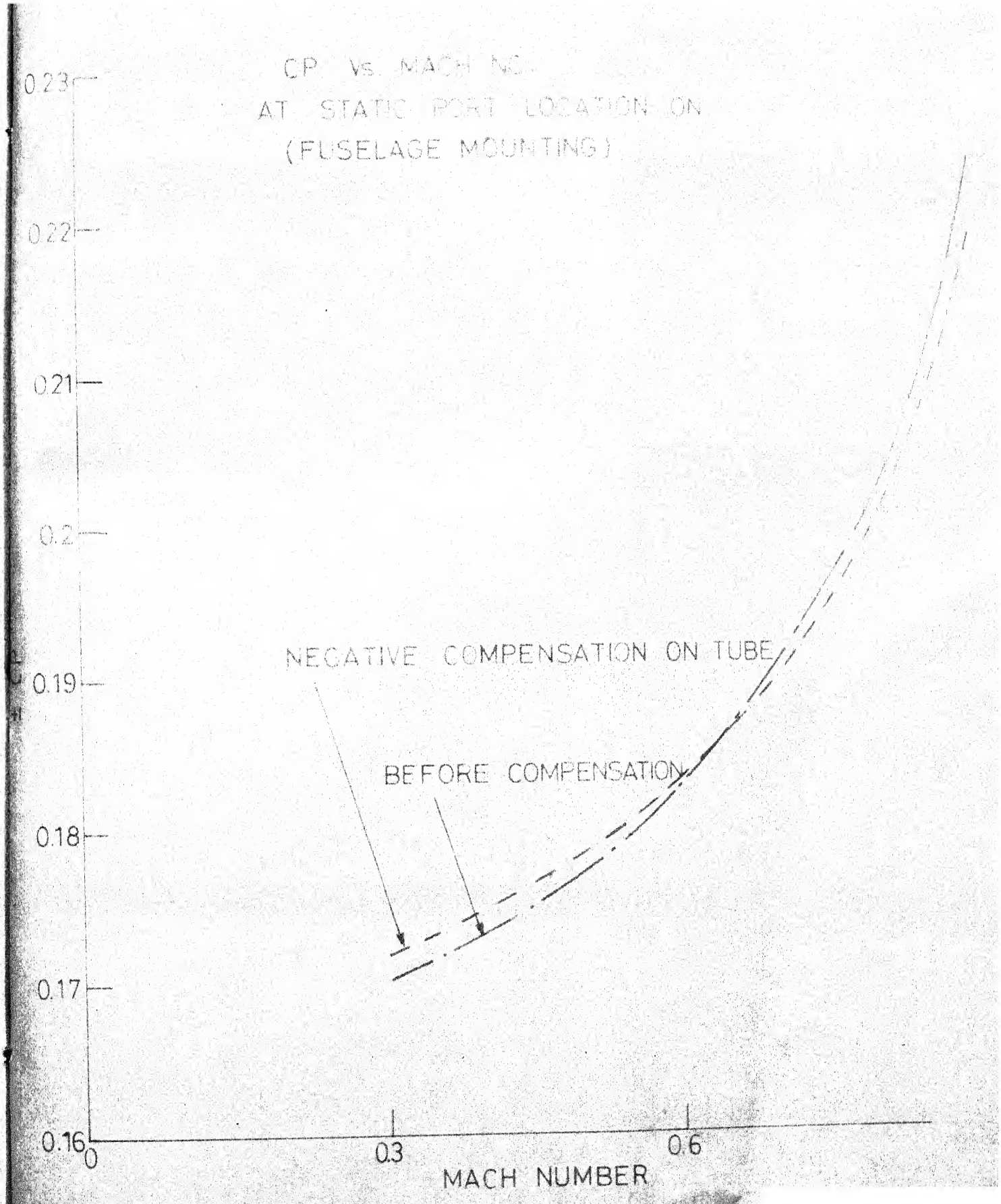
CP Vs. MACH NO.
AT STATIC PORT LOCATION ON
(FUSELAGE MOUNTING)
0.23
0.22
0.21
0.2
0.19
0.18
0.17
0.16
0
0.3
0.6
MACH NUMBER
NEGATIVE COMPENSATION ON TUBE
BEFORE COMPENSATION

FIG._56-A

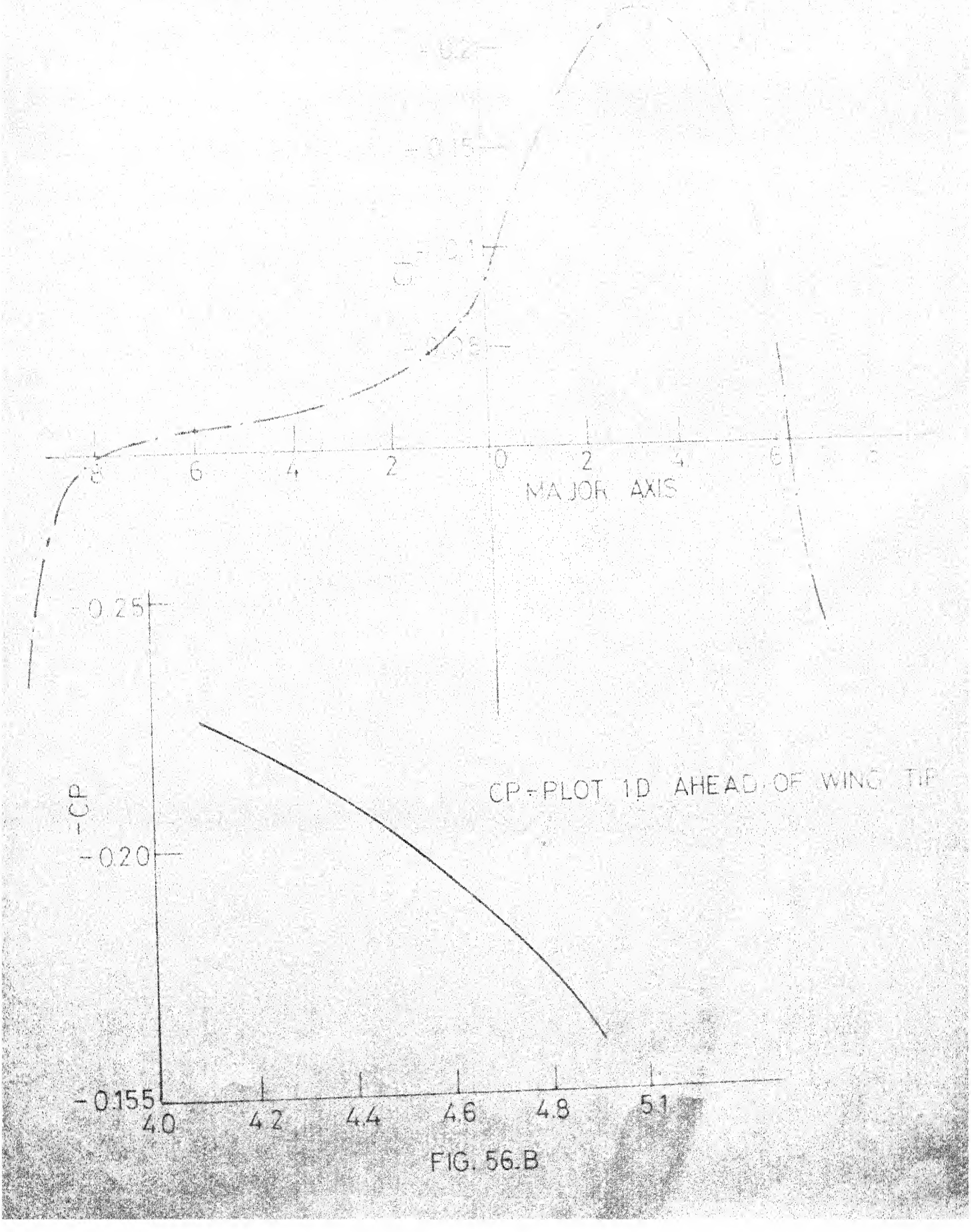
8
6
4
2
0
2
4
6
MAJOR AXIS
-0.25
-0.20
-0.155
4.0
4.2
4.4
4.6
4.8
5.1
CP - PLOT 1D AHEAD OF WING TIP

FIG. 56.B

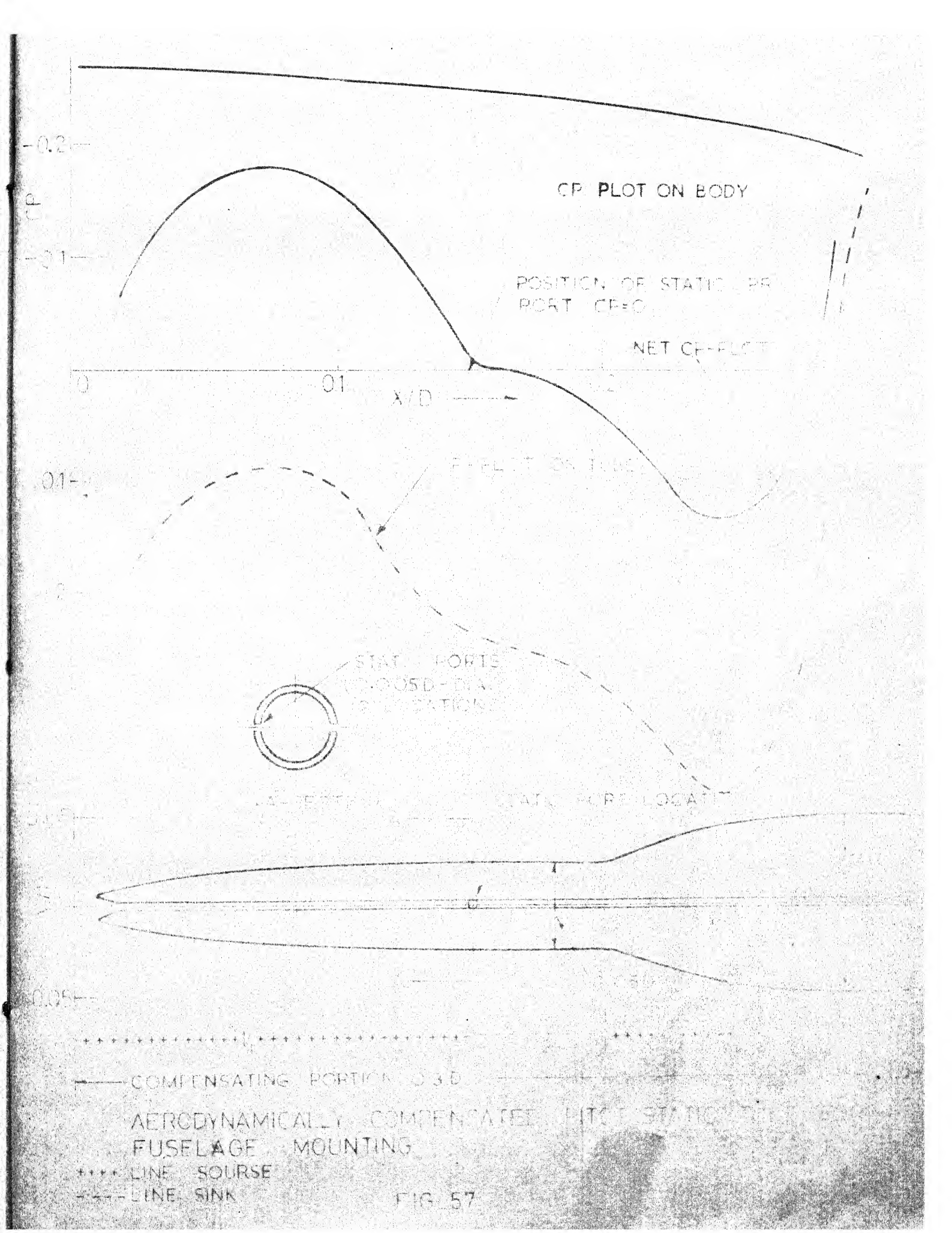
CP PLOT ON BODY
POSITION OF STATIC PR
PORT CP=0
NET CP PLOT
X/D
0
01
-0.2
-0.1
0.1
0.05
COMPENSATING PORTION 0.3 D
AERODYNAMICALLY COMPENSATED
FUSELAGE MOUNTING
++++ LINE SOURSE
---- LINE SINK

FIG. 57

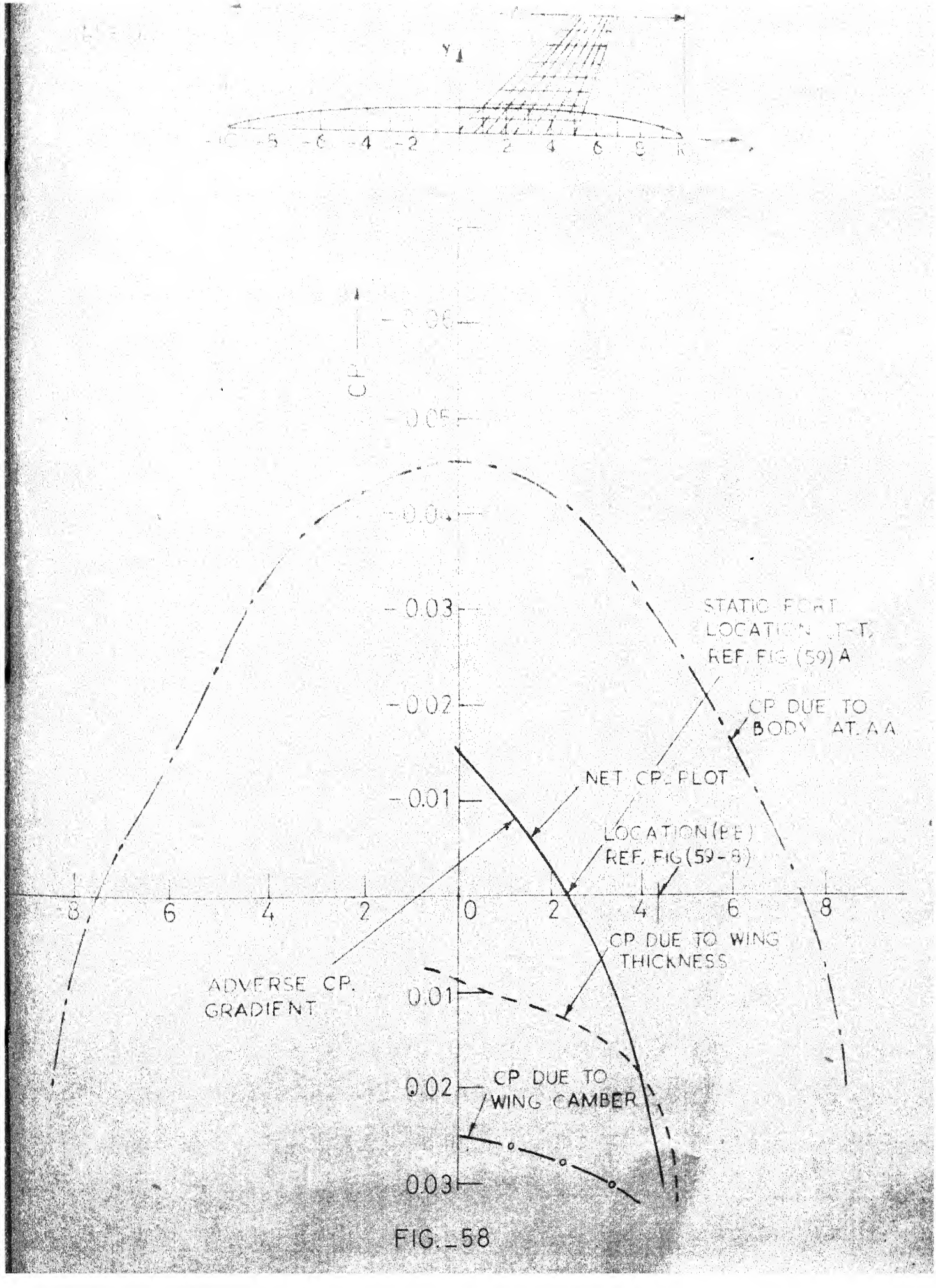
Y
-0.03
-0.02
-0.01
0.01
0.02
0.03
STATIC PORT LOCATION (T-T) REF. FIG (59) A
CP DUE TO BODY AT AA
NET CP PLOT
LOCATION (PE) REF. FIG (59-B)
CP DUE TO WING THICKNESS
ADVERSE CP. GRADIENT
CP DUE TO WING CAMBER
-8
6
4
2
0
2
4
6
8

FIG._58

M = 0.2 - 0.9 AERODYNAMICALLY COMPENSATED
PITOT STATIC TUBE FOR WING-TIP LOCATION

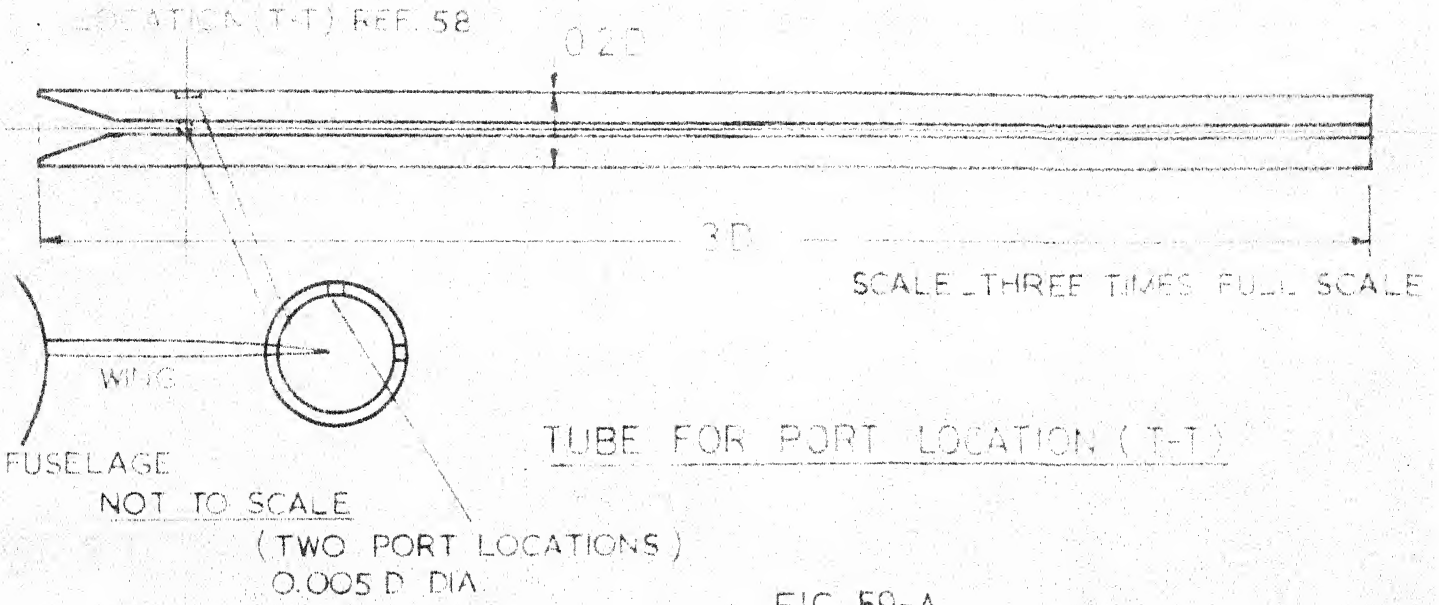

TUBE FOR PORT LOCATION (T-T)

FIG. 59-A

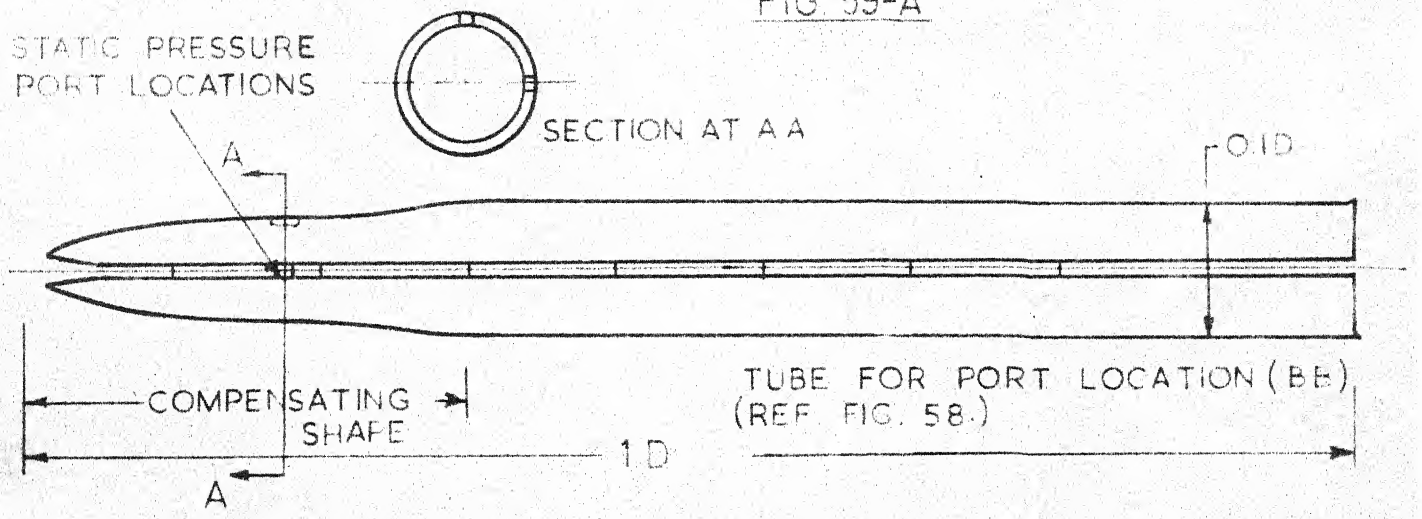

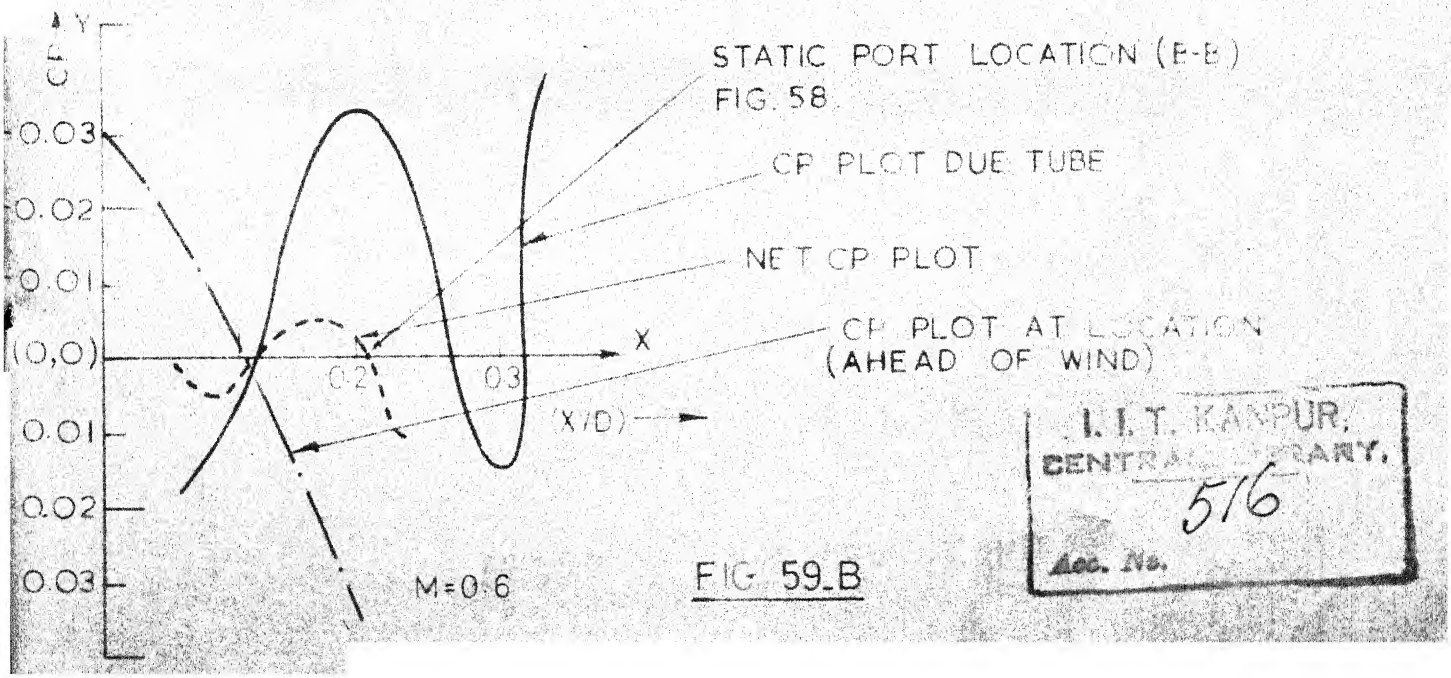

FIG. 59-B